Exploring the use of *in vitro* colorimetric and bioluminescence assays to distinguish between Arf GTPase isoforms and detect Arf GTPase activity

A thesis submitted in fulfilment of the

requirements for the degree of

Master of Science

In Biochemistry

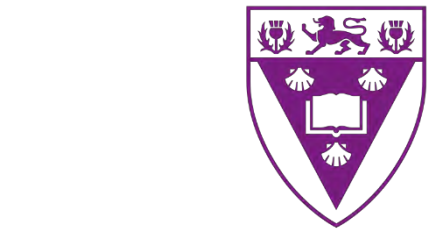

RHODES UNIVERSITY

Where leaders learn

By

Alexander Woolf

May 2021

Abstract

ADP-ribosylation factors (Arfs), part of the Ras superfamily of small GTPases, are involved in various key cellular processes such as the regulation of membrane trafficking and organelle structure. Arfs cycle between a GDP-bound 'inactive' conformation and a GTP-bound 'active' conformation, with the latter exerting its functions on various downstream effector proteins. In eukaryotic organisms, Arf6 regulates traffic in the endocytic pathway and contributes the reorganisation of actin cytoskeleton. Due to its ability to affect health and disease in many ways, Arf6 has been a viable drug target for many diseases, with this study focusing mainly on cancer and malaria. In the *P. falciparum* parasite genome are two genes encoding for Arf GTPase. The first (*Pf*Arf1) has been designated as an Arf1 homologue, and the second shares sequence similarities with both human Arf1 and Arf6 but is otherwise uncharacterised. The potential of the second putative malarial Arf sequence to be a homologue of human Arf6 is important as it would further our understanding of the unusual mechanisms behind malarial endocytosis of the red blood cell cytoplasm. To assign this second putative malarial Arf (*Pf*Arf6) as a human Arf6 or Arf1 homologue, a novel plate-based colorimetric assay system was used involving the Arf effector binding domains of "golgi-localised gamma adaptin ear-containing ARF-binding protein 3" (GGA3), which interacts with Arf1 and Arf6, and "c-Jun NH_2-terminal kinase-interacting protein 4" (JIP4), which interacts with Arf6 only. It was shown that *Pf*Arf6 was able to bind to both GGA3 and JIP4 and that *Pf*Arf6 was distinguishable from *Pf*Arf1. Initial data obtained designated "*Pf*Arf6" as an Arf6 homologue, despite the higher sequence similarity between *Pf*Arf6 and human Arf1. Arf GTPases display notoriously slow intrinsic GTPase activity and so their activity is tightly regulated by their cognate guanine nucleotide-exchange factors (GEFs) and GTPase-activating proteins (GAPs), which cycle Arfs between their GDP- and GTP-bound conformations. Arf6 and its closely associated regulators are involved extensively in the promotion of tumour growth, invasion, and metastasis stages of cancer. Simple and reproducible GTPase activity assays, that are simultaneously amenable to screening compound libraries for Arf inhibitors, are limited in availability due to the difficulties surrounding accurate GTP detection. A novel *in vitro* plate-based bioluminescence assay format developed in this study to detect Arf GTPase activity in the presence of its regulators namely "ARF nucleotide-binding site opener" (ARNO) and ArfGAP1. In cells "nucleoside diphosphate kinase" (NDPK) functions to regulate the available nucleoside triphosphate (NTP) pools to maintain homeostasis. Given the relative ease for accurate ATP detection using firefly luciferase and the ability for NDPK the convert GTP to ATP, NDPK and luciferase were utilised in this coupled assay to detect GTP consumption by Arf. Regulator stimulated Arf GTPase activity was eventually detectable to varying degrees for human Arf1 and Arf6, as well as malarial Arf1. Thus, the groundwork for a simple, plate-based assay system has been laid for the detection of the full Arf GTPase activity cycle, the screening of compound libraries for Arf inhibitors, as well as a means of determining Arf GTPase specificity for regulators (and vice versa) *in vitro*.

Acknowledgements

There are many people I would like to deeply thank for helping me along this journey. Firstly, to my supervisor Prof. Heinrich Hoppe, for his guidance, unwavering patience, and trust in me to push through barriers. I would not have been able to pick myself back up and finish if it were not for his inspiration and understanding. I have enjoyed our conversations thoroughly and have learnt many life lessons. Secondly, to Dustin Laming and Tarryn Swart, for their willingness to answer my silly questions and help steer me in the right direction. I would have been completely lost in the lab without them. Lastly, but not the least noteworthy, to my parents, siblings, and friends for their constant support and motivation, for which without I would have given up.

Table of contents

Abstract……..……**2**

Acknowledgements……..……..**3**

Table of contents…….…...…….…….....…...**4**

List of Abbreviations…….……..……...**7**

List of Figures and tables……..……..….**11**

Chapter 1: Literature review……..…….**13**

1.1. Arf GTPases……13

1.1.1. Classification and structure……..……13

1.1.2. Activity cycle…….....14

1.1.2.1. GTP/GDP cycling……...14

1.1.2.2. Arf GEFs…….15

1.1.2.3. Arf GAPs……16

1.1.2.4. Effectors……..17

1.1.3. Arf6 cellular functions……...……..18

1.1.3.1. Endocytosis…….19

1.1.3.2. Actin dynamics……...21

1.2. Arf6 and disease…….....24

1.2.1. Arf6 GTPase association with cancer…….……..24

1.2.1.1. Cancer development and proliferation……24

1.2.1.2. Arf6 regulator and effector utilisation…….25

1.2.2. Arf6 GTPase association with malaria…….……27

1.2.2.1. Malaria lifecycle…….27

1.2.2.2. Endocytosis in malaria parasites…….28

1.2.2.3. Malarial Arf GTPases……..31

1.3. Overall motivation and objectives……32

Chapter 2: Arf GTPase assay recombinant protein production…..……....**33**

2.1. Introduction…….……33

2.2. Aims and objectives…….34

2.3. Results……..……...35

2.3.1.His-tagged Arf-GTPase proteins…….…….35

2.3.2.NDPK-bioluminescence assay associated proteins……..……39

2.3.3.Arf-GTPase effector proteins……...……44

2.4. Discussion……...……46

Chapter 3: Distinguishing human and malarial Arf1 and Arf6 using of GGA3 and JIP4 …….…...**48**

3.1. Introduction…….……48

3.2. Aims and objectives…….52

3.3. Results……..……...53

3.3.1.Nucleotide exchange optimisation for each Arf GTPase……..……..53

3.3.2.Ni-NTA- and glutathione-immobilised effector-GST interaction assays……..…….57

3.4. Discussion……...……61

Chapter 4: Detection of regulator mediated Arf-GTPase activity using NDPK and luciferase……..…….……**65**

4.1. Introduction…….……65

4.2. Aims and objectives…….68

4.3. Results……...…...……...69

4.3.1.NDPK GTP-to-ATP conversion activity……..69

4.3.2.Arf-NDPK coupled reaction……...…..73

4.4. Discussion……...……78

Chapter 5: Methods and materials……..**82**

5.1. Constructs……...….82

5.2. Transformed *E. coli* stock solution preparation…….……...83

5.2.1. Preparation of competent *E. coli* cells…….……83

5.2.2. Transformation of competent cells…….…….…….83

5.2.3. Alkaline lysis plasmid miniprep…….…..……83

5.2.4. Diagnostic restriction digestion…….…….……..84

5.2.5. Agarose gel electrophoresis …….……84

5.3. Protein expression and purification…….……..…85

5.3.1. Analytical scale expression……..85

5.3.2. Preparative scale expression…….....85

5.3.3. Cell lysis……...86

5.3.4. Preparation of Ni-NTA and glutathione agarose columns……86

5.3.5. Ni-NTA affinity chromatography……...……..87

5.3.6. Glutathione affinity chromatography……...87

5.3.7. Desalting (Buffer exchange)……...….87

5.3.8. Protein concentration and storage……..……..88

5.4. SDS-PAGE and Western blotting analysis……...……88

5.4.1. SDS-PAGE…….……88

5.4.2. Western blotting analysis……...……..89

5.4.3. Detection of His-tagged proteins…….……89

5.4.4. Detection of GST-tagged proteins…….……...89

5.5. Immobilised Arf-Effector interaction assays…….……..90

5.5.1. Nucleotide exchange and intrinsic tryptophan fluorescence…….……90

5.5.2. Ni-NTA immobilised Arf-effector-GST interaction assay…….….90

5.5.3. Glutathione immobilised effector-Arf-GST interaction assay……...……..91

5.6. Coupled bioluminescence assay……...……91

5.6.1. ATP detection using luciferase……91

5.6.2. NDPK-luciferase coupled reaction…….……92

5.6.3. Arf-NDPK coupled bioluminescence assay…….……92

5.6.3.1. 1:1 Arf-NDPK mixture to ATP detection reagent……...92

5.6.3.2. 2:1 Arf-NDPK mixture to ATP detection reagent……...93

5.7. Statistical analysis……93

Appendix……...……**94**

References……....……**99**

List of Abbreviations

ACAP	ArfGAP with coiled-coil, ANK repeat, and PH domains
ADAP	ArfGAP with dual PH domains
AGAP	ArfGAP with GLD, ANK repeat, and PH domains
AGFG	Nucleoporin-related Arf-GAP domain and FG repeat-containing protein
ALPS	Amphipathic lipid packing sensor
ANK	Ankyrin
AP	Adaptor protein
ARAP	ArfGAP with Rho GAP, ANK repeat, and PH domains
Arf	ADP-ribosylation factor
ARNO	ARF nucleotide-binding site opener
ASAP	ArfGAP with SH3, ANK repeat, and PH domains

BAR	Bin/amphiphysin/Rvs
bFGF	Basic fibroblast growth factor
BIG	Brefeldin-A-inhibited guanine nucleotide-exchange factor
BRAG	Brefeldin-A resistant Arf GEF
CDE	Clathrin-dependent endocytosis
CIE	Clathrin-independent endocytosis
COPI	Coat protein complex I
CR3	Compliment receptor 3
DCB	Dimerization and cyclophilin binding
DV	Digestive vacuole
ECM	Extracellular matrix
EFA6	Exchange factor for Arf6
EGF	Epidermal growth factor
EH	Eps15 homology
EHD1	EH domain-containing protein 1
ELMO	Engulfment and cell motility
EPS15	Epidermal growth factor receptor substrate 15
ERC	Endocytic recycling compartment
ERK	Extracellular signal-regulated kinase
EV	Extracellular vesicle
FG	Phenylalanine and glycine
FIP3/4	Rab11 family interacting protein 3/4
GAP	GTPase-activating protein
GBF	Golgi Brefeldin-A-resistance factor
GDP	Guanine diphosphate
GEF	Guanine nucleotide-exchange factor

GGA	Golgi-localised gamma adaptin ear-containing ARF-binding protein
GIT	G protein-coupled receptor kinase-interacting Arf GAP
GLD	G protein-like domain
GSH	Glutathione
GSSG	Glutathione disulfide
GTP	Guanine triphosphate
HCCU	Host cell cytosol uptake
HDS	Homology downstream of Sec7
HGF	Hepatocyte growth factor
iRBC	Infected red blood cell
JIP3/4	JNK-interacting protein 3/4
JNK	c-Jun NH_2-terminal kinase
LZII	Leucine zipper II
MHC	Major histocompatibility complex
MKLP1	Mitotic kinesin-like protein 1
MT1-MMP	Membrane-tethered membrane type 1 – matrix metalloproteinase
MTOC	Microtubule organising centre
Mw	Molecular weight
NMR	Nuclear magnetic resonance
OCRL	OculoCerebroRenal syndrome of Lowe
PA	Phosphatidic acid
PBS	Phosphate-buffered saline
PH	Pleckstrin homology
pI	Isoelectric point
PI3K	Phosphatidylinositol 3-kinase
PI3P	Phosphatidylinositol 3-phoshphate

PIP_2	Phosphatidylinositol 4,5-bisphosphate
PIP_3	Phosphatidylinositol 3,4,5-trisphosphate
PIP5K	Phosphatidylinositol 4-phosphate 5-kinase
PLD	Phospholipase D
PVM	Parasitophorous vacuole membrane
RBC	Red blood cell
scFv	Single chain variable antibody
SH3	SRC homology 3
SMAP	Small Arf GTPase activating protein
SNARE	Soluble *N*-ethylmaleimide-sensitive-factor protein receptor
TBS	Tris-buffered saline
TfnR	Iron-bound transferrin receptor
UBP1	Upstream binding protein 1
uRBC	Uninfected red blood cell
VEGF	Vascular endothelial growth factor
VPS45	Vacuolar protein sorting-associated protein 45
WASP	Wiskott–Aldrich Syndrome protein
WAVE	WASP family verprolin homologous protein
WRC	WAVE regulatory complex

List of Figures and Tables

Figures

Figure 1: Arf GTPase cycle

Figure 2: Plasmodium lifecycle

Figure 3: Analytical scale optimisation of His-tagged *Pf*Arf6 production

Figure 4: Ni-NTA affinity purification of His-tagged Arf GTPases

Figure 5: Diagnostic restriction digestion and analytical scale expression of His-tagged NDPK

Figure 6: Analytical scale optimisation of His-tagged ArfGAP1^{GAP} production

Figure 7: Ni-NTA purification of His-tagged NDPK, ARNO^{Sec7}, and ArfGAP1^{GAP}

Figure 8: Glutathione agarose affinity purification of GST-tagged GGA3^{GAT} and JIP4^{LZII}

Figure 9: Schematic diagram representing the Ni-NTA immobilised Arf-effector-GST interaction assay principle

Figure 10: Schematic diagram representing the glutathione immobilised effector-Arf-GST interaction assay principle

Figure 11: Using tryptophan fluorescence to detect EDTA-mediated nucleotide exchange of *Hs*Arf GTPases

Figure 12: Using tryptophan fluorescence to detect EDTA-mediated nucleotide exchange of *Pf*Arf GTPases

Figure 13: Ni-NTA immobilised Arf-effector-GST interaction assay

Figure 14: Glutathione immobilised effector-Arf-GST interaction assay

Figure 15: Schematic diagram representing the Arf-NDPK coupled bioluminescence assay principle

Figure 16: ATP standard curve (1 nM-1 μM) and use of NDPK to detect GTP

Figure 17: Optimisation of GTP-to-ATP conversion activity of NDPK

Figure 18: Initial attempt to detect regulator mediated *Hs*Arf1 activity using NDPK

Figure 19: Detection of regulator mediated *Hs*Arf1 GTPase activity

Figure 20: Detection of *Hs*Arf6 and *Pf*Arf1 GTPase activity, using *Hs*Arf1 regulators

Figure A1: Sequence alignment of truncated human and malarial Arf-GTPases

Figure A2: Using tryptophan fluorescence to help determine more favourable nucleotide exchange conditions for *Pf*Arf6

Figure A3: Initial attempt to detect regulator mediated *Hs*Arf1 activity using NDPK and an adjusted assay buffer

Figure A4: Detection of regulator mediated *Hs*Arf1 GTPase activity using an adjusted assay buffer

Figure A5: Detection of regulator mediated *Hs*Arf6 and *Pf*Arf1 GTPase activity using *Hs*Arf1 regulators in an adjusted assay buffer

Tables

Table I: Arf-GTPase protein interactions

Table II: Regulators and effectors associated with Arf6-specific cellular functions

Table III: Arf6 GTPase regulators and effectors associated with cancer development

Chapter 1: Literature review

1.1. Arf-GTPases

1.1.1. Classification and structure

ADP-ribosylation factors (Arfs) are a family of low molecular mass (~ 20 kDa) proteins of the Ras superfamily of small GTPases and are ubiquitously expressed in all eukaryotes (Li *et al*., 2004). They were originally named for their ability to function as cofactors for cholera-toxin-mediated ADP-ribosylation of the α-subunit of heterotrimeric G proteins (Kahn & Gilman, 1984; Kahn & Gilman, 1986). The six mammalian Arf proteins have been assigned into three classes based on sequence identity (Kahn *et al*., 2006). Class I Arfs (Arf1, Arf2, and Arf3) regulate the assembly of coat protein onto budding vesicles in the secretory pathway (Manolea *et al*., 2010). Class II Arfs (Arf4 and Arf5) are the least studied and share common/redundant functions with class I Arfs (Liang & Kornfeld, 1998; Volpicelli-Daley *et al*., 2005). The only class III Arf (Arf6), regulates endosomal membrane traffic and modifies the actin cytoskeleton at the cell periphery (D'Souza-Schorey *et al*., 1995; Radhakrishna & Donaldson, 1997; Altschuler *et al*., 1999). Arf1 and Arf6 are the most distinct Arf isoforms, albeit sharing ~70 % sequence identity, where Arf1 is mostly found at the Golgi apparatus and Arf6 at the plasma membrane (Chavrier & Goud, 1999; Peters *et al*., 1995). As with all other Ras GTPases, Arfs cycle between ('inactive') GDP- and ('active') GTP-bound conformations (D'Souza-Schorey & Chavrier, 2006). The regulation of these different nucleotide bound states is mediated by guanine nucleotide-exchange factors (GEFs) and GTPase-activating proteins (GAPs). GEFs catalyse the exchange of bound GDP for GTP, and GAPs catalyse the hydrolysis of bound GTP to GDP (Goldberg, 1998; Jackson & Casanova, 2000). In their GTP bound conformation, Arfs bind to specific effector proteins (D'Souza-Schorey & Chavrier, 2006).

All Arf family members share a canonical G domain, with critical switch I and switch II regions. Arfs also contain an interswitch region between switch I and switch II, unlike other Ras superfamily GTPases (Amor *et al*., 1994; Goldberg, 1998; Ménétrey *et al*., 2000). Arf GTPases are also unique in being post-translationally modified at their N-terminus, specifically their N-terminal glycine is myristoylated. This myristoylated N-terminal extension forms an ordered α-helix which inserts into lipid membranes upon activation brought on by the interswitch region communicating with the N-terminus on the opposite end of the protein (Amor *et al*., 1994; Yu *et al*., 2012). In the GDP-bound form the β2-β3 strand of the interswitch region retract, forming a pocket which accommodates the N-terminal extension (Amor *et al*., 1994; Ménétrey *et al*., 2000). In this retracted conformation a conserved aspartate residue upstream

of switch II mimics the charges of the GTP γ-phosphate, preventing GTP binding. When GDP is replaced by GTP, the interswitch region changes its conformation (the 'interswitch toggle') simultaneously allowing GTP to bind the nucleotide biding site and releasing the N-terminal helix for integration into the membrane (Goldberg, 1998; Pasqualato *et al*., 2001). Positive charges on the main Arf domain and the linker connecting it to the N-terminal helix facilitate lipid binding by interacting with their negatively charge phosphate groups (Liu *et al*., 2010). Nuclear magnetic resonance (NMR) studies have shown that the main Arf domain has a "flat" side that associates with the membrane (Liu *et al*., 2010). This association with membranes restricts the functions of these small GTPases to specific cellular locations.

1.1.2. Activity cycle

1.1.2.1. GTP/GDP cycling

In the cytosol 'inactive' Arf (Arf-GDP) is activated when a GEF catalyses the exchange of bound GDP for GTP, allowing membrane association. The 'active' membrane bound Arf (Arf-GTP) binds effector proteins to propagate signals. When a GAP stimulates the hydrolysis of the bound GTP to GDP and Pi, signal transduction is terminated and the GDP-bound Arf dissociates from the effector protein and the membrane. By associating with membranes, Arfs generate positive membrane curvature. This leads to further recruitment of Arfs as well as regulators or effectors (Lundmark *et al*., 2008). Arfs interact with downstream effector proteins in the GTP-bound form to propagate a signal (D'Souza-Schorey & Chavrier, 2006).

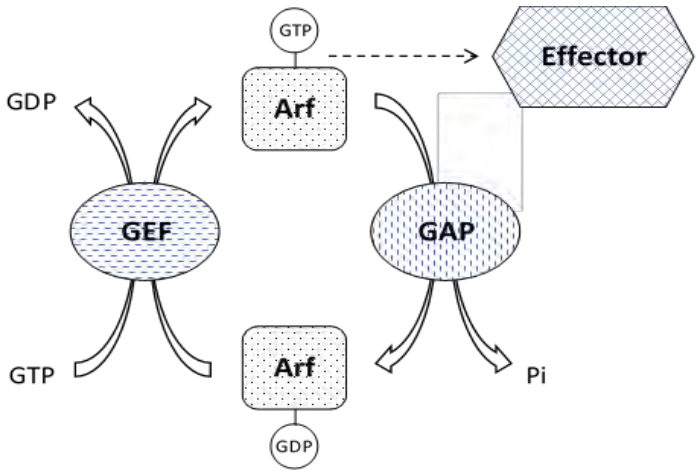

Figure 1: Arf-GTPase activity cycle. GEF = guanine nucleotide exchange factor; GAP = GTPase activating protein.

1.1.2.2. Arf GEFs

Nucleotide exchange of GDP by GTP is catalysed by GEFs (Goldberg, 1998). All GEFs share a canonical catalytic Sec7 domain of ~ 200 amino acids involved in inducing nucleotide exchange, with different GEF isoforms having unique regulatory functions (Chardin *et al*., 1996; Peyroche *et al*., 1996; Jackson & Casanova, 2000). A glutamic finger motif within the Sec7 domain is inserted into the nucleotide binding site, where it displaces the GDP phosphate groups, prompting GDP dissociation and a transient nucleotide-free intermediate (Beraud-Dufour *et al*., 1998; Renault *et al*., 2003). As the cellular concentration of GTP is about ten times that of GDP, GTP rapidly occupies the Arf nucleotide-free pocket (Goldberg, 1998). The human genome encodes for 15 GEFs, assigned to six families based on sequence identity, domain organisation, and phylogenetic analysis. The six human GEF families fall into two groups distinguished molecular weight (Mw) below or above 200 kDa (**Table I**). Low Mw GEFs include cytohesins, EFA6 and BRAG, while high Mw GEFs include BIG and GBF (Casanova, 2007; Gillingham & Munro, 2007; Cherfils & Chardin, 1999).

The GEF Sec7 domain displaces the Arf N-terminal amphipathic extension, activating the 'interswitch toggle' to stimulate membrane binding of Arf-GDP before GDP is exchanged for GTP (Antonny *et al*., 1997; Renault *et al*., 2003). The low Mw GEFs (cytohesin, EFA6, and BRAG) function mainly along endosomal and plasma membranes. They have a pleckstrin homology (PH) domain, C-terminal of the Sec7 domain, involved in membrane binding and cell orientation (Casanova, 2007; Frank *et al*., 1998; Ogasawara *et al*., 2000; Sakagami, 2008). The PH domain of cytohesins specifically recognise phosphatidylinositol 4,5-bisphasphate (PIP_2) and phosphatidylinositol 3,4,5-triphosphate (PIP_3), and blocks the Sec7 domain (DiNitto *et al*., 2003; Cronin *et al*., 2004; Li *et al*., 2012; Hiester & Santy, 2013). The PH domain of BRAGs bind several anionic lipids but does not block the Sec7 domain. Cytohesin activity positively correlates with Arf-GTP levels, whereas this is not observed for BRAG activity (Aizel *et al*., 2013; Jian *et al*., 2012; Karandur *et al*., 2017). The PH domain and a C-terminal polybasic region of EFA6s function together to target membranes, and Arf-GTP levels inhibit EFA6 activity in negative-feedback loop (Padovani *et al*., 2014). Cytohesins, BRAGs and EFA6s serve to regulate Arf6 more strongly than other Arf family members. They typically localise near plasma and endosomal membranes (Casanova, 2007; Hongu & Kanaho, 2014). Unlike low Mw GEFs, high Mw GEFs (BIG, GBF) function mainly at endosomal and secretory membranes, and associate with membranes through both their "dimerization and cyclophilin binding" (DCB) and "homology downstream of Sec7" (HDS) domains (Galindo *et al*., 2016; Meissner *et al*., 2018; Quilty *et al*., 2018; Wright *et al*., 2014).

1.1.2.3. Arf GAPs

All Arf GAPs share canonical GAP domains that hydrolyse Arf-bound GTP, returning Arf to the inactive (Arf-GDP) state (Kahn *et al*., 2008). Within the GAP domain is an 'arginine finger' motif containing a catalytic arginine residue (Ahmadian *et al*., 1997; Scheffzek *et al*., 1998). This 'arginine finger' is inserted into the nucleotide binding site and stabilises the transition state of the hydrolysis reaction, which requires a conserved glutamine residue in switch II (Cherfils & Zeghouf, 2013; Ismail *et al*., 2010). Currently, there are 31 genes encoding for proteins containing a GAP domain, assigned to 10 families based on sequence identity and domain structure similarity (**Table I**) (Kahn *et al*., 2008). These families are ArfGAP1, ArfGAP2/3, ADAP, GIT, SMAP, AGFG, ASAP, ACAP, AGAP, and ARAP. Membrane association of GAPs allosterically controls GAP activity as well as localises their activity to specific subcellular locations. The four GAP subfamilies ASAP, ACAP, AGAP, and ARAP, which contain 21 of the 31 known GAPS, contain a N-terminal PH domain often associated with membrane recruitment (Campa *et al*., 2009; Jian *et al*., 2015; Kam *et al*., 2000; Nie *et al*., 2002). The "Bin/amphiphysin/Rvs" (BAR) domain in ASAP and ACAP presumably function as membrane curvature sensors (Gallop & McMahon, 2005; Jian *et al*., 2009). Furthermore, the tandem BAR-PH domains function to inhibit ASAP1 GAP activity, whereby the N-terminal extension of the BAR domain interacts with the PH and GAP domain to affect enzyme activity (Jian *et al*., 2009).

ArfGAP1, the most widely studied Arf GAP, contains an "amphipathic lipid packing sensor" (ALPS) motif, which forms as an amphipathic helix when recognising and binding curved lipid membranes (Drin *et al*., 2007). The amphipathic lipid packing sensor (ALPS) motif seems to regulate GAP activity, as the activity of ArfGAP1 increases with membrane curvature, suggesting a feedback loop which controls the direct timing of GAP activity during vesicle budding (Bigay *et al*., 2005). In addition to their core roles in deactivating Arfs by stimulating GTP hydrolysis, Arf GAPs are involved in a number of cellular processes, with most of the studies centred around coat/adaptor recruitment to membranes (Gillingham & Munro, 2007; Weimer *et al*., 2008; Spang *et al*., 2010; Shiba & Randazzo, 2012). Arf GAPs are also involved in the regulation of the actin cytoskeleton and integrin adhesion complexes (Hoefen & Berk, 2006; Randazzo *et al*., 2007; Zhou *et al*., 2016; Vitali *et al*., 2017). Specific GAPs associated with Arf6 functions are GITs, SMAPs, ACAPs, and ARAPs, which are involved in endocytic vesicle budding, actin remodelling, and focal adhesion formation (Chen *et al*., 2014; Donaldson & Jackson, 2011; Huang & Sidney, 2010; Sangar *et al*., 2013).

1.1.2.4. Effectors

Of the known Arf GTPase effectors, most are essential components of membrane trafficking within the cell (**Table I**). The best-characterised Arf effectors are coat adaptor proteins (APs), as well as the coat proteins themselves, such as "golgi-localized gamma adaptin ear-containing ARF-binding proteins" (GGAs) and coat protein complex I (COPI) (Serafini *et al*., 1991; Stamnes & Rothman, 1993; West *et al*., 1997; Boman *et al*., 2000; Dell'Angelica *et al*., 2000; Donaldson & Jackson, 2011). All Arfs are also able to activate the lipid modifying enzymes phospholipase D (PLD) and phosphatidylinositol 4-phosphate 5-kinase (PIP5K), which generate phosphatidic acid (PA) and phosphatidyl 4-5-bisphosphate (PIP2), respectively. These lipid metabolites mediate the recruitment of proteins to membranes and assist in membrane curvature dynamics (Brown *et al*., 1993; Cockcroft *et al*., 1994; Honda *et al*., 1999; Jones *et al*., 2000). The majority of known effectors, which differ widely in structure, size and shape, bind Arfs via an invariant triad of aromatic residues, in both the switch and interswitch regions of Arf (Khan & Ménétrey, 2013). In their GDP-bound form the conformations of Arf switch regions are different, allowing effectors to differentiate between inactive Arf1 and Arf6 isoforms. However, in the GTP-bound form, there are no structural differences between Arf1 and Arf6 switch regions (Pasqualato *et al*., 2001). This, coupled with the fact that the switch region sequences are highly conserved between Arfs, raises the question about regulator and effector specificity toward Arfs. Either specific sequences outside of the switch regions or the subcellular localisations of Arfs, or a combination of both, dictate regulator and effector specificity toward Arf isoforms (Peters *et al*., 1995; Donaldson & Jackson, 2000; Kawasaki *et al*., 2005). Just as with GEFs and GAPs, the membrane plays a role in Arf-GTP and effector interactions, whereby both the N-terminal extension of Arf and regions in the effector simultaneously interact with membranes (Isabet *et al*., 2009; Malaby *et al*., 2013; Ren *et al*., 2013; Shiba *et al*., 2003). Arf-effector complexes keep the GAP binding site on Arf-GTP open, suggesting possible ternary Arf-effector-GAP complexes. This has been demonstrated for Arf1 bound to COPI and ArfGAP1, where binding of ArfGAP1 to Arf1-COPI increases GAP activity and induces the disassembly of the coat complex on curved membranes (Dodonova *et al*., 2017; Yu *et al*., 2012). Arf GAPs also function as effectors and not merely as inactivators of Arf as they also propagate Arf signals by driving coat assembly and cargo selection during vesicle formation (Bai *et al*., 2011; Gillingham & Munro, 2007; Lee *et al*., 2005; Yang *et al*., 2002).

Table I: Arf-GTPase protein interactions. GEFs have a greater affinity for inactive Arf (Arf-GDP), whereas GAPs and effector proteins have a higher affinity for active Arf (Arf-GTP). ACAP = ArfGAP with coiled-coil, ANK repeat, and PH domains; ADAP = ArfGAP with dual PH domains; AGAP = ArfGAP with GLD, ANK, and PH domains; AGFG = nucleoporin-related Arf-GAP domain and FG repeat-containing protein; AP = adaptor protein; ARAP = ArfGAP with Rho GAP, ANK repeat, and PH domains; ASAP; ArfGAP with SH3, ANK, and pH domains; BRAG = Brefeldin-A resistant ArfGEF; BIG = Brefeldin-A inhibited guanine nucleotide-exchange factor; EFA6 = exchange factor for Arf6; EPI64 = EBP50-PDZ interactor of 64 kDa; FIP = Rab 11 family interacting protein; GBF = golgi Brefeldin-A resistance factor; GGA = Golgi associated, gamma adaptin ear-containing, ARF binding protein; GIT = G protein-coupled receptor kinase-interacting ArfGAP; JIP = JNK-interacting protein; MKLP = mitotic kinesin-like protein; SMAP = small ArfGTPase activating protein. * = interacts with Arf6 isoform.

Arf-GDP interactors		**Arf-GTP interactors**		
GEFs		**GAPs**		**Effectors**
< 200 kDa	**> 200 kDa**			
*Cytohesins	BIG	*SMAP	*ASAP	Coat proteins (*AP1-3, *GGA1-3, coatomer)
*EFA6	GBF	*GIT	AGAP	*Phospholipid-metabolising enzymes (*PIP5K, *PLD)
*BRAG		*ACAP	ArfGAP1	Arf and Rab GAPs (*FIP3/4, *EPI64B; *arfaptin)
		*ARAP	ArfGAP2/3	Motor/scaffolding proteins (*MKLP1, *JIP3/4)
		*ADAP	AGFG	

1.1.3. Arf6 cellular functions

Arf6 exerts its wide range of functions through a diverse set of effectors. These can be categorised into two main functions, namely 1) endocytosis, and 2) remodelling of the actin cytoskeleton (**Table II**). It activates the lipid modifying enzymes PIP5K and PLD, producing PIP_2 and PA, respectively, where the increased concentration of PA leads to a secondary enhancement of PIP_2 production due to the stimulatory effect of PA on PIP5K (Honda *et al*., 1999; Bach *et al*., 2010). Arf6-mediated increase in PIP_2 concentration is crucial for: clathrin-dependent (CDE) and clathrin-independent endocytosis (CIE), endosomal recycling (fast and slow), as well as actin polymerisation and remodelling of the plasma membrane (Bach *et al*., 2010; D'Souza-Schorey *et al*., 1995; Honda *et al*., 1999; Radhakrishna & Donaldson, 1997; Shome *et al*., 1998; Sugita *et al*., 1999; Toda *et al*., 1999). Tools used to analyse

the functions of Arf6 include: Arf6 silencing/gene disruption, the overexpression of Arf6 or its canonical GAPs/GEFs, as well as overexpression of Arf6 mutants with altered GTP/GDP affinity and GTPase activity (Macia *et al*., 2001; Donaldson, 2003; Donaldson & Jackson, 2011). Arf6 mutants used most frequently include the 'constitutively active' Arf6-Q67L, which binds GTP but lacks GTPase activity, and the 'dominant negative' Arf6-T27N, which has low nucleotide affinity and mimics the GDP-bound state (D'Souza-Schorey *et al*., 1995). However, the low nucleotide affinity of Arf6-T27N destabilises the protein, leading to denaturation and requiring to interpret experimental observations. Arf6-T44N was proposed by Macia *et al*. (2004) as a better alternative, as it has a low binding affinity for GTP but retains near-normal affinity for GDP.

1.1.3.1. Endocytosis

In both CDE and CIE, Arf6-GTP is crucial for downstream transport and recycling of cargo proteins (Montagnac *et al*., 2011). In CDE, the cytoplasmic domains of plasma membrane proteins are recognised specifically by adaptor proteins and recruited into clathrin coated vesicles (Conner & Schmid, 2003; Doherty & McMahon, 2009). Multiple GEFs and GAPs are involved in the Arf6-mediated regulation of CDE, depending on the endocytosed material. Arf6-GTP, activated by dynamin-2 through EFA6B and EFA6D, recruits AP-2 to clathrin-coated pits to regulate transferrin endocytosis, whereas activation of Arf6 through BRAG2 regulates the endocytosis of β1-integrins (Dunphy *et al*., 2006; Okada *et al*., 2015). The GAP SMAP1 regulates transferrin endocytosis by binding specifically to the heavy chain of clathrin as well as Arf6-GTP (Tanabe *et al*., 2005). Rab35 and Arf6 are antagonists of each other and these GTPases are sequentially required for endocytic recycling. In the early stages of CDE, Rab35 GTPase interacts with endocytosed vesicles and recruits "OculoCerebroRenal syndrome of Lowe" (OCRL) (Dambournet *et al*., 2011; Cauvin *et al*., 2016). OCRL hydrolyses PIP_2 to PIP, creating a need for Arf6-mediated PIP_2 production. Arf6-GTP inhibits Rab35 by binding the Rab GAP EPI64B, and conversely, Rab35 inhibits Arf6, by binding the Arf6 GAP ACAP2 (Chesneau *et al*., 2012; Kobayashi & Fukuda, 2012). In CIE, which is much less studied than CDE, particular cargo proteins are first internalised and transported in Arf6-enriched vesicles before being recycled to the plasma membrane (Grant & Donaldson, 2009; Mayor & Pagano, 2007). A class of trafficking motifs in CIE cargo proteins are presumed to prevent internalisation and/or facilitate the Arf6-mediated recycling of these cargo by associating with EFA6 (Gong *et al*., 2007). At the sorting endosome, Arf6-GTP hydrolysis to Arf6-GDP and the removal of PIP_2 are both required for fission of recycling vesicles (Brown *et al*., 2001; Chesneau *et al*., 2012). Rab35 and Arf6 recruit ACAP2 and EPI64B in CIE vesicles as well, suggesting the two act synergistically in the internalisation and sorting of early cargo (Chesneau *et al*., 2012; Dutta & Donaldson, 2015; Kobayashi & Fukuda, 2013)

Accurate and efficient endocytic recycling is crucial for processes such as cell division, cell migration, cell junction formation and maintenance, cell-cell fusion events, neuronal signalling control in learning and memory, as well as cell polarity. The fast and slow recycling of endosomal cargo, from both CDE and CIE pathways to the plasma membrane, is mediated by Arf6 (Grant & Donaldson, 2009). Regardless of the mode of entry into the cell, endocytosed cargo is usually transported to the early/sorting endosome (Maxfield & McGraw, 2004). Fast recycling of cargo involves direct transport from sorting endosomes to the plasma membrane, involving the hydrolysis of Arf6-GTP as well as Rab35-GTP (Kouranti *et al*., 2006). Upon clathrin uncoating, Arf6-GTP binds the scaffolding proteins JIP3 and JIP4, in so doing mediating fast recycling (Montagnac *et al*., 2011). JIP3/4 preferentially bind to the plus-ended motor protein kinesin-1, though Arf6-GTP binding to JIP3/4 causes JIP3/4 to bind to the minus-ended motor protein dynein of the dynactin complex (Kelkar *et al*., 2005). JIP3/4 interaction with Arf6 on endocytic vesicles is crucial for the fast microtubule-mediated recycling of iron-bound transferrin receptor (TfnR), a well-known CDE protein, back to the plasma membrane (Montagnac *et al*., 2011). EFA6 is involved in the redistribution of TfnR from the sorting endosome to the cell periphery (Franco *et al*., 1999).

Whereas the adaptor protein AP-2 localises to the plasma membrane to facilitate CDE, AP-1 as well as AP-3 and AP-4 localise to endomembranes to facilitate the sorting of cargo in the biosynthetic and/or endocytic pathway (Nakatsu & Ohno, 2003). AP-1B localises specifically to recycling endosomes to mediate the sorting of cargo targeted for the plasma membrane (Fölsch, 2005). Arf6 colocalised with TfnR as well as AP-1B on recycling endosomes, suggesting Arf6 directs the membrane recruitment of AP-1B and regulates its function (Shteyn *et al*., 2011). Rab35 is also associated with Arf6- and "Eps15 homology domain-containing protein" (EHD1)-positive tubular recycling endosomes that carry CIE-cargo back to the plasma membrane. Whether Rab35 is a merely a passenger or actively contributes is not known (Walseng *et al*., 2008). Slow recycling of cargo involves transport from sorting endosomes to the endocytic recycling compartment (ERC) before shuttling to the plasma membrane via Rab8- and Rab11-dependent recycling pathways (Goldenring, 2015). Both Rab11 and Arf6-GTP bind FIP3 and FIP4, and the Arf6-FIP3-Rab11 complex has been implicated in at least one form of slow endosomal recycling (Fielding *et al*., 2005; Wilson *et al*., 2005; Horgan *et al*., 2010). FIP3 and FIP4 are associated with dynein, ensuring minus-ended transport to the ERC, situated near the microtubule organising centre (MTOC) (Horgan *et al*., 2010). The motor switch from dynein to kinesin-1 is induced by the site-specific phosphorylation of FIP3, reversing the direction of transport toward to the plasma membrane (Simon & Prekeris, 2008; Otani *et al*., 2011). The Arf6 GAPs ACAP1 and ARAP2 are presumed to differentially regulate α5β1-integrin recycling based on localisation. ACAP1 is localised to the ERC and promotes α5β1 recycling, whereas ARAP2 is localised to "adaptor protein containing a PH domain, PTB domain, and leucine zipper motif" (APPL)-containing endosomes and inhibits α5β1 recycling (Chen *et al*., 2014).

1.1.3.2. Actin dynamics

Multiple Arf6 GAPs and effectors are recruited to alter the actin cytoskeleton. During cytokinesis in animal cells the actin cytoskeleton and membrane are dynamically remodelled to promote ingression of the cleavage furrow, forming a narrow cytoplasmic bridge. (Glotzer, 2005). The targeted traffic of secretory and endocytic recycling vesicles has been observed at the ingression furrow and within the intercellular bridge (Schweitzer & D'Souza-Schorey, 2002; Albertson *et al*., 2005). The association of recycling endosomes with, and donation of membrane to, the cleavage furrow depends on Rab11 (Riggs *et al*., 2003). Arf6 has less of an effect on furrowing than Rab11 but contributes to severing the intercellular bridge during abscission (Schweitzer & D'Souza-Schorey, 2002). EFA6 activates Arf6 around the cleavage furrow, but only Arf6 was targeted to the Flemming body (Ueda *et al*., 2013). Binding of Arf6 to FIP3 targets Arf6 to the cleavage furrow at the midbody during late telophase (Schonteich *et al*., 2007). MKLP1 has also been observed in recruiting Arf6 to the cleavage furrow, implying the importance of Arf6 during cytokinesis (Makyio *et al*., 2012). Arf6 interaction with JIP4 is required for trafficking of recycling endosomes in and out of the intercellular bridge as well as for abscission (Montagnac *et al*., 2009).

Phagocytosis is initiated by a foreign particle binding to specific cell surface receptors, such as Fcγ (FCγR) or complement receptors, on professional phagocytes, like neutrophils and macrophages (Egami *et al*., 2011). PIP_2 and PIP5Kα have both been observed at the site of phagocytosis, implying the Arf6-mediated activation of PIP5K is involved (Botelho *et al*., 2000; Coppolino *et al*., 2002). FcγR-mediated phagocytosis requires the normal GDP/GTP cycling of both Arf6 and Arf1, as expression of GTP-cycling-deficient mutants halted phagocytosis (Beemiller *et al*., 2006; Beemiller *et al*., 2010). Upon foreign particle binding, Arf6 is activated immediately, with the peak active Arf6 levels reached within 2 minutes of the initiation of phagocytosis. Localisation of active Arf6 is concentrated at the leading edge of the phagocytic cup, whereas Arf1 appeared more broadly distributed along the phagocytic cup (Beemiller *et al*., 2010). Arf6 activation is regulated by BRAG2 and cytohesin-1 in the initial stages of phagocytosis, as they regulate both FcγR- and "complement receptor 3" (CR3)-mediated phagocytosis. BRAG2 depletion inhibits both FcγR- and CR3-mediated phagocytosis, whereas the depletion of cytohesin-1 enhances CR3-mediated phagocytosis (El Azreq *et al*., 2011; Someya *et al*., 2010). The deactivation of Arf6 during phagocytosis is facilitated by the Arf6 GAPs ASAP2 and ACAP2. ASAP2 regulates FCγR-mediated phagocytosis, whereas ACAP2 regulates FcγR- and CR3-mediated phagocytosis under the control of Rab35. During phagocytosis of IgG-erythrocytes and zymosan, Rab35 is recruited early to the phagocytic cup, where it recruits ACAP2 (Egami *et al*., 2011; Egami *et al*., 2015; Uchida *et al*., 2001). In the amoeba *Dictyostelium discoideum*, the knockout of an OCRL orthologue inhibits phagosome closure, suggesting the importance of Rab35 recruitment

of OCRL to hydrolyse Arf6-induced PIP_2 (Loovers *et al*., 2007). Arf6 has also been linked to autophagy since it colocalises with proteins essential for phagophore or pre-autophagic structure formation. Arf6-mediated activation of PIP5K and PLD contributes to autophagy, as PIP_2 and PA regulates membrane endocytosis and influences membrane delivery to forming phagophores. (Moreau *et al*., 2012).

At the plasma membrane, accumulation of Arf6-GTP and PIP3 leads to the recruitment of ARF nucleotide-binding site opener (ARNO), which both activates Arf1 and further amplifies the activation of Arf6 (Humphreys *et al*., 2013). Both activated Arf1 and Rac1 work together to recruit and activate the "WAVE regulatory complex" (WRC), which in turn activates the Arp2/3 complex leading to actin polymerisation (Koronakis *et al*., 2011; Humphreys *et al*., 2013). The cooperation between Arf1 and Rac1 may be promoted by the binding of ARNO to the dock180/ELMO complex, a GEF for Rac1 (Santy *et al*., 2005). Actin polymerisation and remodelling is further influenced by Arf6, as it both directs the transport of lipid rafts, Rho GTPases, and Rho signalling components to the sites of actin polymerisation, as well as releasing PIP_2, which acts on a number of actin modulating proteins (Boshans *et al*., 2000; Balasubramanian *et al*., 2007; Frank & Hansen, 2008; Myers & Casanova, 2008; Osmani *et al*., 2010). Membrane ruffle formation at the plasma membrane is facilitated by EFA6 as it regulates both Arf6 and Rac1 activation (Franco *et al*., 1999). EFA6-mediated Arf6 activation, together with Arf1, causes WRC-dependent actin polymerisation in *Salmonella enterica* invasion. ADAP1 and ACAP1 facilitate Arf6 deactivation and the formation of the invading ruffle (Davidson *et al*., 2015). ACAP3-mediated Arf6 deactivation is involved in regulating neurite outgrowth in hippocampal cells, in part due to the increased concentration of PIP_2 at the plasma membrane (Miura *et al*., 2016). ARAP2 functions to partially regulate focal adhesion (FA) size by influencing the interactions between Arf6 and Rac1 and RhoA (Chen *et al*., 2013; Yoon *et al*., 2006). Independently of Rac1 activity, Arf6 regulates membrane ruffle formation through binding the effector arfaptin-2, a known Rac-interacting protein (D'Souza-Schorey *et al*., 1997). In epithelial cells, microvillar structure is negatively regulated by EPI64 when in contact with Arf6-GTP (Hanono *et al*., 2006).

Table II: Regulators and effectors associated with Arf6-specific cellular functions. The interaction between Arf6 and specific effectors mediates two main cellular functions: 1) endocytosis as well as 2) remodelling of the actin cytoskeleton. CDE = clathrin-dependent endocytosis; CIE = clathrin-independent endocytosis; FAs = focal adhesions.

Arf6 function		Arf6 GEF	Arf6 GAP	Arf6 effector
Endocytosis and recycling	CDE	EFA6B/D BRAG2	ACAP2 SMAP1	JIP3/4 AP-2 EPI64B PIP5K
	CIE	EFA6	ACAP2	PIP5K
	Fast and slow recycling	EFA6 BRAG2	ARAP2 ACAP1	JIP3/4 AP-1B FIP3/4 PIP5K
Actin dynamics	Cytokinesis	EFA6A		FIP3 JIP4 MKLP1
	Phagocytosis and autophagy	Cytohesin-1 BRAG2	ACAP2 ASAP2	PIP5K PLD
	Actin polymerisation (ruffles, FAs, neurite outgrowth)	EFA6	ADAP1 ACAP1/3 ARAP2 ASAP2	EPI64B PIP5K Arfaptin-2

1.2. Arf6 and disease

1.2.1. Arf6 GTPase association with cancer

1.2.1.1. Cancer development and proliferation

Most malignant tumours metastasise, a complex process involving modified genes and cellular pathways. This allows the intravasation of cancer cells into lymphatic and blood vessels, followed by their extravasation into and colonisation in distal organs away from the initial tumour (Nguyen *et al*., 2009). A series of coordinated membrane processes involving cell adhesion, cytoskeletal remodelling, cell shape changes, and the proteolytic degradation of the extracellular matrix, all control the movement of tumour cells through tissue. All these cellular processes are regulated by Arf6, which controls the subcellular locations of both membrane and cytoplasmic proteins (Schweitzer *et al*., 2011). The signalling from intracellular endosomes appears key to the effect Arf6 has on multiple cellular pathways and cancer types (Hongu *et al*., 2016). Disassembling cell-cell junctions allow cancer cells to detach from their primary tumour lesion sites, initiating local tissue invasion. E-cadherin mediates cell-cell adhesion and helps to maintain the structure and normal function of epithelial cell layers. Its internalisation in epithelial tissue, mediated by Arf6 and NM23-H1, correspondingly triggers the disassembly of the cell-cell junction (Palacios *et al*., 2001; Palacios *et al*., 2002). Most experiments investigating Arf6 in cancer metastasis focused on tissue invasion using various cancer cell lines.

After the disassembly of cell-cell junctions, the extracellular matrix (ECM) barriers have to be degraded in order for cancer cells to invade into the surrounding stroma (Nguyen *et al*., 2009). Arf6 has been implicated in ECM degradation by regulating both the formation of invadopodia and the release of plasma membrane-derived microvesicles (Schweitzer *et al*., 2011). There are many proteins involved in the formation of invadopodia, most notably actin binding proteins, adhesion molecules and membrane-associated proteases (Murphy & Courtneidge, 2011). Arf6 is central in recruiting these molecules to the plasma membrane initiating invadopodia formation. Plasma membrane derived microvesicles, in addition to invadopodia, are also essential for ECM degradation. Cancer cells shed microvesicles by outward budding and fission of the plasma membrane, and microvesicles contain selective proteolytic cargo proteins such as MT1-MMP, MMP2 and MMP9 (Webb *et al*., 2017). The protease "membrane-tethered membrane type 1 – matrix metalloproteinase" (MT1-MMP), vital for invadopodia-induced ECM degradation, is presumed to be transported to the plasma membrane by Arf6 (Hotary *et al*., 2006). The endocytic/exocytic transport of MT1-MMP is mediated by numerous molecules to ensure the constant flow of proteinases at the leading edge. Whereas invadopodia mediate

the degradation of the pericellular ECM, microvesicles degrade the distal ECM to create a pathway for invasion (D'Souza-Schorey & Clancy, 2012). The tumour microenvironment (surrounding blood vessels, immune cells, fibroblasts, signalling molecules and the ECM), is also vital for tumour proliferation in addition to autonomous signalling. Neovascularisation is essential for a tumour to grow beyond a relatively small size, as oxygen and nutrients are supplied from the tumour microenvironment (Carmeliet & Jain, 2011; Baghban *et al*., 2020). Tumour and tumour stroma cells, contained in the tumour microenvironment, secrete angiogenic factors such as vascular "endothelial growth factor" (VEGF), "basic fibroblast growth factor" (bFGF), and "hepatocyte growth factor" HGF, to induce tumour angiogenesis (Montag *et al*., 2009). β1-integrin (a transmembrane glycoprotein), involved in the adhesion of cell-cell and cell-ECM interactions, is essential for tumour angiogenesis (Abraham *et al*., 2008), and Arf6 is involved in its recycling to the plasma membrane (Powelka *et al*., 2003). β-catenin is also internalised under Arf6 control and is involved in two functions: 1) helps fortify cadherin-based adhesion at the plasma membrane and 2) serve as a transcription factor. The Arf6-stimulated release of β-catenin from N-cadherin at the plasma membrane increases the cytosolic pool of free β-catenin (Grossmann *et al*., 2013). Tumour proliferation is promoted when β-catenin is trafficked from the plasma membrane to the nucleus (Yoo *et al*., 2016). Arf6 is involved in the invasion, metastasis, and/or proliferation of various cancers, most notably breast and skin (melanoma) cancer (Donaldson, 2003; Grossmann *et al*., 2013; Marchesin *et al*., 2015; Zhao *et al*., 2015; Yoo *et al*., 2016). Other cancers in the body known to utilise Arf6 include: brain, cervical, colon/colorectal, endometrial, eye, gastric, head and neck, kidney, liver; lung, ovarian, pancreatic, prostate, and tongue cancer (Li *et al*., 2006; Li *et al*., 2009; Menju *et al*., 2011; Rueckert & Haucke, 2011; Attar *et al*., 2012; Hu *et al*., 2012; Sato *et al*., 2012; Hashimoto *et al*., 2016; Matsumoto *et al*., 2016; Otsuka *et al*., 2016; Shan *et al*., 2016; Chabu *et al*., 2017; Chou *et al*., 2017; Liang *et al*., 2017.

1.2.1.2. Arf6 regulator and effector utilisation

Multiple Arf GEFs, GAPs, and effectors, some yet to be observed, are utilised in the development of cancer (**Table III**). The Arf6 GEF BRAG2 has been linked both the invasion and proliferation of a number of cancer cell lines. BRAG2 activation of Arf6, stimulated by "epithelial growth factor" EGF or HGF, disrupts E-cadherin cell-cell contacts and promotes breast and liver carcinoma cell invasion (Hiroi *et al*., 2006; Morishige *et al*., 2007; Xu *et al*., 2015). In glioma and breast cancer cells, BRAG2 and EFA6A activation of Arf6 may regulate microvesicle shedding as they activate the ERK/MAPK pathway (Li *et al*., 2006; Hu *et al*., 2013). BRAG2, along with GRP1 (/cytohesin-3), EFA6B and EFA6D in epithelial tissue, regulate different steps along the HGF-induced β1-integrin recycling

pathway. The release and trafficking of β-catenin to the nucleus is promoted by the activation of Arf6 by BRAG2 in uveal and cutaneous melanoma (Grossmann *et al*., 2013; Yoo *et al*., 2016). SMAP1, a GAP involved in Arf6-mediated receptor endocytosis, localises to adherence junctions and regulates E-cadherin internalisation in epithelial tissue (Tanabe *et al*., 2005; Kon *et al*., 2008). In breast cancer, the deactivation of Arf6 by ARAP3 targets MT1-MMP to late endosomes to be trafficked to invadopodia at the plasma membrane (Loskutov *et al*., 2014). ASAP1 acts as an effector for Arf6 and is upregulated along with Arf6 and BRAG2 to promote pancreatic cancer invasion (Hashimoto *et al*., 2019). EGF-induced activation of Arf6 by BRAG2 also recruits ASAP1, along with cortactin and paxillin, to the sites of invadopodia formation at the plasma membrane in breast cancer (Morishige *et al*., 2007; Sabe *et al*., 2009). JIP4 also interacts with Arf6 in breast cancer, as it recruits dynactin or kinesisn-1 to transport MT1-MMP to the plasma membrane to promote invadopodia formation (Marchesin *et al*., 2015). The Arf6-dependent activation of PLD recruits ERK along the MAPK pathway to activate MLC downstream to facilitate microvesicle budding in melanoma (Muralidharan-Chari *et al*., 2009).

Table III: Arf6 GTPase regulators and effectors associated with cancer development. The coordinated processes of cell adhesion molecule internalisation and extracellular matrix degradation, mediated by Arf6, leads to the eventual movement of tumour cells through tissue. GRP1 (cytohesin-3) = general receptor for phosphoinositides isoform 1. (Carcinoma) = (epithelial cell model used in experimentation).

Arf6 interactors		**Arf6 associated cancer**
GEF	BRAG2	Breast; glioma; (carcinoma); liver; melanoma; pancreas
	EFA6	Breast; (carcinoma); glioma
	GRP1	Carcinoma
GAP	ARAP3	Breast
	SMAP1	(Carcinoma)
Effector	ASAP1	Breast; pancreas
	PLD	Melanoma
	MT1-MMP	Melanoma
	JIP4	Breast

1.2.2. Arf6 GTPase association with malaria

1.2.2.1. Malaria lifecycle

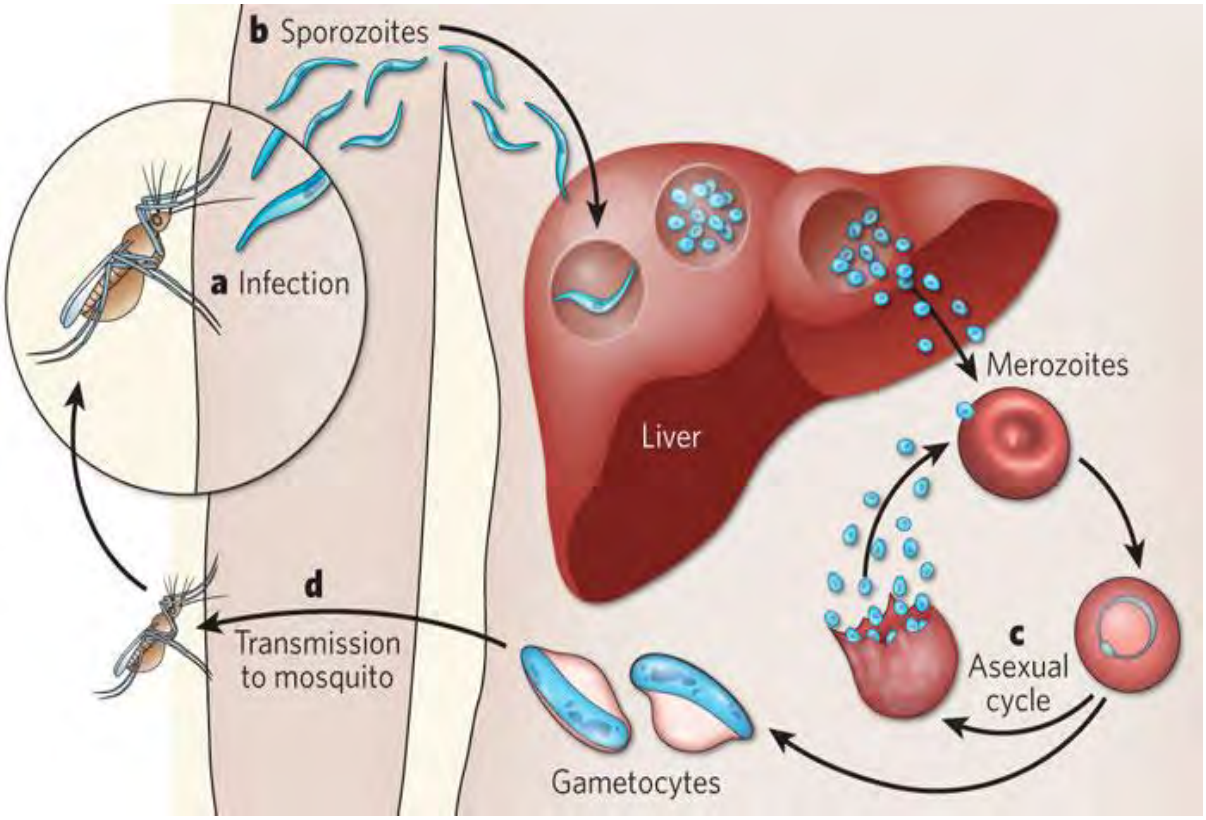

Figure 1: Plasmodium lifecycle. (A) Mosquito bites the human host, injecting sporozoites. (B) Sporozoites infect liver cells, proliferate, and become merozoites, which in turn infect red blood cells. (C) Merozoites proliferate in red blood cells, bursting the cell and allowing infection of new cells. (D) Gametocytes produced from the merozoites, can be transmitted to feeding mosquitoes. Over the course of 10-14 days, the gametocytes in the mosquito will produce sporozoites, which localize to the mosquito's salivary glands. (Image adapted from Michalakis *et al*., 2009).

Malaria is caused by *Plasmodium*, a genus of parasitic protozoans, with *Plasmodium falciparum* as the most virulent strain (Snow *et al*., 2005). The lifecycle of *Plasmodium falciparum* is complex, having both an asexual and sexual stage as well as requiring two hosts (vertebrate and invertebrate) for its completion (**Figure 1**). In humans, two parasitic phases develop during the asexual cycle, namely initial pre-erythrocytic liver-stage parasites, and later erythrocytic stages that cyclically produce asexual merozoites. A sub-population of the erythrocytic stage parasites differentiate into sexual gametocytes. In the female *Anopheles* mosquito (definitive host), the parasite undergoes sexual development to produce sporozoites (Talman *et al*., 2014). When the female *Anopheles* takes a blood meal, it

simultaneously transmits a small number of sporozoites from its salivary glands into the human host bloodstream. the sporozoites invade hepatocytes, after reaching the liver, and undergo multiple rounds of mitotic division to produce thousands of merozoite progeny (Prudêncio *et al*., 2011). After around seven days of hepatocyte development, each infected hepatocyte ruptures and releases up to tens of thousands merozoites into the peripheral bloodstream. Merozoites quickly invade circulating red blood cells (RBCs), initiating the intraerythrocytic asexual replication cycle (Hisaeda *et al*., 2005). Over the course of around 48 hours, the parasites in RBCs progress through ring and trophozoite stages before developing 16 to 32 daughter merozoites in the schizont stage (Lyon & Haynes, 1986; Wickham *et al*., 2003). At this point the RBCs rupture, releasing merozoites into circulation to continue the asexual replication.

During each round of asexual replication, a small subset of merozoites that have invaded RBCs produce sexual progeny, namely male and female gametocytes (Alano, 2007; Liu *et al*., 2011). This small subset of merozoites migrate to the extravascular space in bone marrow, where gametocytes mature and progress through stages I-V of gametocytogenesis in around eight to ten days. The mature male and female gametocytes re-enter the peripheral circulation, where they infect mosquitos (de Niz *et al*., 2018). The male and female gametocytes are ingested by the female *Anopheles* mosquito during its bloodmeal where they rapidly mature into gametes (gametogenesis). Within the mosquito midgut, the male gametocyte undergoes exflagellation, whereby it divides into eight flagellated microgametes, whereas the female gametocyte develops into a singular macrogamete (Sinden *et al*., 2010). A zygote is formed when a microgamete fertilises the macrogamete, which develops into an invasive ookinete after meiosis. The ookinete penetrates the mosquito gut wall and forms an oocyst, which rapidly divides via mitosis to produce several thousand daughter sporozoites. After the oocyst ruptures, the sporozoites migrate to the salivary glands, whereby they can be transmitted back to the human host when the mosquito takes another bloodmeal (Guttery *et al*., 2012). Malaria symptoms in humans are caused during the asexual RBC stages of the parasite (intraerythrocytic cycle).

1.2.2.2. Endocytosis in malaria parasites

Within the RBC, the parasite plasma membrane is not in direct contact with the surrounding host cell, as it is surrounded by an additional membrane the ‘parasitophorous vacuole membrane’ (PVM). The parasite develops within the PVM during this symptomatic phase, and modifies the host RBC to support its growth and survival (Kwiatkowski & Nowak, 1991). In *Plasmodium falciparum*, the only endocytic process to be studied as yet is the uptake of host cell cytosol. Within RBCs, the parasite endocytoses

and digests more than two-thirds of host cell content, primarily haemoglobin (Francis *et al*., 1997). The RBC cytosol is transported to, and digested in, the digestive vacuole (DV), an organelle similar to the mammalian lysosome. Digested haemoglobin produces free heme which is converted into hemozoin as well as amino acids, which function as building blocks for the growing parasite (Sherman, 1977; Hanssen *et al*., 2012). Host cell cytosol uptake (HCCU) also provides additional space for the growing parasite, and maintains an osmotic balance in the infected RBC (iRBC) (Lew *et al*., 2003). The exact mechanisms of how HCCU occurs is still speculative though, as the cellular structures involved have only been partially defined. Host cell cytosol-filled invaginations at the parasite periphery, such as the cytostome and phagotroph, are assumed to initiate HCCU (Bakar *et al*., 2010; Milani *et al*., 2015). The cytostome is a flask-shaped invagination of the parasite plasma membrane and PVM with a narrow (~100 nm) neck, which contains an electron-dense collar (appears as two flanking dots in electron microscope sections) (Liu *et al*., 2019). Phagotrophs, on the other hand, are invaginations much larger than cytostomes, which possess a wider (>200 nm) neck without a collar (Elliott *et al*., 2008; Milani *et al*., 2015). There are two general theories as to how cytostomes or phagotrophs could generate endosomal structures destined for the DV: 1) the 'cytostome maturation model' and 2) the 'cytostome hub model'. In the 'cytostome maturation model', the cytostome itself detaches from the membrane and is transported to the DV. The cytostome then goes through a cycle of initiation, maturation, followed by 'pinching off' (Jonscher *et al*., 2019).

In the 'cytostome hub model' the cytostome remains at the membrane while smaller HCC-filled vesicles pinch off from its body. These vesicles are either delivered directly to the DV or coalesce in larger endosomal structures before reaching the DV (Aikawa *et al*., 1966). Genetic and chemical inhibitor studies resulted in the accumulation of HCC-filled vesicular intermediates, which were not in contact with the host cell, and some were positive for phosphatidylinositol 3-phoshphate (PI3P) (Lazarus *et al*., 2008; Milani *et al*., 2015; Jonscher *et al*., 2019). PI3P, a known endosomal membrane signature is found on the DV, but not if these intermediates are unable to be transported to the DV (Tawk *et al*., 2010). A subset of these accumulated endosomal vesicles also contained smaller internal vesicles, typical of endosomes in other organisms. The trafficking of host cell cytosol to the DV is thus presumably similar to the process of endosomal maturation in model organisms. However, the precise structures involved in HCCU and how exactly these endosomal intermediates reach the DV remain unsolved (Jonscher *et al*., 2019). Until very recently it has been unclear which proteins exactly are involved in HCCU. Inhibition studies though have implicated actin, dynamin, PI3K, and "soluble *N*-ethylmaleimide-sensitive-factor protein receptor" (SNARE) proteins (Smythe *et al*., 2007; Lazarus *et al*., 2008; Vaid *et al*., 2010; Howe *et al*., 2012; Dalal & Klemba, 2015). The parasite ortholog of "vacuolar protein sorting-associated protein 45" (VPS45) is directly involved. Conditional inactivation of VPS45 caused HCC-filled vesicles to accumulate in the parasite, indicating that these vesicles represent transport

intermediates and that possibly more classical endosomal proteins are involved in trafficking internalised HCC to the DV (Jonscher *et al*., 2019).

Other proteins implicated in the early phases of HCCU are "adaptor-related protein complex 2 μ subunit" (AP2μ), a protein resembling "epidermal growth factor receptor substrate 15" (EPS15), Kelch13, and Kelch13 interaction candidates (KIC1-6, 8, 9; and "upstream binding protein 1" (UBP1)), which all form part of the Kelch13 complex (Birnbaum *et al*., 2020). Kelch13 complex inhibition terminated HCC delivery to the DV without HCC-filled vesicles forming, suggesting the Kelch13 complex may play a role in the initial stages of vesicle formation. Kelch13 and its interactors appeared in loci near the DV and near the cytostomes (Birnbaum *et al*., 2017; Birnbaum *et al*., 2020). In model organisms, AP2 and ESP15 are involved together in initiating cargo-dependent CDE (Ma *et al*., 2016), however clathrin was absent from the complex (Birnbaum *et al*., 2020). The unusual initial stages of endocytosis, with regards to AP2 and the lack of clathrin (Mayor *et al*., 2014), may likely be due adaptations of endocytosis to ensure parasite survival while being harboured in a foreign environment surrounded by the PVM. The possible lack of endocytosis-specific receptors may be why the PVM is internalised along with the parasite plasma membrane and that the mechanisms behind parasite endocytosis does not follow canonical endocytosis measures (Mayor *et al*., 2014). The uptake of host cell cytosol may be receptor-independent bulk uptake, though the rate of uptake has to be regulated based on the multiple stages of growth and in response to other factors such as metabolic cues (Mayor *et al*., 2014). Haemoglobin lacks isoleucine, explaining the need for an exogenous supply of this amino acid (Liu *et al*., 2006). Less than 20 % of the haemoglobin-derived amino acids are actually used up by the parasite, surprisingly, and large amounts of amino acids are released from iRBCs (Sherman, 1977; Krugliak *et al*., 2002; Dalal & Klemba, 2015).

Extracellular vesicles (EVs) have been observed to be exchanged between host and parasite, as well as between parasites. These vesicles may help mediate cell-cell communication as well as promote host immune system evasion and the spread virulence factors (Mantel *et al*., 2013). Quantitative and kinetic experiments of EV release showed that iRBCs released ten-fold more than uninfected red blood cells (uRBCs), and the vast majority of EV release occurs just prior to iRBC rupture and release of merozoite progeny (Mantel *et al*., 2013). Time-lapse analysis of parasite development revealed that the mass EV release coincides with the disappearance of Maurer's clefts – membrane bound structures found in the cytoplasm of RBCs infected with maturing parasites (Grüring *et al*., 2011). EVs are also internalised by iRBCs as well, and are transferred to the parasite cytosol, suggesting possible intercellular communication (Mantel *et al*., 2013; Regev-Rudzki *et al*., 2013). The appearance of both PVM and parasite plasma membrane in internalised EVs implies that some phagocytic/endocytic process may be occuring (Luse & Miller, 1971). Since the machinery for these processes are missing from mature RBCs, these pathways are likely mediated by parasite-derived components of iRBCs (Lauer, 1997; Hiller *et al*., 2004; Sargeant *et al*., 2006).

1.2.2.3. Malarial Arf GTPases

A putative malarial Arf1 GTPase (Stafford *et al*., 1996), as well as a single malarial Arf GEF (Baumgartner *et al*., 2001), and Arf GAP (Senkovich & Chattopadhyay, 2004), have already been discovered and subjected to limited characterisation. However, there exists a second putative gene in the *Plasmodium falciparum* genome encoding for an Arf GTPase (Gardner *et al*., 2002). This Arf is suspected by us to be homologous to human Arf6 based on confocal microscopy data revealing *Pf*Arf6-GFP did not conform to the behaviour of typical class I and II Arfs by localising to the Golgi apparatus, but instead at the parasite plasma membrane and peripheral puncta (Swart *et al*., 2020), as well as based on primary structural information (explored further in Chapter 3).

1.3. Overall motivation and objectives

Arf6 plays essential roles in cell division, cell migration, cell spreading, cell polarity, and cell adhesion, due to its ability to affect actin polymerisation, membrane remodelling, internalisation, and recycling. Thus, Arf6 affects health and disease in many ways, and is a viable therapeutic target for drug discovery. A second putative malarial Arf in *P. falciparum* being a homologue of human Arf6 would expand our understanding of the unusual parasitic endocytosis of the red blood cell cytoplasm. With JIP4 as a known human Arf6 effector and GGA3 known to interact with both Arf1 and Arf6, we hypothesise that their Arf binding domains might distinguish between Arf1 and Arf6 homologues, and could thus be used to address the question whether the behaviour (differential effector binding) of the putative malarial Arf protein is more consistent with Arf6 vs. Arf1.

A simple and effective way of monitoring Arf GTPase activity, by a high-throughput method, would allow rapid and cheap screening for potential Arf6 GTPase cycle inhibitors. NDPK can reversibly exchange terminal phosphates between nucleoside diphosphates and triphosphates (NDPs and NTPs), e.g. ADP and GTP, and ATP can be detected using firefly luciferase. By measuring the depletion of GTP (through its conversion to ATP by NDPK) in Arf reactions containing Arf regulators (the Sec7 and GAP domains of ARNO and ArfGAP1), we hypothesise that Arf activity can be detected in a 96-well plate format.

To achieve these aims, the following objectives were pursued using techniques and resources detailed in Chapter 5 (Methods and materials):

- Recombinantly express and purify N-terminally truncated human and malarial Arf1 and Arf6, the GAT and LZII effector binding domains of GGA3 and JIP4, the Sec7 and GAP domains of ARNO and ArfGAP1 and NDPK.
- Load separate mixtures of each Arf isoform with GTP and GDP and confirm ‘active’ and ‘inactive’ conformations by internal tryptophan fluorescence.
- Use colorimetric *in vitro* immobilisation assays in 96-well plates to establish whether GGA3 and JIP4 effector binding domains distinguish between Arf-GTP and Arf-GDP, as well as between Arf1 and Arf6.
- Establish an NDPK-based, *in vitro* coupled-bioluminescence assay to detect Arf GTPase activation of Arf isoforms by ARNO and/or ArfGAP1 regulatory domains (Sec7 and GAP domains, respectively).

Chapter 2: Arf GTPase assay recombinant protein production.

2.1. Introduction

Protein structural or functional studies demand a high-yield recombinant expression system for optimum levels of soluble and active protein. Prokaryotic organisms, such as bacteria, have been widely utilised for the simple and cost-effective production of recombinant proteins (Demain & Vaishnav, 2009). It is due to their fast growth rates and capability of being manipulated, that *E. coli* has become the most popular expression platform (Rosano & Ceccarelli, 2014). Despite a wealth of experience, many proteins still remain difficult to produce in a soluble form using *E. coli*, especially if they need extensive post-transitional modifications (Zhu *et al*., 2012). Variables affecting protein solubility include culture incubation time and temperature, the concentration of the inducer, as well as fusion of the target protein to a soluble protein (Donovan *et al*., 1996). Fusion partners are a simple and common strategy to facilitate the recovery and verification of recombinant proteins (Uhlén *et al*., 1992). Two of the most widely used fusion partners are the "poly-histidine tag" (His-tag) and the "glutathione-S-transferase tag" (GST-tag) (Lichty *et al*., 2005), both of which were used in this study to assist in the purification of the recombinantly expressed truncated Arf GTPase constructs, and the Sec7 and GAP domains (His-tagged), as well as the GAT and second leucine zipper (LZII) effector binding domains (GST-tagged). Histidine tags are used most frequently because their small size reduces the probability of interference with protein structure and function, as well as their simple purification by Ni-NTA affinity chromatography. In this study, the N-terminal lipid anchors of the Arf GTPases were truncated and replaced with a His-tag. GST tags are widely used to increase the solubility of the proteins they are fused to and are also recovered cost-effectively using glutathione affinity chromatography (Bell *et al*., 2013). However, there is no 'one size fits all' set of expression conditions to ensure viable and soluble protein is obtained, as each protein has its own unique and distinct features. In this study various conditions were adjusted in order to express detectable levels of the soluble form of the N-terminally His-tagged Arf constructs and regulator domains (Sec7 and GAP), as well as the N-terminally GST-tagged effector binding domains (GAT and LZII).

2.2. Aims and objectives

To explore whether immobilised effector binding assays and a coupled bioluminescence activity assay could be used to determine the effector binding properties and activity of Arf GTPases, respectively, a panel of recombinant proteins were needed. The required proteins, produced and purified in a soluble form from *E. coli*, were His-tagged *Hs*Arf1, *Hs*Arf6, *Pf*Arf1, *Pf*Arf6, ArfGAP1^{GAP}, ARNO^{Sec7}, and NDPK, as well as GST-tagged GGA3^{GAT} and JIP4^{LZII}. Of these proteins, NDPK had not been produced in our research group before, while *Pf*Arf6 and ArfGAP1^{GAP} produced low yields under standard induction conditions (37°C, 4 incubation,1 mM IPTG) for *E. coli*. To achieve these aims, the following objectives were pursued using techniques and resources detailed in Chapter 5 (Methods and materials):

- Determine sufficient induction conditions for *Pf*Arf6 and ArfGAP1^{GAP}, to generate a sufficient amount of soluble recombinant protein, by varying: incubation time, incubation temperature, and IPTG concentration.
- Determine whether NDPK could be produced under standard induction conditions (37°C, 4 h incubation, 1 mM IPTG) in a soluble conformation.
- Produce all recombinant proteins according to standard induction conditions or by their specific/modified conditions (*Pf*Arf6 and ArfGAP1^{GAP}).
- Purify all His-tagged and GST-tagged recombinant proteins by Ni-NTA and glutathione affinity chromatography, respectively.

2.3. Results

2.3.1. His-tagged Arf-GTPase proteins

An analytical scale expression optimisation of Rosetta (DE3) *E. coli* containing the pET-*Pf*Arf6$^{N\Delta17}$ construct was performed in order to determine the optimal expression conditions to obtain sufficient soluble His-tagged *Pf*Arf6 (truncated *P. falciparum* Arf6 lacking the N-terminal 17 amino acids). Six sets of two analytical scale expression cultures were prepared by inoculating Luria broth, containing kanamycin, with overnight culture. Once exponential growth phase was reached, one expression culture was induced using IPTG (1 mM, unless stated otherwise), while the other was left uninduced. The various incubation conditions once IPTG induction was initiated were: 37°C for 4 h, 30°C for 6 h, 25°C for 12 h, 16°C for 16 h, followed by 16°C for 16 h with 0.4 and 0.1 mM IPTG. Induced and uninduced *E. coli* cells were collected, lysed, and the soluble and insoluble fractions prepared. The soluble and insoluble fractions were analysed by SDS-PAGE, with the approximate sizes of overexpressed proteins of interest being determined by plotting log (Mw) against the retardation factor (Rf) of the molecular weight ladder used (results not shown) (**Figure 3**). His-tagged *Pf*Arf6 had a predicted molecular weight of 20.6 kDa. Overexpressed proteins, ranging from 21 to 21.8 kDa were observed in the induced insoluble fraction lanes and were not present in the uninduced insoluble lanes (**Figure 3 A-F**, lane II vs. UI). By contrast, the induced soluble fraction lanes contained faint protein bands of the expected size, however these could not be confidently distinguished from endogenous *E. coli* proteins migrating in the same position in the uninduced soluble fractions (**Figure 3 A-D**, lane IS vs. US). The exceptions were cultures where the induction had been carried out at 16°C for 16 h with lower IPTG concentrations (0.4 mM and 0.1 mM), which produced a marked improvement in the ratio of soluble to insoluble *Pf*Arf6 protein (**Figure 1 E-F**). The latter condition, namely the induction using 0.1 mM IPTG (**Figure 3F**), was selected for the preparative scale production and purification of *Pf*Arf6.

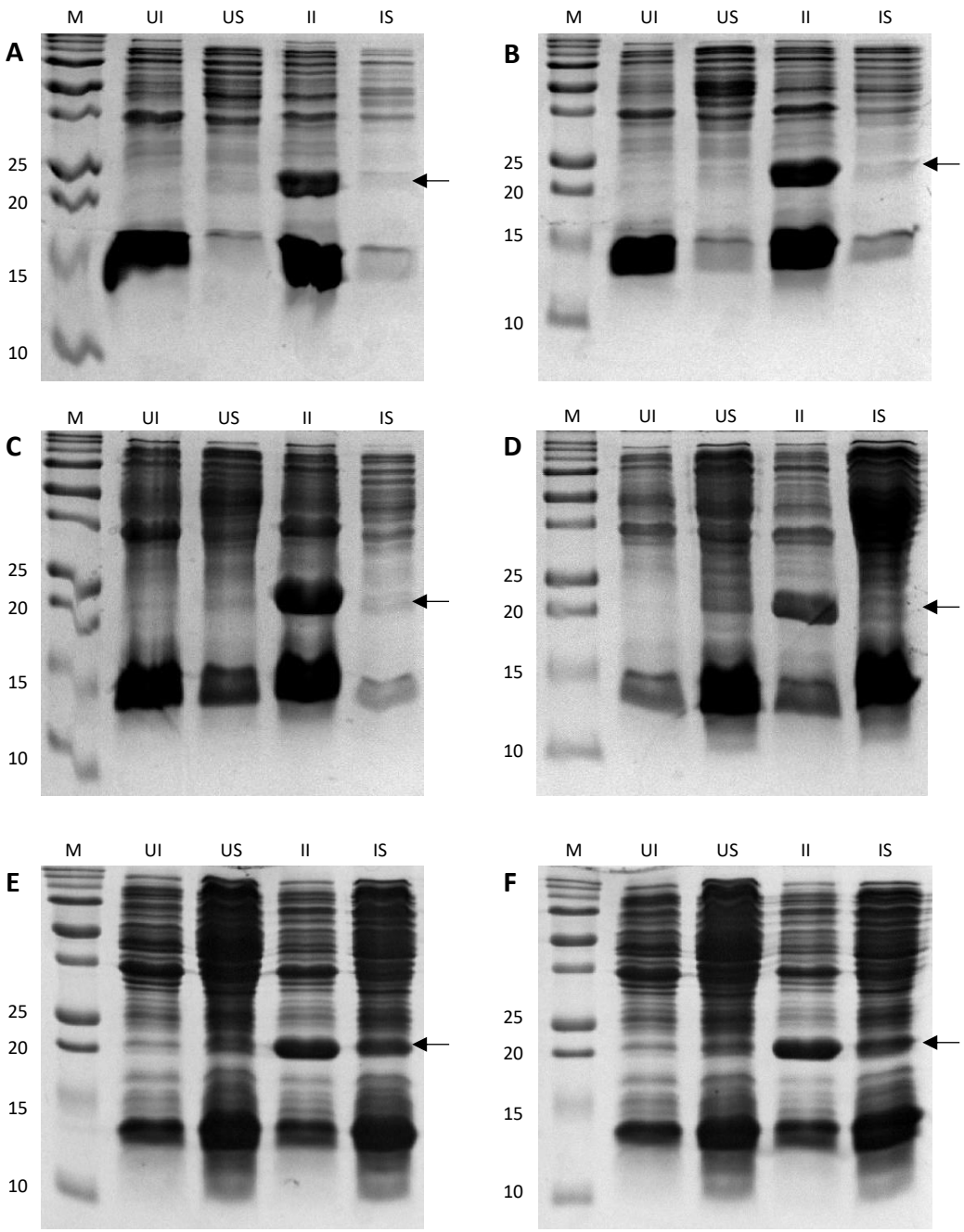

Figure 3: Analytical scale optimisation of His-tagged *Pf*Arf6 production. (Arrows indicate the migration position of *Pf*Arf6). Lanes: **M**: Precision Plus Protein All Blue standard (10 – 250 kDa), **UI**: uninduced insoluble fraction, **US**: uninduced soluble fraction, **II**: induced insoluble fraction, **IS**: induced soluble fraction. Induction conditions: **(A)** 37°C, 4 h; **(B)** 30°C, 6 h; **(C)** 25°C, 12 h; **(D)** 16°C, 16 h**; (E)** 16°C, 6 h, 0.4 mM IPTG; **(F)** 16°C, 6 h, 0.1 mM IPTG. Protein production was conducted at varying incubation conditions, where the soluble and insoluble fraction of 1 mM (unless otherwise stated) IPTG-induced and uninduced *E. coli* were collected after centrifugation. Samples were analysed by SDS-PAGE (15 % gels) and stained with Coomassie.

Preparative scale production of His-tagged *Hs*Arf1, *Hs*Arf6 and *Pf*Arf1 (N-terminally truncated human and malarial Arf1 and human Arf6) were all performed in 500 mL culture under standard induction conditions (37°C, 4 h, 1mM IPTG). His-tagged *Pf*Arf6 expression, however, was performed in 1000 mL culture under its modified conditions (16°C, 16 h, 0.1 mM IPTG). The expression cultures were lysed, the soluble fractions purified using Ni-NTA affinity chromatography and the purified proteins desalted into Arf assay buffer using size exclusion columns. The purification profiles were analysed by SDS-PAGE to visually assess the purity and yield of the desalted protein fractions (**Figure 4,** Top). The predicted sizes for His-tagged *Hs*Arf1, *Hs*Arf6, *Pf*Arf1 and *Pf*Arf6 were 21.1, 21.0, 21.1 and 20.6 kDa, respectively. Clear and distinct bands were observed in the whole soluble fraction (SF), eluate (E) and desalted eluate (DE) lanes. This yielded values of 21.5, 21.2, 22.0 and 21.0 kDa for *Hs*Arf1, *Hs*Arf6, *Pf*Arf1 and *Pf*Arf6, respectively, which agreed with their predicted molecular weights. The approximate sizes of the desalted, purified proteins were determined by plotting log (Mw) against the retardation factor (Rf) of the molecular weight ladder used (results not shown). However, residual *E.coli* proteins were also observed in the eluate and desalted eluate lanes of *Hs*Arf1, *Pf*Arf1 and *Pf*Arf6 (**Figure 4 A, C-D;** Top; lanes E and DE). The purification profile samples, resolved on SDS-PAGE gels, were also transblotted onto nitrocellulose membranes. The membranes were then probed for His-tagged proteins using HisDetector Nickel-HRP followed by an incubation in TMB membrane peroxidase substrate (**Figure 4,** Bottom). Prominent bands were visible in the whole soluble fraction, eluate, and desalted eluate lanes, confirming the successful production and purification of soluble His-tagged *Hs*Arf1, *Hs*Arf6, *Pf*Arf1 and *Pf*Arf6. Less prominent bands were also observed in the eluate and desalted eluate lanes of *Hs*Arf1, *Pf*Arf1 and *Pf*Arf6 (**Figure 4 A, C-D;** Bottom; lanes E and DE). Desalted protein concentrations were determined using the protein $Abs_{260/280nm}$ feature of the NanoDrop 2000/2000c spectrophotometer (Thermo Scientific). Quintuplicate recordings were taken, with Arf assay buffer used as a blank. The concentrations obtained for His-tagged *Hs*Arf1, *Hs*Arf6, *Pf*Arf1 and *Pf*Arf6 were 1.31, 0.93, 1.57 and 0.92 $mg.mL^{-1}$, respectively. This translated to 72.6, 44.2, 74.2 and 44.6 µM purified *Hs*Arf1, *Hs*Arf6, *Pf*Arf1 and *Pf*Arf6, respectively in 50% (v/v) glycerol stocks (6 mL total). The small amount of residual *E.coli* proteins in the final desalted *Hs*Arf1, *Pf*Arf1, and *Pf*Arf6 preparations (**Figure 4A, C–D**), may indicate an overestimation of final concentration.

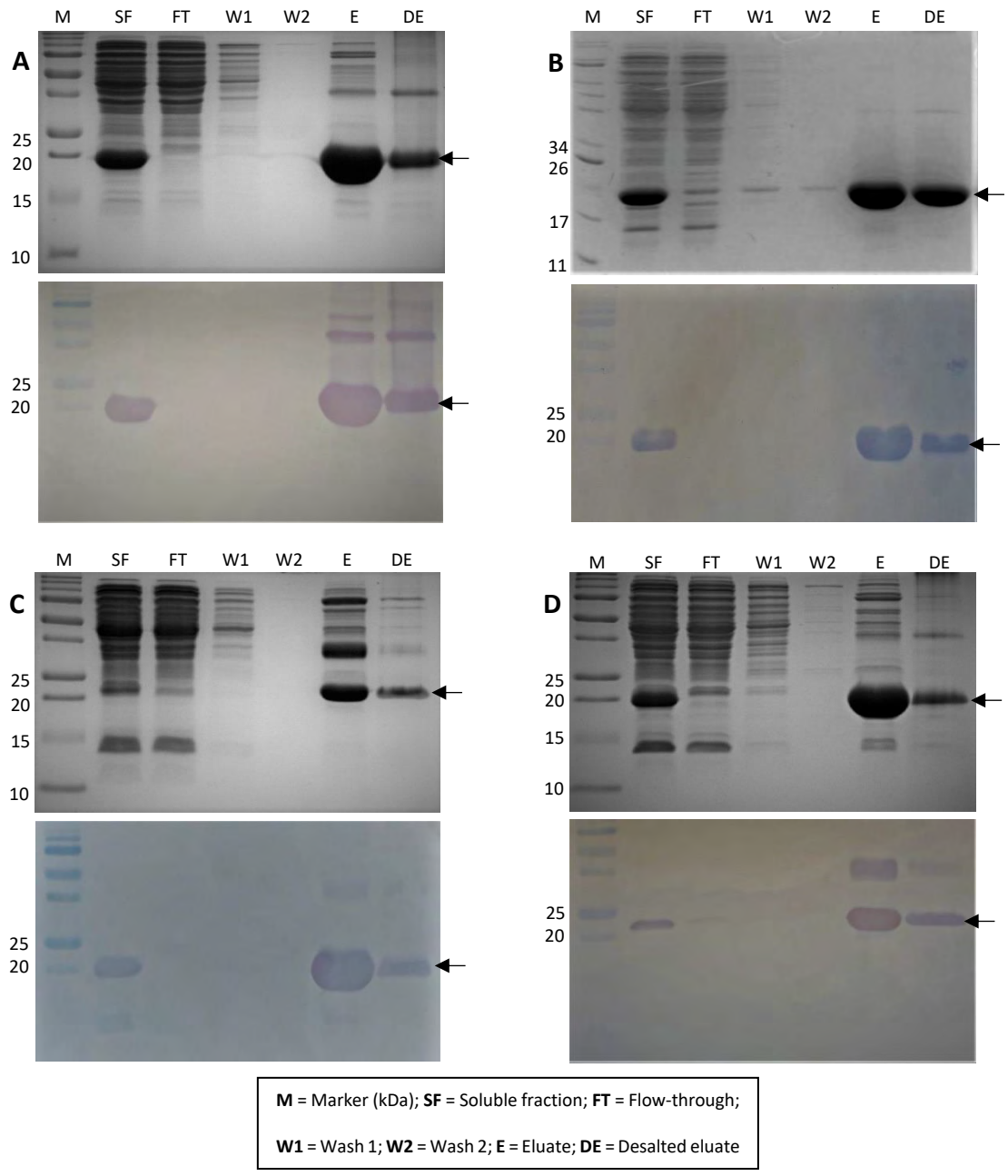

Figure 4: Ni-NTA affinity purification of His-tagged Arf GTPases. (Top: SDS-PAGE, Bottom: Western blot; Arrows indicate the migration position of: **(A)** *Hs*Arf1; **(B)** *Hs*Arf6; **(C)** *Pf*Arf1; and **(D)** *Pf*Arf6.) Induced protein production was conducted at 37°C for 4 h with 1 mM IPTG **(A – C)**; or at 16°C for 16 h with 0.1 mM IPTG **(D)**. Fractions obtained during Ni-NTA affinity chromatography were analysed by SDS-PAGE (15 % gels) and either, Top: stained with Coomassie, or Bottom: transblotted onto nitrocellulose membranes, probed for His-tagged proteins using HisDetector Nickel-HRP substrate, followed by an incubation in TMB membrane peroxidase substrate. Lanes: **M**: Precision plus protein all blue standard (10 – 250 kDa); (**B,** top) Blue Prestained Protein standard, broad range (11 – 250 kDa).

2.3.2.NDPK-bioluminescence assay associated proteins

Both competent XL-10 Gold and T7 lysY/Iq *E. coli* cells were transformed with the pET-NDPK construct (Genscript), then grown overnight in the presence of kanamycin. An alkaline lysis miniprep was performed to isolate recombinant plasmid from the overnight cultures. A diagnostic restriction digest was performed, whereby plasmids were digested with *Nhe*I and *Xho*I, and then analysed by agarose gel electrophoresis, to confirm that transformation was successful. The approximate sizes of restriction digestion products were determined by plotting log (bp) against the relative migration distance plots (Rf) of the 1kb DNA ladder used (results not shown). In theory, digesting the pET-NDPK construct with *Nhe*I and *Xho*I should lead to two linear bands representing the pET-28a plasmid (5369 bp) and the NDPK coding sequence (444 bp). The diagnostic restriction digestion produced two digestion products of approximately 5304 and 377 bp, respectively, correlating with the predicted digestion sizes (**Figure 5A**).

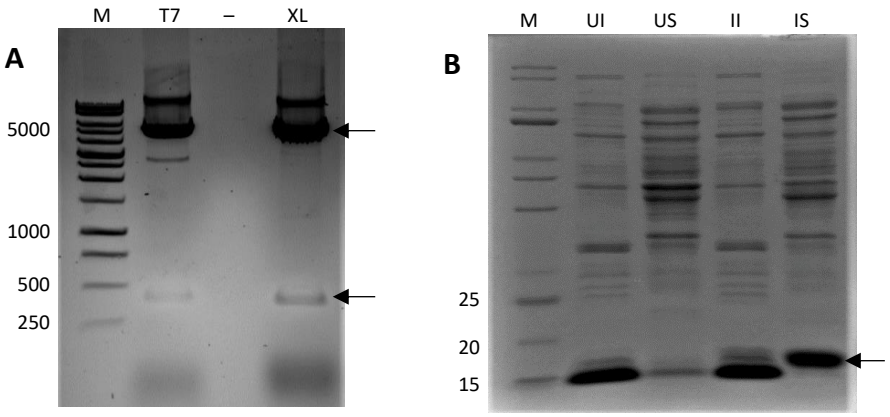

Figure 5: Diagnostic restriction digestion and analytical scale expression of His-tagged NDPK. **(A)** Arrows – top: pET-28a plasmid (5304 bp), bottom: insert (377 bp). Lanes: **M**: 1kb DNA ladder (bp), **T7**: T7 Express lysY/Iq plasmid miniprep, (**–**): empty, **XL**: XL10-Gold miniprep. An alkaline lysis plasmid miniprep was performed on transformed *E. coli* colonies and digested with *Xho*I and *Nhe*I restriction enzymes. Digests were analysed on a 0.8 % agarose gel stained with ethidium bromide. **(B)** Arrow indicates the migration position of NDPK. Lanes: **M**: Unstained protein standard, broad range (10 – 200 kDa), **UI**: uninduced insoluble fraction, **US**: uninduced soluble fraction, **II**: induced insoluble fraction, **IS**: induced soluble fraction. SDS-PAGE analysis of NDPK samples, on a 12 % gel stained with Coomassie. Induced (1 mM IPTG) protein production was conducted at 37°C for 4 h, where the soluble and insoluble fractions were collected after centrifugation.

To determine whether His-tagged NDPK could be produced, and to what degree the recombinant protein was soluble, an analytical scale expression of the transformed T7 lysY/Iq bacteria was performed. Two analytical scale expression cultures were prepared by inoculating Luria broth, containing kanamycin, with an overnight culture. Once exponential growth phase was reached, one expression culture was induced using IPTG (1 mM), while the other was left uninduced. Induced and uninduced *E. coli* cells were collected and lysed, and the soluble and insoluble fractions collected. The soluble and insoluble fractions were then analysed by SDS-PAGE, with the approximate sizes of overexpressed proteins of interest being determined by plotting log (Mw) against the Rf of the molecular weight ladder used (results not shown). His-tagged NDPK had a predicted molecular weight of 17.8 kDa. An overexpressed protein of approximately 16.9 kDa was observed in the induced soluble fraction lane, which was not present in the uninduced soluble lane (**Figure 5B**, lane IS vs .US).

An analytical scale expression optimisation of T7 lysY/Iq *E. coli*, containing the pET-ArfGAP1^{GAP} construct, was performed to determine favourable induction conditions to obtain sufficient soluble His-tagged ArfGAP1^{GAP} (GAP domain of ArfGAP1). Three sets of two analytical scale expression cultures were prepared by inoculating Luria broth, containing kanamycin, with overnight culture. Once exponential growth phase was reached, one expression culture was induced using IPTG (1 mM), while the other was left uninduced. The various incubation conditions once induced were: 37°C for 4 h, 30°C for 6 h, and 25°C for 12 h. Induced and uninduced *E. coli* cells were collected and lysed, and the soluble and insoluble fractions collected. The soluble and insoluble fractions were then analysed by SDS-PAGE, with the approximate sizes of overexpressed proteins of interest being determined by plotting log (Mw) against the Rf of the molecular weight ladder used (results not shown). His-tagged ArfGAP1^{GAP} had a predicted molecular weight of 18.5 kDa. Overexpressed proteins of approximately 17.5, 17.7 and 18.0 kDa respectively, were observed in the induced soluble fraction lanes, which were not present in the uninduced soluble lanes (**Figure 6A – C**, lane IS vs. US). When comparing the intensity of the overexpressed protein band in the induced soluble to the induced insoluble lane, the 6 h induction at 30°C (**Figure 6B**), displayed the greatest ratio of soluble to insoluble protein.

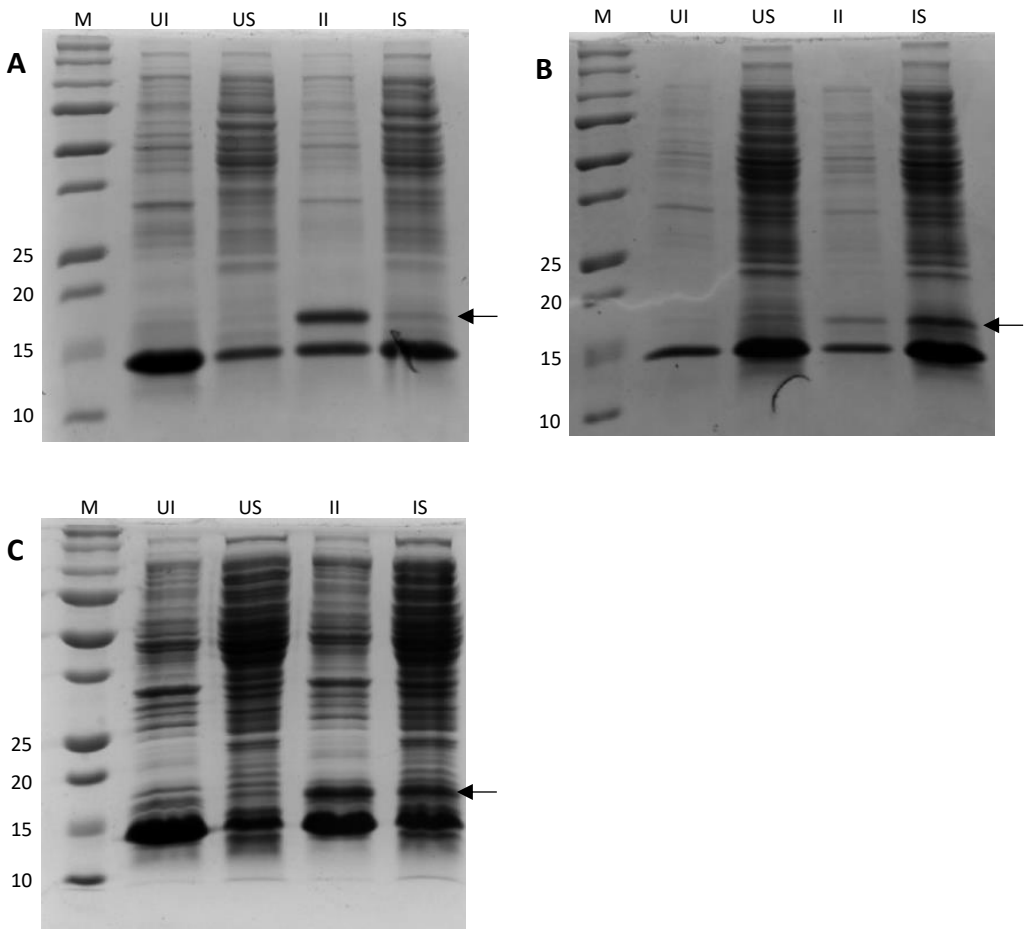

Figure 6: Analytical scale optimisation of His-tagged ArfGAP1^{GAP} production. (Arrows indicate the migration position of ArfGAP1^{GAP}). Lanes: **M**: Precision Plus Protein All Blue standard (10 – 250 kDa), **UI**: uninduced insoluble fraction, **US**: uninduced soluble fraction, **II**: induced insoluble fraction, **IS**: induced soluble fraction. Induction conditions: **(A)** 37°C, 4 h; **(B)** 30°C, 6 h; **(C)** 25°C, 12 h. Protein production was conducted at varying incubation conditions, where the soluble and insoluble fractions of induced (1 mM IPTG) and uninduced *E. coli* were collected after lysis by centrifugation. Samples were analysed by SDS-PAGE (15 % gels) and stained with Coomassie.

Preparative scale expressions of His-tagged NDPK, ARNO^{Sec7} (Sec7 domain of ARNO), and ArfGAP1^{GAP} were all performed in 500 mL culture under standard induction conditions (37°C, 4 h, 1 mM IPTG), except for ArfGAP1^{GAP}, which was performed under its modified conditions (30°C, 6 h, 1 mM IPTG). The expression cultures were lysed, the soluble fractions purified using Ni-NTA affinity chromatography and the purified proteins were desalted into Arf assay buffer (NDPK assay buffer for NDPK). The purification profiles were analysed by SDS-PAGE to visually assess the purity of the desalted protein fractions (**Figure 7,** Top). The predicted sizes for His-tagged NDPK, ARNO^{Sec7} and ArfGAP1^{GAP}, were 17.8, 25.6 and 18.5 kDa, respectively. Clear and distinct bands were observed in the eluate and desalted eluate lanes, corresponding to 17.1, 24.8 and 18.1 kDa, which all agreed with the predicted sizes of His-tagged NDPK, ARNO^{Sec7} and ArfGAP1^{GAP}, respectively. However, residual *E.coli* proteins were also observed in the eluate and desalted eluate lanes of ArfGAP1^{GAP} (**Figure 7C,** Top, lanes E and DE). The purification profile samples, resolved on SDS-PAGE gels, were also transblotted onto nitrocellulose membranes. The membranes were probed for His-tagged proteins using HisDetector Nickel-HRP followed by an incubation in TMB membrane peroxidase substrate (**Figure 7,** Bottom). Prominent bands were visible in the whole soluble fraction, eluate and desalted eluate lanes, confirming the successful production and purification of soluble His-tagged NDPK, ARNO^{Sec7} and ArfGAP1^{GAP}. Less prominent bands were also observed on the nitrocellulose membranes in the eluate and desalted eluate lanes of NDPK, ARNO^{Sec7} and ArfGAP1^{GAP} (**Figure 7,** Bottom, lanes E and DE). Desalted protein concentrations were determined using the protein $Abs_{260/280nm}$ feature of the NanoDrop 2000/2000c spectrophotometer (Thermo Scientific). Quintuplicate recordings were taken, with Arf assay buffer used as a blank (NDPK buffer for NDPK). The concentrations obtained for His-tagged NDPK, ARNO^{Sec7} and ArfGAP1^{GAP} were 0.50, 1.48 and 0.80 $mg.mL^{-1}$, respectively. This translated to 28.1, 57.8 and 43.1 µM purified NDPK, ARNO^{Sec7} and ArfGAP1^{GAP}, respectively in 50% (v/v) glycerol stocks (6 mL total). The small amount of residual *E.coli* proteins in the final desalted NDPK, ARNO^{Sec7} and ArfGAP1^{GAP} preparation (**Figure 7**), may indicate an overestimation of final concentration.

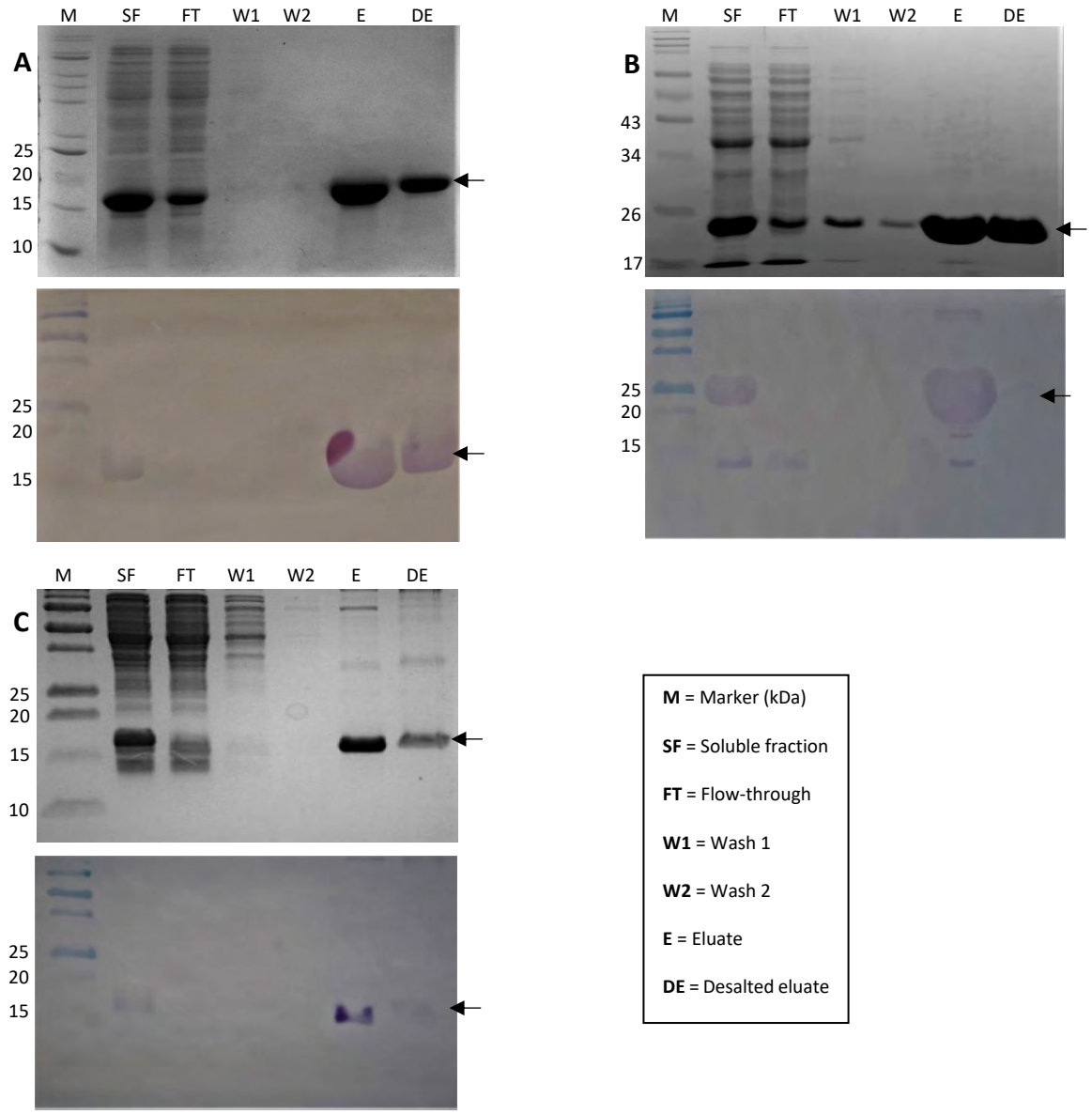

Figure 7: Ni-NTA purification of His-tagged NDPK, ARNO^{Sec7}, and ArfGAP1^{GAP}. (Top: SDS-PAGE, Bottom: Western blot; Arrows indicate the migration position of: **(A)** NDPK; **(B)** ARNO^{Sec7}; and **(C)** ArfGAP1^{GAP}). Induced (1 mM IPTG) protein production was conducted at 37°C for 4 h **(A – B)**; or at 30°C for 6 h **(C)**. Fractions obtained during Ni-NTA affinity chromatography were analysed by SDS-PAGE (15 % gels) and either, Top: stained with Coomassie, or Bottom: transblotted onto nitrocellulose membranes, probed for His-tagged proteins using HisDetector Nickel-HRP substrate, followed by an incubation in TMB membrane peroxidase substrate. Lanes: **M**: Precision plus protein all blue standard (10 – 250 kDa); (**B,** top) Blue Prestained Protein standard, broad range (11 – 250 kDa).

2.3.3. Arf-GTPase effector protein domains for immobilised assays

Preparative scale expression of GST-tagged GGA3^{GAT} (GAT domain of GGA3) and JIP4^{LZII} (leucine zipper II domain of JIP4), in 250 mL culture each, were conducted under standard induction conditions (37°C, 4 h, 1 mM IPTG). The expression cultures were lysed, the soluble fractions purified using glutathione agarose affinity chromatography, and purified proteins desalted into Arf assay buffer. The purification profiles were analysed by SDS-PAGE to visually assess the purity of the desalted protein fractions (**Figure 8,** Top). The predicted sizes of GST-tagged GGA3^{GAT} and JIP4^{LZII}, were 58.0 and 38.8 kDa, respectively. Distinct bands were observed in the eluate and desalted eluate lanes, corresponding to approximately 57 and 38 kDa, respectively. However, residual *E. coli* proteins were also observed in the eluate and desalted eluate lanes of GGA3^{GAT} and JIP4^{LZII} (**Figure 8,** Top, lanes E and DE). The purification profile samples, resolved on SDS-PAGE gels, were also transblotted onto nitrocellulose membranes. The membranes were probed for GST-tagged proteins using anti-GST primary and HRP-conjugated secondary antibodies, followed by an incubation in TMB membrane peroxidase substrate (**Figure 8,** Bottom). Prominent bands were visible in the whole soluble fraction, eluate and desalted eluate lanes, confirming the successful production and purification of soluble GST-tagged GGA3^{GAT} and JIP4^{LZII}. Residual bands were also observed on the nitrocellulose membranes in the eluate and desalted eluate lanes of GGA3^{GAT} and JIP4^{LZII} (**Figure 8,** Bottom, lanes E and DE). Desalted protein concentrations were determined using the protein $Abs_{260/280nm}$ feature of the NanoDrop 2000/2000c spectrophotometer (Thermo Scientific). Quintuplicate recordings were taken, with Arf assay buffer used as a blank. The concentrations obtained for GST-tagged GGA3^{GAT} and JIP4^{LZII}, were 1.82 and 2.35 $mg.mL^{-1}$, respectively. This translated to 15.7 and 30.3 µM purified GGA3^{GAT} and JIP4^{LZII}, respectively in 50 % (v/v) glycerol stocks (6 mL total).

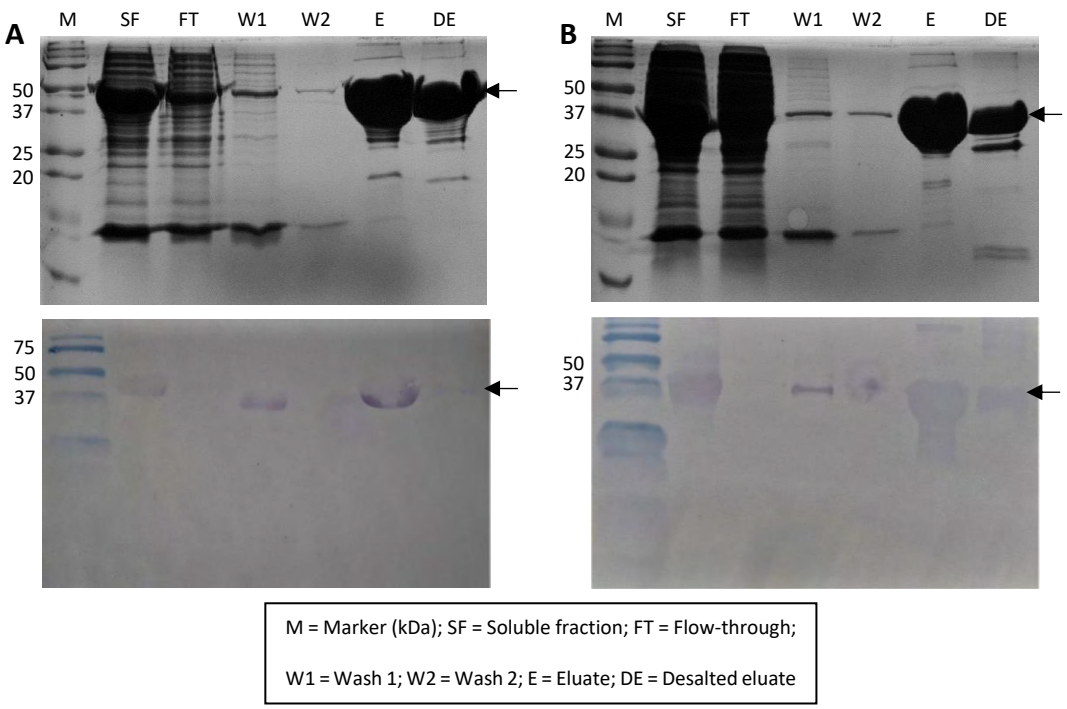

Figure 8: Glutathione agarose affinity purification of GST-tagged $GGA3^{GAT}$ and $JIP4^{LZII}$. (Top: SDS-PAGE, Bottom: Western blot; Arrows indicate the migration position of: **(A)** $GGA3^{GAT}$; and **(B)** $JIP4^{LZII}$). Induced (1 mM IPTG) protein production was conducted at 37°C for 4 h. Fractions obtained during glutathione affinity chromatography were analysed by SDS-PAGE (15 % gels) and either, Top: stained with Coomassie, or Bottom: transblotted onto nitrocellulose membranes, probed for GST-tagged proteins using anti-GST primary and HRP-conjugated secondary antibodies, followed by an incubation in TMB membrane peroxidase substrate. Lanes: **M**: Precision plus protein all blue standard (10 – 250 kDa).

2.4. Discussion

Malarial (*P. falciparum*) parasite gene sequences often prove difficult to recombinantly express in *E. coli*, due to the AT bias of their codons (Berg & Silva, 1997; Baca & Hol, 2000). In order to combat this in a previous *in vivo* study in our research group (expressed in HeLa cells), both the His-tagged *Pf*Arf1 and *Pf*Arf6 codons were optimised for human expression (Genscript, Hong Kong), thus avoiding the AT codon bias. Indeed, a high yield of both *Pf*Arf1 and *Pf*Arf6, particularly under optimised conditions, were expressed from *E. coli*. However, the higher levels of expression under standard induction conditions may have contributed to the higher levels of insoluble *Pf*Arf6, thus prompting the analytical scale expression to determine conditions suitable to yield sufficient soluble *Pf*Arf6, like *Pf*Arf1. Rosano & Ceccarelli (2009), showed that higher levels in protein expressed in Rosetta (DE3) and Tuner (DE3) *E. coli* cells were often met with decreased protein solubility. When recombinantly expressing and purifying a target protein from a bacterial organism, such as *E. coli*, certain expression conditions are altered in order to increase the level of soluble expression. Some of these conditions, which were varied in this study, are the incubation time and temperature after induction, as well as the concentration of the inducer used (Gräslund *et al*., 2008; Shirano & Shibata, 1990; Turner *et al*., 2005). The standard induced incubation temperature and time employed was 37°C and 4 h, respectively, and the standard concentration of IPTG used was 1 mM (Zerbs *et al*., 2014). Under these standard conditions His-tagged *Hs*Arf1, *Hs*Arf6, *Pf*Arf1, NDPK, and ARNO^{Sec7}, as well as GST- tagged GGA3^{GAT} and JIP4^{LZII} displayed soluble expression, whereas the expression conditions of *Pf*Arf6 and ArfGAP1^{GAP} had to be optimised. ArfGAP1^{GAP} displayed soluble expression when the induced incubation temperature was lowered to 30°C and incubation time increased to 6 h. *Pf*Arf6 only displayed any soluble expression when the incubation temperature and time was 16°C and 16 h respectively, with the IPTG concentration lowered ten-fold to 0.1 mM. A high-throughput recombinant expression study performed by Mühlmann *et al*. (2017), explored the effects on expression when the induced incubation time and temperature, as well inducer concentration was varied. They showed that the concentration of IPTG used had a greater effect on expression than the incubation time and temperature. As long the correct IPTG concentrations were used, expression levels were increased even at higher temperatures. This study made use of the Tuner (DE3) *E. coli* strain, lacking lacZY, which allowed for uniform entry of ITPG into the cells and detection of inducer concentration-dependent expression. Based on this *Pf*Arf6 expression could be investigated in future studies at a higher temperature than 16°C, but still with 0.1 mM IPTG, in order to reduce the overall time taken to obtain pure *Pf*Arf6. *Pf*Arf6 could also be expressed using Tuner (DE3) *E. coli* in order to further optimise the expression conditions needed to express higher levels of soluble protein. The initial *Pf*Arf6, expressed and stored in 50 % (v/v) glycerol (in Eppendorf tubes in a -20°C freezer), started to precipitate after 3-5 days, whereas all the other stored purified assay proteins remained in solution upwards of 3 weeks. The addition of ± 1

mg.mL^{-1} BSA may help improve the stability of the stored *Pf*Arf6 (Scopes, 1998), as the concentration of expressed *Pf*Arf6 was just short of 1 mg.mL^{-1}. A possible explanation for the stored (50%) *Pf*Arf6 precipitating may be the difference between the elution buffer pH and the isoelectric point (pI) of *Pf*Arf6. In a study performed by Kirkwood *et al*. (2015), they analysed the pI and pH of around 24000 proteins and observed that acidic proteins (pI < 7) would precipitate above 1 pH unit of their pI's, whereas basic proteins tended to precipitate 1.5 -3 pH units below their pI. They also stated that proteins are soluble within 1 pH unit of, but not equal to, their pI. With *Pf*Arf6 being a basic protein (pI ~ 8.6, discussed further in next chapter), and the pH of the Arf buffer used being 7.4, it was possible that the final pH of the stored *Pf*Arf6 was 1.5-3 pH units below its pI, thus causing it to crystalise. In future *Pf*Arf6 can be expressed and eluted into Arf buffer with different pH values (around 8.0-8.5) to assess whether a higher buffer pH allows *Pf*Arf6 to be soluble and stable for longer.

In terms of recombinant protein production, solubility has often been linked with the conformational quality of the protein, i.e. if its soluble it must be fully active and if insoluble it must be inactive. However soluble expressed recombinant proteins may still display incomplete folding, whereby they adopt a soluble conformation, but the active site arrangement is still unsuitable for its full potential of activity (González-Montalbán *et al*., 2007; Mart nez-Alonso *et al*., 2008). There are advantages to the formation of insoluble inclusion bodies though, such as relatively high levels of protein expression and purity. Hence if efficient refolding protocols are applied, of which there are many (de Bernardez Clark, 1998; Rosano & Ceccarelli, 2014; Simpson, 2010), relatively large amounts of active protein can be obtained. The inclusion bodies may also protect the protein from proteolytic degradation, thus one could store several batches of *Pf*Arf6 inclusion bodies to explore the optimum refolding conditions for protein stability. Gutiérrez-González *et al*. (2019) were able to refold a single chain variable antibody (scFv), directed against major histocompatibility complex (MHC) class I chain-related protein A, using a fast dilution protocol and the additions of arginine and the redox pair glutathione/glutathione disulfide (GSH/GSSG). These techniques were adapted from Basu *et al*. (2011), de Marco (2009) and Yamaguchi *et al*., (2012), thus a basis for exploring *Pf*Arf6 refolding from inclusion bodies is present for future *Pf*Arf6 stability studies. Overall, the recombinant proteins used in the subsequent assays were all expressed and purified in a soluble conformation, with just the stability of *Pf*Arf6 being in question.

Chapter 3: Distinguishing between human and malarial Arf1 and Arf6 using GGA3 and JIP4.

3.1. Introduction

In addition to the sequence encoding the previously characterised *P. falciparum* homologue of Arf1, *Pf*Arf1 (PF3D7_1020900), the *P. falciparum* genome contains a second sequence (PF3D7_1034700) which is annotated as encoding for another Arf-GTPase. Jalview was used to view a pairwise alignment of the truncated human and malarial Arf GTPases (**Figure A1**), in which this second Arf sequence displayed a higher sequence identity of 53.42 % with human Arf1 compared to a 49.07 % sequence identity with human Arf6. Despite this higher sequence homology with *Hs*Arf1, we have tentatively designated this second malarial Arf sequence as *Pf*Arf6 for a number of reasons. As mentioned earlier in chapter 1 (literature review), fluorescence microscopy analysis has shown that *Pf*Arf6-GFP is distributed along the parasite cell periphery and localises with cytoplasmic puncta, which aligns with human Arf6 function in endocytosis and recycling from endosomes (T.Swart, PhD thesis). *Pf*Arf1-GFP, on the other hand, has been shown to localise to the Golgi apparatus of the parasite cell, which aligns with the localisation and function of human Arf1 (Swart *et al*., 2020). In addition to this, the *Pf*Arf6 predicted amino acid sequence contains features which are more consistent with human Arf6 than with Arf1. Mammalian Arf1 GTPases all contain an MXXE motif that localises the Arf to the Golgi apparatus (Honda *et al*., 2005). A QS motif within the switch I region of Arf6 helps to induce actin protrusions at the plasma membrane (Song *et al*., 1998; Al-Awar *et al*., 2000). While the MXXE motif is present and the QS motif absent in *Pf*Arf1, in *Pf*Arf6 the MXXE motif is partly mutated to IXXE, while a QT motif is present in a primary sequence position corresponding to that of the QS motif in *Hs*Arf6. (**Figure A1**). The predicted basic isoelectric point (pI) of *Pf*Arf6 (8.6) conforms with Arf6 homologues from other organisms, which are basic proteins with pIs > 8 (Yang *et al*., 1998; Donaldson, 2003). Arf1 homologues, such as *Hs*Arf1 and *Pf*Arf1 are relatively more acidic with pIs < 7 (Qin *et al*., 2010).

Effector proteins recognise key sequences on Arf when bound to GTP, usually at a common ‘‘hydrophobic area” containing the switch I C-terminal, middle interswitch, and switch II N-terminal regions. This has been shown to be the binding site for various GTPase effectors. Two effector binding motifs have been described in this hydrophobic area, namely the critical hydrophobic pocket and the adjacent triad patch, consisting of a tryptophan residue in the interswitch region and a phenylalanine and tyrosine/phenylalanine residue situated adjacent to the switch I and switch II regions, respectively (Chavrier & Ménétrey, 2010; Khan & Ménétrey, 2013). Unlike Rab GTPases, the phenylalanine adjacent to switch I is found two residues upstream in Arf GTPases (Merithew *et al*., 2001). These two binding motifs allow effectors to distinguish between GTPase families but cannot account fully for how

Arf GTPase effectors distinguish between members of the Arf GTPases subfamily, even as different as Arf1 and Arf6 (Chavrier & Goud, 1999; Peters *et al*., 1995; Isabet *et al*., 2009). Nonetheless, the research presented in this chapter explores the possibility that Arf binding domains of effector proteins can distinguish between human Arf1 and Arf6, and consequently assign the putative *Pf*Arf6 as either an Arf6/Arf1 homologue using *in vitro* binding assays.

The Mg^{2+} in GTPases stabilise the attached nucleotide and so stabilises the GTPase in an active (GTP-bound) or inactive (GDP-bound) state. GTPases are rarely found in a nucleotide-free state and so favour the binding of guanine nucleotides present around them. In *in vitro* EDTA-mediated nucleotide exchange of Arf GTPases, the Arf isoforms are incubated with EDTA and excess GTP/GDP. EDTA chelates the Mg^{2+}, the GTPases favour binding of the nucleotide present in excess, and excess $MgCl_2$ relative to the EDTA concentration added subsequently stabilises the Arf GTPases in a GTP/GDP-bound state. Nucleotide exchange is monitored by intrinsic tryptophan fluorescence (Ex_{297nm}/Em_{340nm}) to differentiate Arf GTPase 'preloaded' with GTP/GDP (Higashijima *et al*., 1987). An invariant tryptophan residue, within the switch II region of Arf GTPases (**Figure A1**), is exposed during the conformational shift which occurs as Arf-GDP transitions to Arf-GTP. The tryptophan residue is shielded from detection in the protein core when Arf-GTP is deactivated to Arf-GDP. Hence, the tryptophan residue acts a probe for the activation status of Arf GTPases whereby higher and lower fluorescence emission values at 340 nm represent Arf-GTP and Arf-GDP, respectively (Higashijima *et al*., 1987). These 'preloaded' Arf GTPases could then be used to study Arf-effector interactions *in vitro*. The effector GGA3 has been shown to interact with all mammalian Arfs (class I – III) *in vitro* (Parachoniak *et al*., 2011), through its catalytic GAT domain (Takatsu *et al*., 2002; Collins *et al*., 2003). JIP4, an effector protein only for Arf6, binds through its LZII domain (Montagnac *et al*., 2011). Thus, the difference in binding affinity of these effectors to Arf-GTP should be able to distinguish Arf1 from Arf6 GTPase. Two novel *in vitro* assay formats were explored that focus on the interaction between Arf-GTP and an effector protein's Arf binding domain, using either a Ni^{2+} (nickel) or glutathione coated 96-well plate (**Figure 9 – 10**).

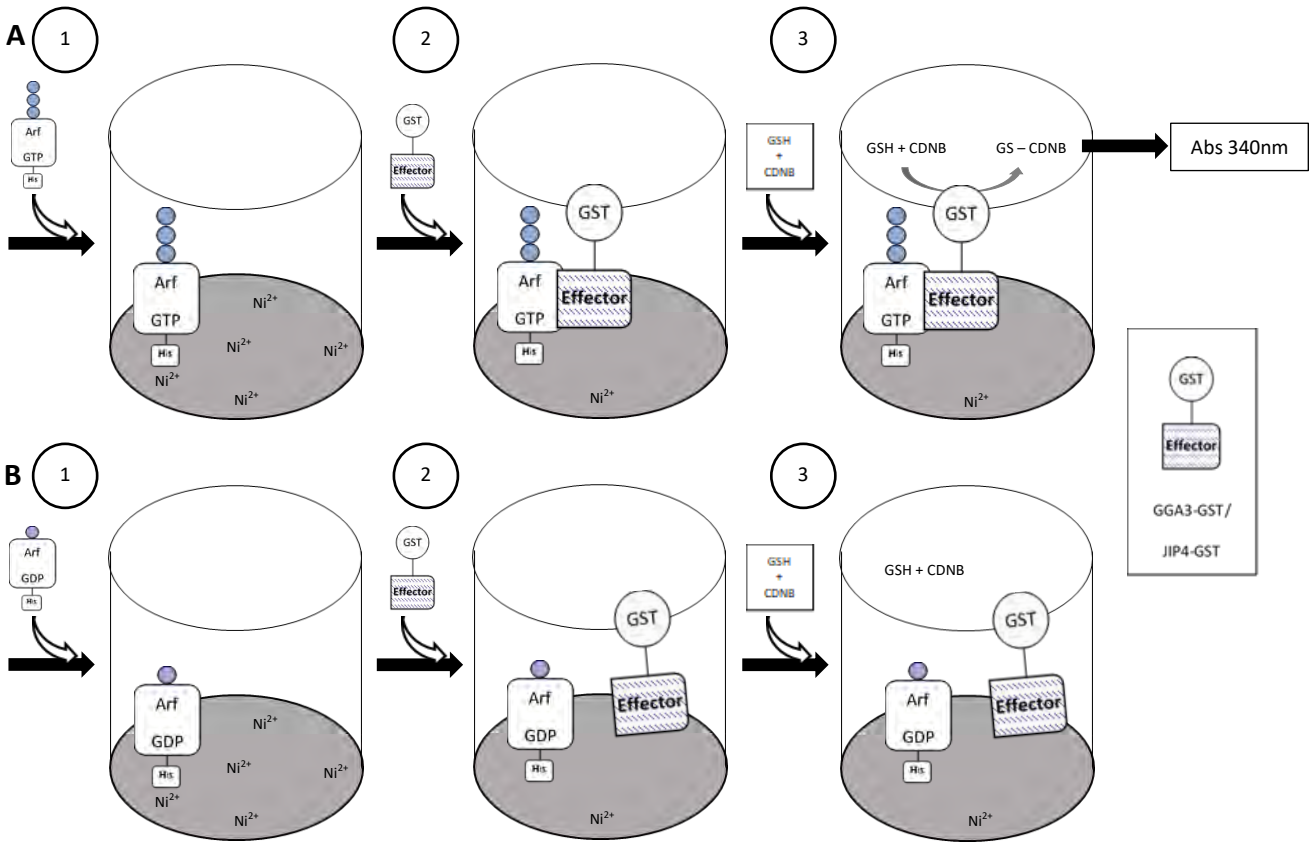

Figure 9: Schematic diagram representing the Ni-NTA immobilised Arf-effector-GST interaction assay principle. **(A)** '**Active' Arf** Step 1: GTP preloaded His-tagged Arf-GTPase (*Hs*Arf1; *Hs*Arf6; *Pf*Arf1; or *Pf*Arf6) is added to a Ni-NTA coated 96-well plate, allowing His-tag immobilisation to the plate. Step 2: An Arf-GTPase effector protein bound to GST (GST-GGA3^{GAT} / GST-JIP4^{LZII}) is added to the plate, allowing for the GAT and LZII (leucin zipper II) domains to selectively bind Arf-GTP. Step 3: Unbound proteins are washed off, followed by the addition of a bound GST substrate mix, including 1-chloro-2,4-dinitrobenzene (CDNB), reduced glutathione (GSH) and 1 × PBS. The reaction product, glutathione conjugated to CDNB (GS-CDNB), is formed and absorbance measured at 340 nm. **(B)** '**Inactive' Arf** Step 1: GDP preloaded His-tagged Arf-GTPase (*Hs*Arf1; *Hs*Arf6; *Pf*Arf1; or *Pf*Arf6) is added to a Ni-NTA coated 96-well plate, allowing His-tag immobilisation to plate. Step 2: An Arf-GTPase effector protein bound to GST (GST-GGA3^{GAT} / GST-JIP4^{LZII}) is added to the plate. Step 3: Unbound proteins are washed off, followed by the addition of a GST substrate mix. It is anticipated that the GST-tagged effector proteins would be incapable of binding effectively to Arf-GDP, leading to less formation of the reaction product, GS-CDNB, and lower absorbance at 340 nm compared to active Arf.

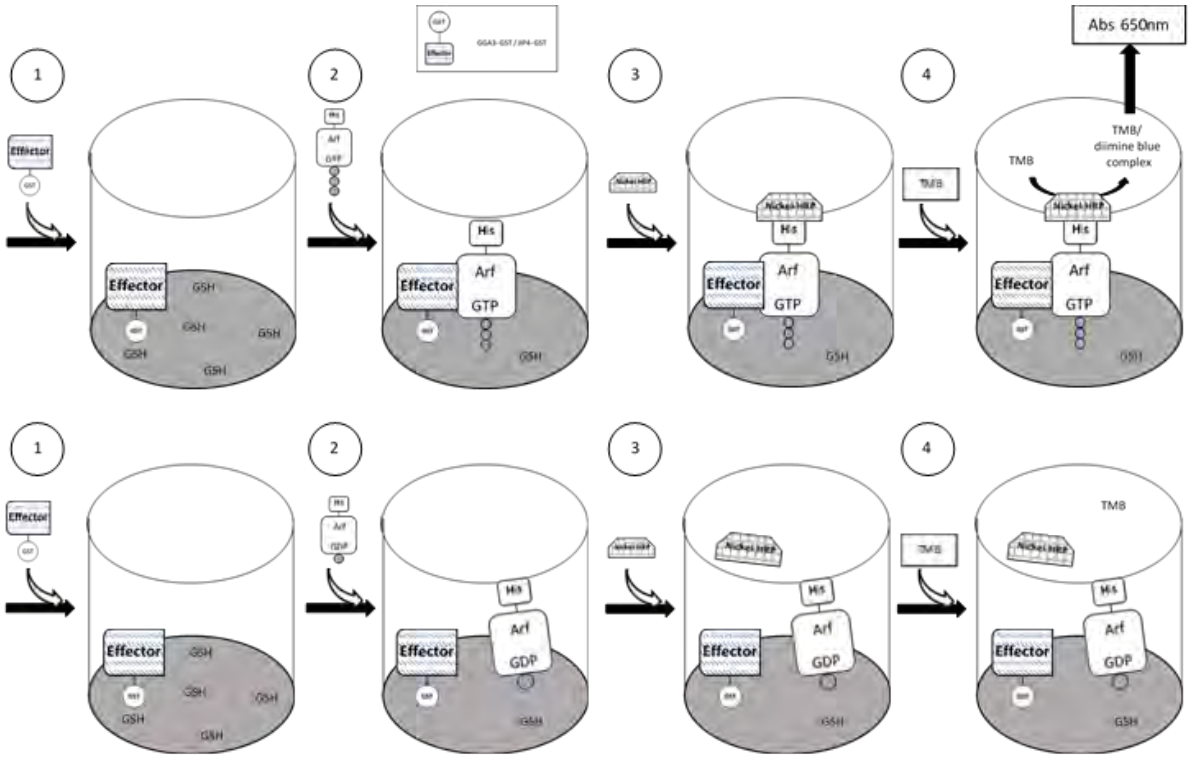

Figure 10: Schematic diagram representing the glutathione immobilised effector-Arf-GST interaction assay principle. **(A)** '**Active' Arf** Step 1: An Arf-GTPase effector protein bound to GST (GST-GGA3^{GAT} / GST-JIP4^{LZII}) is added to a glutathione (GSH) coated 96-well plate, allowing for GST-tag immobilisation. Step 2: GTP preloaded His-tagged Arf-GTPase (*Hs*Arf1; *Hs*Arf6; *Pf*Arf1; or *Pf*Arf6) is added to the plate, allowing for the GAT and LZII (leucin zipper II) domains to selectively bind Arf-GTP. Step 3: Unbound proteins are washed off, followed by the addition of a His-Detector reagent (nickel-HRP). Step 4: The plate is washed further, to remove unbound nickel-HRP, before an HRP-substrate (TMB) is added. The HRP oxidizes the TMB to form a TMB/diimine blue complex and absorbance is measured at 650 nm. **(B)** '**Inactive' Arf** Step 1: An Arf-GTPase effector protein bound to GST (GST-GGA3^{GAT} / GST-JIP4^{LZII}) is added to a glutathione (GSH) coated 96-well plate, allowing for GST-tag immobilisation. Step 2: GDP preloaded His-tagged Arf-GTPase (*Hs*Arf1; *Hs*Arf6; *Pf*Arf1; or *Pf*Arf6) is added to the plate. Step 3: Unbound proteins are washed off, followed by the addition of His-Detector (Nickel-HRP). Step 4: The plate is washed further before a TMB substrate is added, and absorbance is measured at 650 nm. In principle, the His-tagged Arf-GDP should not bind to the immobilised effector domains, leading to less nickel-HRP binding and lower absorbance at 650 nm.

3.2. Aims & objectives

To assess whether the *in vitro* binding of Arf GTPases to the GGA3 and JIP4 Arf-binding domains could be used to: i) confirm whether the *Pf*Arf6 recombinant protein is able to interact with the effector domains, ii) determine whether *Pf*Arf6 could be distinguished from *Pf*Arf1, iii) determine whether the *Pf*Arf6 effector domain binding readings correlate more with human Arf6 than Arf1. To achieve these aims, the following objectives were pursued using techniques and resources detailed in Chapter 5 (Methods and materials):

- Determine the concentration of EDTA required to facilitate effective nucleotide exchange on *Hs*Arf1 and *Hs*Arf6, to produce Arf-GTP and Arf-GDP.
- Determine the concentration of EDTA required to facilitate effective nucleotide exchange on *Pf*Arf1 and *Pf*Arf6, to produce Arf-GTP and Arf-GDP.
- Confirm whether the GAT domain of GGA3 binds preferentially to the active *Hs*Arf6-GTP and *Pf*Arf6-GTP conformations, using a Ni^{2+} coated plate (as has been previously reported for *Hs*Arf1 and *Pf*Arf1; Swart et al., 2020)
- Determine whether the Arf-binding LZII domain of JIP4 can distinguish between both human and *P. falciparum* Arf1 and Arf6 *in vitro*, using the Arf proteins immobilised onto a Ni^{2+} coated plate.
- Determine whether JIP4 can distinguish between human and *P. falciparum* Arf1 and Arf6 *in vitro*, with the reversed assay format, whereby the effector domains are immobilised onto a glutathione coated plate.

3.3. Results

3.3.1. Nucleotide exchange optimisation for each Arf-GTPase

As effector proteins only bind active Arf-GTPases, it was necessary to prepare both 'active' (Arf-GTP) and 'inactive' (Arf-GDP) Arf complexes, to be used in the subsequent effector interaction assays. Intrinsic tryptophan fluorescence was used to distinguish between the Arf-GTP and Arf-GDP conformations. As GDP is exchanged for GTP the detected internal fluorescence signal should increase, and vice versa the signal should decrease as GTP is exchanged for GDP. Nucleotide exchange was performed with varying amounts of EDTA in order to chelate the Mg^{2+} and obtain the greatest Arf-GTP to Arf-GDP signal differences (Arf-GTP minus Arf-GDP) for each of the expressed His-tagged Arf constructs. EDTA-mediated nucleotide exchange was conducted by incubating 5 µM Arf-GTPase (*Hs*Arf1, *Hs*Arf6, *Pf*Arf1, and *Pf*Arf6) with EDTA (2, 5, 10 and 20 mM) and 50 µM GTP/GDP at 25°C for 60 min, with gentle agitation. The Arf-GTP and Arf-GDP complexes were stabilised with 30 mM $MgCl_2$ and incubated further at 25°C for 10 min, with gentle agitation. Intrinsic tryptophan fluorescence was measured as an end-point reading (excitation wavelength 297 nm; emission wavelength 340 nm). For the His-tagged *Hs*Arf-GTPase constructs (**Figure 11**; Left: *Hs*Arf1, Right: *Hs*Arf6), the differences between the Arf-GTP and Arf-GDP reaction mixture fluorescence signals increased with the amount of EDTA used. For *Hs*Arf1, the significant differences between *Hs*Arf1-GTP and *Hs*Arf1-GDP fluorescence readings were 107 ($p = 0.0000042$), 224 ($p = 0.0000017$), 252 ($p = 0.0000501$) and 264 ($p = 0.0000067$) for the 2, 5, 10 and 20 mM EDTA reaction mixtures, respectively (**Figure 11A,** Left). For *Hs*Arf6 in contrast, the only significant differences between *Hs*Arf6-GTP and *Hs*Arf6-GDP fluorescence readings were 86 ($p = 0.000039$) and 162 ($p = 0.000321$) for the 10 and 20 mM EDTA reaction mixtures, respectively (**Figure 11A,** Right). Continuous tryptophan fluorescence readings were recorded every 5 min over the 60 min incubation with 20 mM EDTA, for both *Hs*Arf1 and *Hs*Arf6, including both Arf mixtures on their own (without addition of exogenous nucleotides). Both the Arf-GTP and Arf only fluorescence values followed near identical trajectories, whereas the Arf-GDP fluorescence values decreased below the other values over the hour, suggesting the *Hs*Arf GTPases were purified from *E. coli* predominantly in an active GTP-bound conformation (**Figure 11B**). Preloading incubation conditions for *Hs*Arf1 and *Hs*Arf6, for the subsequent assays, were set at 5 µM Arf-GTPase with 20 mM EDTA and 50 µM GTP/GDP (25°C, 60 min, gentle agitation). This translated to *Hs*Arf1-GTP/GDP fluorescence values averaging 580 and 330, respectively (difference ~ 250 units), and *Hs*Arf6-GTP/GDP absorbance values averaging 560 and 440, respectively (difference ~ 120 units) (**Figure 11C**).

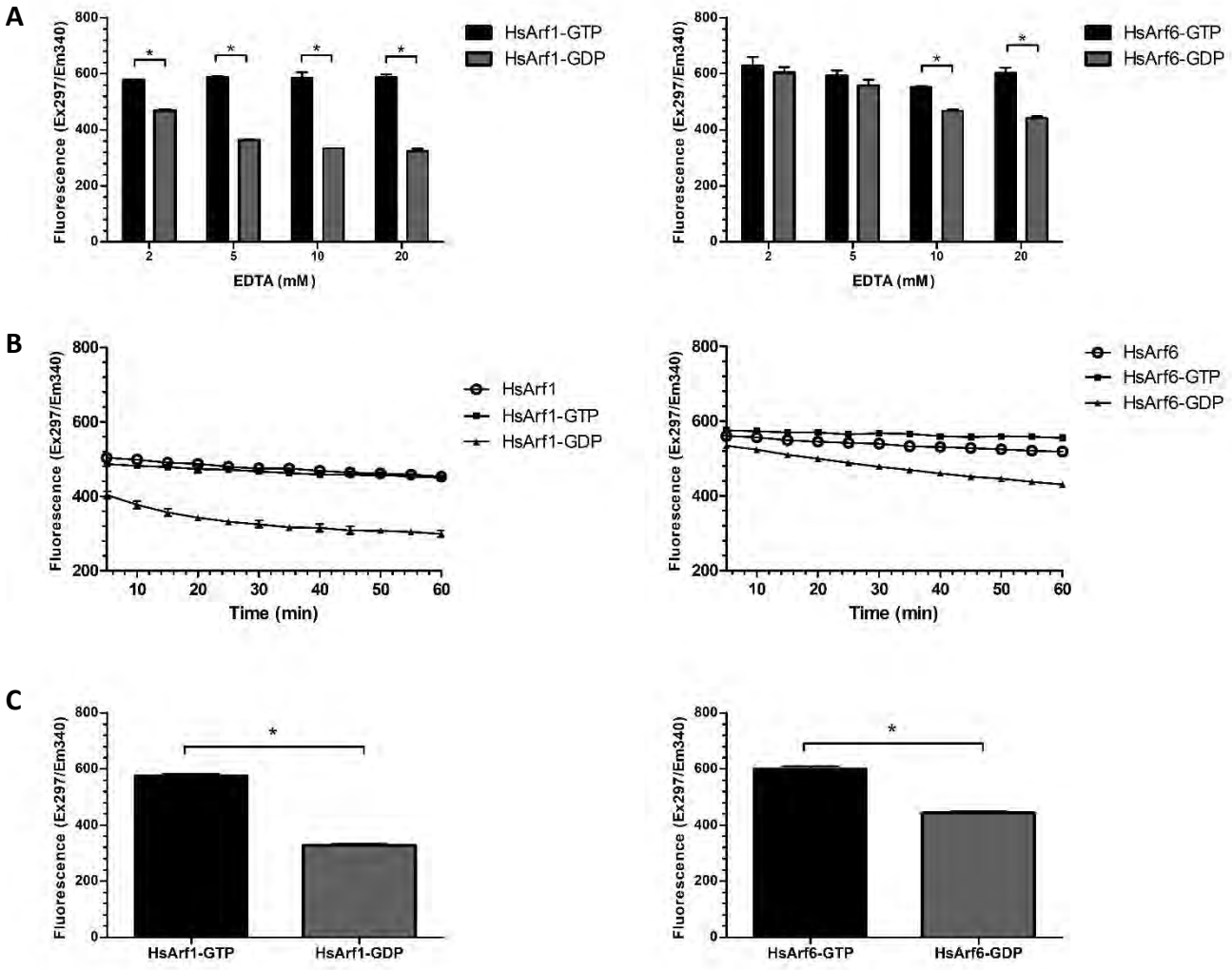

Figure 11: Using tryptophan fluorescence to detect EDTA-mediated nucleotide exchange of *Hs*Arf GTPases. (Left) *Hs*Arf1, (Right) *Hs*Arf6. **(A)** Nucleotide exchange was performed by incubating 5 µM *Hs*Arf GTPase with 50 µM GTP/GDP, in the presence of varying amounts of EDTA (2, 5, 10, 20 mM), for 60 min at 25°C, with gentle agitation. $MgCl_2$ (30 mM) was added, and the *Hs*Arf-GTP and *Hs*Arf-GDP complexes were stabilised after a 10 min incubation at 25°C, with gentle agitation. Tryptophan fluorescence was measured as an end-point reading (Ex_{297}/Em_{340}). **(B – C)** 5 µM *Hs*Arf GTPase, in the presence of 50 µM GTP/GDP and 20 mM EDTA, was incubated for 60 min at 25°C, with gentle agitation. A continuous reading of tryptophan fluorescence (Ex_{297}/Em_{340}), including *Hs*Arf without any nucleotide, was measured every 5 min for 60 min **(B)**; or as an end-point reading after 60 min (**C**); using a Spectramax M3 (Molecular Devices) plate reader. Each point represents the mean and standard deviation of triplicate readings. (*) = p-value < 0.05.

For the His-tagged *Pf*Arf-GTPase proteins (**Figure 12**; Left: *Pf*Arf1, Right: *Pf*Arf6), the differences between the Arf-GTP and Arf-GDP reaction mixture fluorescence signals decreased slightly with increasing concentrations of EDTA used. For *Pf*Arf1, the significant differences between *Pf*Arf1-GTP and *Pf*Arf1-GDP absorbance readings were 148.17 ($p = 0.000099$), 116.50 ($p = 0.000041$), 119.82 ($p = 0.002334$) and 113.68 ($p = 0.000120$) for the 2, 5, 10 and 20 mM EDTA reaction mixtures, respectively (**Figure 12A,** Left). For *Pf*Arf6 on the other hand, the significant differences between *Pf*Arf6-GTP and *Pf*Arf6-GDP absorbance readings were 206.29 ($p = 0.00029$), 156.80 ($p = 0.00017$), 136.15 ($p = 0.00024$), and 36.88 ($p = 0.00026$) for the 2, 5, 10 and 20 mM EDTA reaction mixtures, respectively (**Figure 12A,** Right). Continuous tryptophan fluorescence readings were recorded every 5 min over the 60 min incubation with 2 mM EDTA, for both *Pf*Arf1 and *Pf*Arf6, including both Arf proteins on their own (without added excess nucleotide). Both the Arf-GTP and Arf only absorbance values followed near identical trajectories, whereas the Arf-GDP absorbance values decreased below the other values over the hour (**Figure 12B**). As with the human proteins, this suggested that both the malarial Arf GTPases were purified from *E. coli* predominantly in a GTP-bound state. Preloading incubation conditions for *Pf*Arf1 and *Pf*Arf6, for the subsequent assays, were set at 5 µM Arf-GTPase with 2 mM EDTA and 50 µM GTP/GDP (25°C, 60 min, gentle agitation). This translated to *Pf*Arf1-GTP/GDP absorbance values averaging 480 and 330, respectively (difference ~ 150 units), and *Pf*Arf6-GTP/GDP absorbance values averaging 540 and 340, respectively (**Figure 12C**).

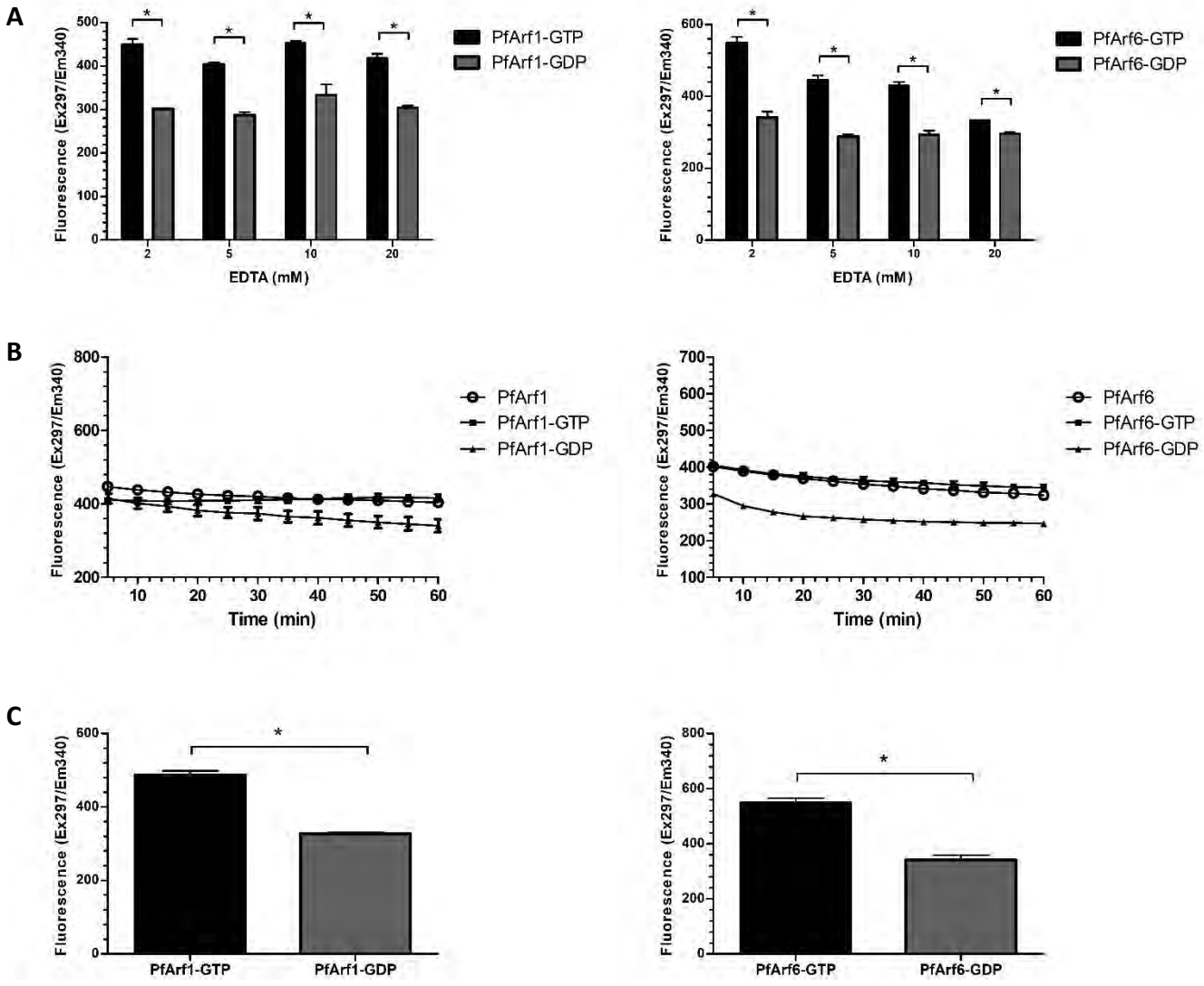

Figure 12: Using tryptophan fluorescence to detect EDTA-mediated nucleotide exchange of *Pf*Arf GTPases. (Left) *Pf*Arf1, (Right) *Pf*Arf6. **(A)** Nucleotide exchange was performed by incubating 5 µM *Pf*Arf GTPase with 50 µM GTP/GDP, in the presence of varying amounts of EDTA (2, 5, 10, 20 mM), for 60 min at 25°C, with gentle agitation. $MgCl_2$ (3 mM) was added, and the *Pf*Arf-GTP and *Pf*Arf-GDP complexes were stabilised after a 10 min incubation at 25°C, with gentle agitation. Tryptophan fluorescence was measured as an end-point reading (Ex_{297}/Em_{340}). **(B – C)** 5 µM *Pf*Arf GTPase, in the presence of 50 µM GTP/GDP and 2 mM EDTA, was incubated for 60 min at 25°C, with gentle agitation. A continuous reading of tryptophan fluorescence (Ex_{297}/Em_{340}), including *Pf*Arf without added nucleotide, was measured every 5 min for 60 min **(B)**; or as an endpoint reading after 60 min **(C);** using a Spectramax M3 (Molecular Devices) plate reader. Each point represents the mean and standard deviation of triplicate readings. (*) = p-value < 0.05.

Issues arose with the *Pf*Arf6-GTP/GDP preloaded samples, where the *Pf*Arf6-GTP and *Pf*Arf6-GDP average fluorescence values both showed a notable decrease during storage, translating to differences of 80 units only. These values dropped over the space of 3 – 4 days after *Pf*Arf6 expression, whereas all the other preloaded samples generated the same Arf-GTP/GDP fluorescence values and differences even 2 weeks after expression. A new batch of purified *Pf*Arf6 was prepared from *E. coli* and the nucleotide exchange conditions were altered in an attempt to generate a more discernible difference between *Pf*Arf6-GTP and *Pf*Arf6-GDP. The conditions varied one by one were: incubation temperature (37°C), EDTA concentration (2, 1, 0.5 and 0.25 mM), and lastly incubation time (90 and 120 min). The 120 min incubation showed the most promise, so preloading incubation conditions for *Pf*Arf6, for the subsequent assays, were set at 5 µM Arf-GTPase with 2 mM EDTA and 50 µM GTP/GDP (25°C, 120 min, gentle agitation). This translated to *Pf*Arf6-GTP/GDP fluorescence values 390 and 275, respectively with a difference ~ 115 units (refer to **Figure A2**). Since the observed decrease in *Pf*Arf6-GTP/GDP fluorescence readings may have been caused by instability of the *Pf*Arf6 protein samples during storage, protein purification was carried out at a maximum of 5 days prior to nucleotide preloading, which was conducted immediately before the effector binding assays

3.3.2. Ni-NTA- and glutathione-immobilised effector-GST interaction assays

It is well known that the binding of Arf GTPases to GGA3, through the GAT domain of the latter, occurs in the 'active' GTP-bound conformation of the Arf. It has been used to discriminate between both active and inactive His-tagged *Hs*Arf1 and *Pf*Arf1 complexes *in vitro* in our research group (Swart *et al*., 2020). In order to determine whether the GGA3 GAT domain can also discriminate between both active and inactive His-tagged *Hs*Arf6 and *Pf*Arf6 complexes *in vitro*, the Ni-NTA 96-well plate assay described earlier (**Figure 9**) was used. Both *Hs*Arf1 and *Pf*Arf1 were also included to serve as controls due to their previously established differential binding to the GGA3 GAT domain. The His-tagged Arf constructs (*Hs*Arf1, *Pf*Arf1, *Hs*Arf6 and *Pf*Arf6) were preloaded with GTP and GDP and immobilised on a nickel coated 96-well plate. Purified GST-GGA3^{GAT} was added to the plate and incubated before the plate was washed to remove any unbound proteins. A GST substrate mix (containing CDNB and GSH) was added to assess the extent of GST-GGA3^{GAT} binding to the plate by absorbance at 340 nm (**Figure 13A**). All values obtained were corrected for a GST-GGA3^{GAT} only background mixture (wells lacking immobilised Arf proteins). The Arf-GTP absorbance values (all between 0.6 to 0.8 units) were all statistically higher than their corresponding Arf-GDP values ($p < 0.005$), confirming that both active and inactive forms of His-tagged Arf constructs could be detected. Both *Hs*Arf1- and *Pf*Arf1-GDP absorbance values were close to zero (similar to background control), whereas the *Hs*Arf6- and *Pf*Arf6-GDP values were higher at approximately half of their corresponding -GTP values (49 % and 52 % of

the GTP-loaded absorbance values for *Hs*Arf6 and *Pf*Arf6, respectively). This suggests that, unlike the two Arf1 isoforms, the GAT domain of GGA3 maintains some residual binding affinity for inactive forms of both the human and malarial Arf6 proteins.

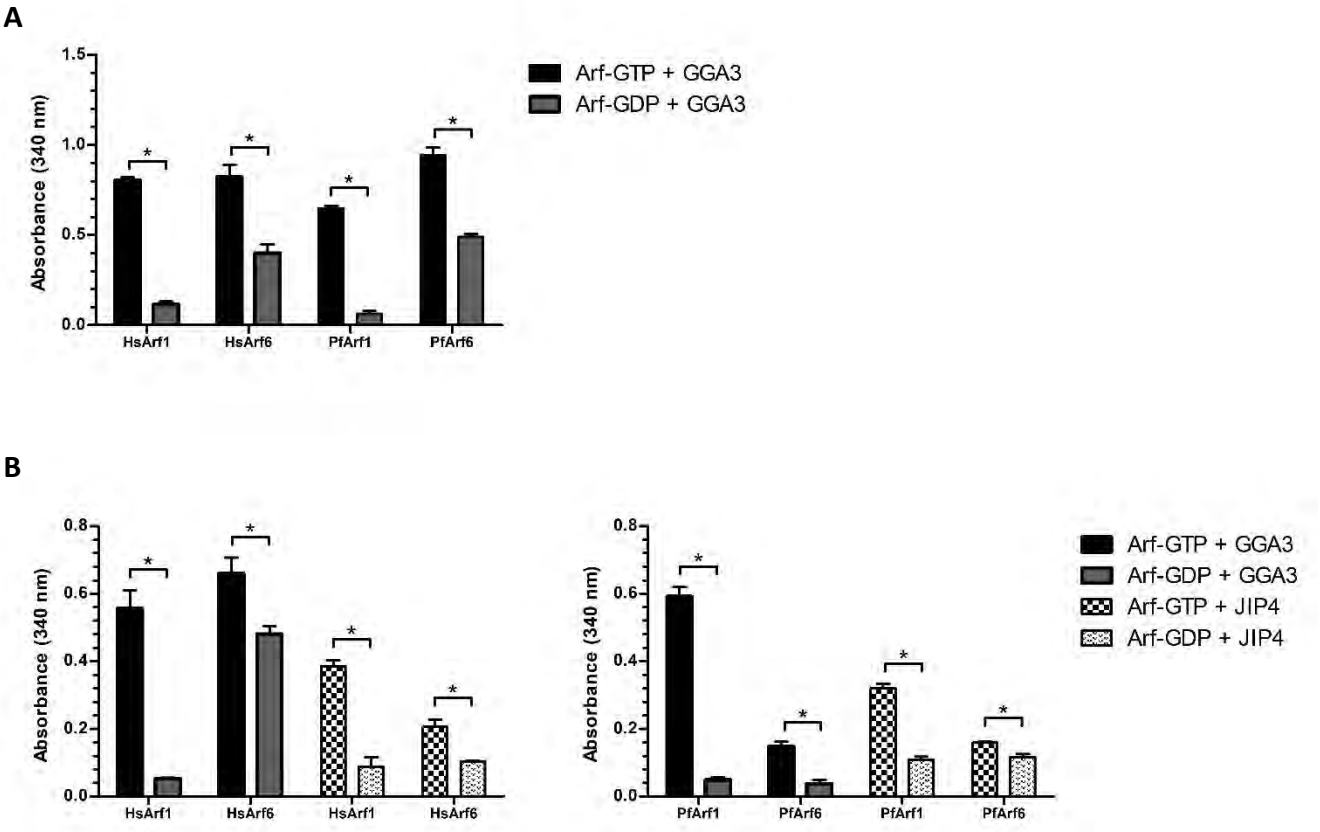

Figure 13: Ni-NTA immobilised Arf-effector-GST interaction assay. **(A)** GTP and GDP preloaded Arf GTPase (*Hs*Arf1, *Hs*Arf6, *Pf*Arf1, and *Pf*Arf6) were added to the wells of a Ni-NTA coated clear 96-well plate and incubated for 30 min at 4°C, with gentle agitation. An equal volume of GST-GGA3^{GAT} was added to each well (1 µM Arf GTPase, 1 µM GST-GGA3^{GAT} final concentrations) and plate incubated for 60 min at 4°C, with gentle agitation. **(B)** GTP and GDP preloaded Arf GTPase (*Hs*Arf1, *Hs*Arf6, *Pf*Arf1, and *Pf*Arf6) were added to the wells of a Ni-NTA coated clear 96-well plate and incubated for 30 min at 4°C, with gentle agitation. An equal volume of GST-GGA3^{GAT}/GST-JIP4^{LZII} was added to each well (1 µM Arf GTPase, 1 µM GST-GGA3^{GAT}/GST-JIP4^{LZII}) and plate incubated for 60 min at 4°C, with gentle agitation. **(A – B)** The wells were washed before a GST substrate master mix (2 mM reduced L-glutathione, 1 mM 1-chloro-2,4-dinitrobenzene (CDNB) in 1 × PBS) was added to each well and incubated for 30 min at room temperature. Absorbance was measured at 340 nm, using a Spectramax M3 (Molecular Devices) plate reader. All values were corrected for background absorbance obtained from wells incubated with GGA3^{GAT}/GST-JIP4^{LZII} in the absence of immobilised Arf proteins. Each point represents the mean and standard deviation of triplicate readings. (*) = p-value < 0.05.

As differential GTP vs. GDP-bound *Hs*Arf6 and *Pf*Arf6 detection by GST-GGA3^{GAT} was confirmed, the next step was to determine whether the same was true for GST-JIP4^{LZII}. In addition, a question was to what extent it could distinguish between the respective malarial and human Arf1 and Arf6 isoforms, since JIP4 has been reported to be an Arf6 effector in cells (Montagnac *et al*., 2011). The same procedure was followed as before with preloaded His-tagged Arf-GTP/GDP, except now GST-JIP4^{LZII} was used in parallel with GST-GGA3^{GAT} (**Figure 13B**). Absorbance readings of background controls including GST bound effectors only were subtracted from their corresponding Arf and GST-GGA3^{GAT}/-JIP4^{LZII} mixtures. Negative controls (preloaded Arf-GTP/GDP on its own, i.e. omitting the GST-tagged effector domain in the incubation) for each Arf construct were also used in the assay. For each Arf construct, the negative controls were all below the GST-GGA3^{GAT} and GST-JIP4^{LZII} background controls (data not shown). As was the case with GST- GGA3^{GAT}, GST- JIP4^{LZII} could distinguish between the GTP- and GDP-bound forms of all the Arf isoforms, though less robustly so in the case of *Pf*Arf6. Despite being reported to be an Arf6 effector in cells, it produced lower Abs_{340} values than GST- GGA3^{GAT} when incubated with *Hs*Arf6-GTP, and similar values to GST- GGA3^{GAT} with *Pf*Arf6-GTP. In addition, it appeared to bind more efficiently to the Arf1-GTP vs. Arf6-GTP proteins of both species, though still less efficiently than GST- GGA3^{GAT}. Thus, it did not behave as an Arf6-specific probe in this specific *in vitro* assay format.

Due to the relatively low absorbance values obtained using GST-JIP4^{LZII} on the Ni-NTA coated plate, a glutathione coated plate was also used in order to investigate if this would improve the efficiency and specificity of GST-JIP4^{LZII} binding to the Arf6 isoforms (**Figure 14**). The glutathione assay was very similar to the Ni-NTA assay method, except that GST-tagged effectors (GST-GGA3^{GAT} or GST-JIP4^{LZII}) were immobilised to the plate instead and incubated with Arf proteins in solution (**Figure 10**). The His-tag on all the Arf constructs, bound to an immobilised effector, was detected by a subsequent incubation with Nickel-HRP, followed by a colorimetric HRP substrate (TMB). Working in this reverse format, the new background controls were absorbance readings obtained with the preloaded His-tagged Arf constructs on their own (Arf-GTP and Arf-GDP), i.e. incubated in wells lacking immobilised effector proteins, which were subtracted from their corresponding Arf-GTP or Arf-GDP reaction mixture with each GST-tagged effector. The negative controls were the GST-tagged effectors on their own. For each respective Arf construct, the negative controls were all below the Arf-GTP and Arf-GDP background controls (data not shown). As was the case with the Ni-NTA plate experiment (**Figure 13A**), GST-GGA3^{GAT} could distinguish between GTP- vs. GDP-bound Arf proteins in all cases and there was significant residual binding to both Arf6-GDP homologues. In addition, the stronger binding of GST-GGA3^{GAT} to Arf6 than Arf1 was more pronounced in this assay format, particularly for the malarial proteins. Importantly, by rather immobilising the effector domains using their GST tags, GST-JIP4^{LZII} could now robustly distinguish between the Arf6 and Arf1 proteins. Absorbance readings obtained with the Arf1 proteins were close to background, in contrast to the comparatively high readings

obtained with Arf6. It produced absorbance values that were 13-fold higher for *Hs*Arf6-GTP vs *Hs*Arf1-GTP, and 6-fold higher for *Pf*Arf6-GTP vs *Pf*Arf1-GTP. Though GST-JIP4^{LZII} could distinguish between the active GTP-bound and inactive GDP-bound conformations of both Arf6 proteins, it mimicked GST-GGA3^{GAT} by still displaying significant binding to the GDP-bound forms of the Arf6 isoforms. Using GST-GGA3^{GAT}, the GDP values obtained were 43 % and 62 % of the *Hs*Arf6- and *Pf*Arf6-GTP values, respectively. Whereas for GST-JIP4^{LZII}, the GDP values obtained were 60 % and 72 % of the *Hs*Arf6- and *Pf*Arf6-GTP values, respectively (**Figure 14**).

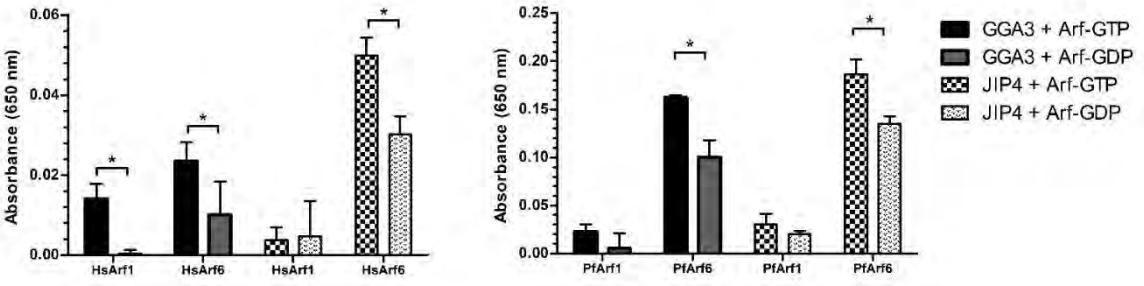

Figure 14: Glutathione immobilised effector-Arf-GST interaction assay. GST-GGA3^{GAT}/GST-JIP4^{LZII} (1 µM) was added to the wells of a glutathione coated clear 96-well plate, and incubated for 30 min at 25°C, with gentle agitation. The wells were washed before GTP and GDP preloaded Arf GTPase (*Hs*Arf1, *Hs*Arf6, *Pf*Arf1, and *Pf*Arf6) were added (1 µM), and incubated for 60 min at 25°C, with gentle agitation. A His-tag detection reagent (HisDetector Nickel-HRP (Sera Care) diluted 1: 10 000 in Arf assay buffer) was added to each well, followed by a further incubation for 60 min at 25°C, with gentle agitation. The wells were washed again before being incubated, in SureBlue Reserve (Sera Care), for 30 min at 25°C. Absorbance was measured at 650 nm, using a Spectramax M3 (Molecular Devices) plate reader. All values were corrected for background absorbance from a GGA3^{GAT}/GST-JIP4^{LZII} free reaction mixture, containing only preloaded Arf-GTP/GDP. Each point represents the mean and standard deviation of triplicate readings. (*) = p-value < 0.05.

3.4. Discussion

As for most small GTPases, Arf GTPases as well as their cognate regulators and effectors have been implicated in many human diseases. Many GTPases in the Ras superfamily have strong links to cancer but the mechanism by which Arf GTPase signalling is altered in cancers differs from other families such as Ras and Rho GTPases. The most common alteration of Ras/Rho GTPase signalling is through missense mutation, whereas the most common Arf GTPase genetic alterations are seen through amplification events (Ehlers *et al*., 2005; Jang *et al*., 2012). The increased amount of available Arf GTPases leads to the eventual increase in Arf-GTP and effector interactions, thus an increased rate in signal propagation. Hence, Arf GTPase effector binding is a plausible therapeutic target, as weakening this interaction would interrupt the Arf GTPase signal demand threshold for diseases such as cancer. In the case of malaria, genome-wide knock-out studies have reported that *Pf*Arf1 and its predicted regulatory GEF and GAP are essential for blood-stage parasite viability (Zhang *et al*., 2018; Bushell *et al*., 2017), and well-known Arf1 activation inhibitors, e.g. Brefeldin A, inhibit parasite viability at low micromolar concentrations (Swart *et al*., 2020). *Pf*Arf6 appears less important for blood-stage parasite viability in the knock-out studies, though an essential role in other stages cannot be ruled out. GGA3 and JIP4 do not have homologues in malaria parasites and the endogenous Arf effector proteins are not known. However, conservation of GGA3 and JIP4 binding to the malaria Arf proteins may present an opportunity to probe Arf-effector binding as a malaria drug target.

The human and *P. falciparum* kinetic fluorescence readings for both Arf1 and Arf6 in the absence of added nucleotide, shared very similar readings to those obtained during GTP loading. This suggests that the His-tagged Arf proteins expressed in *E. coli* were purified in a predominantly active GTP bound form. For human Arf1, effective nucleotide exchange occurred using 2 mM EDTA but was more effective up to 20 mM EDTA. On the other hand, for human Arf6, effective nucleotide exchange with a sufficient fluorescence difference only occurred at 20 mM EDTA, thus 20 mM EDTA was chosen for the preloading of *Hs*Arf GTPase. For *P. falciparum* Arf1 and Arf6, unlike their human homologues, the most effective nucleotide exchange occurred using 2 mM EDTA. The Ni-NTA immobilised interaction assay involving only GGA3, showed that the GAT domain of GGA3 preferentially binds the active GTP-bound form of *Hs*Arf6 and *Pf*Arf6, as is the case for the *Hs*Arf1 and *Pf*Arf1. The GST-GGA3^{GAT} binding of *Pf*Arf6 showed more of a correlation to *Hs*Arf6 than that of *Hs*Arf1. GST-GGA3^{GAT} binding could robustly distinguish between the GTP- and GDP-bound forms of *Hs*Arf1 and *Pf*Arf1, as the GDP-bound values were relatively close to zero. The ability of GST-GGA3^{GAT} to distinguish between *Hs*Arf6 and *Pf*Arf6 on the other hand, was less effective due to the more significant binding of GGA3 to the GDP-bound forms. The subsequent Ni-NTA immobilised interaction assay that included the LZII domain of JIP4 showed that it preferentially bound the active GTP-bound forms of *Hs*Arf1, *Pf*Arf1,

*Hs*Arf6 and *Pf*Arf6, just like with the GAT domain of GGA3. Given that JIP4 is a known Arf6 effector *in vivo*, it was unexpected to find that the LZII domain of JIP4 bound more effectively to *Hs*Arf1 and *Pf*Arf1, compared to their Arf6 counterparts. This also showed that *Pf*Arf6 correlated more with *Hs*Arf6 than *Hs*Arf1.

Except for *Pf*Arf6, JIP4 binding to the active GTP-bound conformations of the Arfs was notably weaker than that of GGA3. In light of this another assay format was considered, whereby the effector domains were immobilised to a glutathione coated plate instead of the Arf-GTP/-GDP constructs being immobilised to a Ni-NTA coated plate. This assay format was reversed in order to assess whether JIP4 could distinguish between Arf1 and Arf6. The glutathione immobilised interaction assay showed that JIP4 could robustly distinguish between both human and malarial Arf1 and Arf6, by preferentially binding to both the Arf6 homologues. An interesting observation was that GGA3 also preferentially bound to the Arf6 homologues, especially *Pf*Arf6. Despite *Pf*Arf6 sharing a greater sequence alignment with *Hs*Arf1 than *Hs*Arf6, the immobilised interaction assays provided support for the designation of *Pf*Arf6 as an Arf6 homologue, in addition to the parasite localisation data and sequence features mentioned in the introduction. As was the case with *Hs*Arf6, the GDP-bound *Pf*Arf6 showed considerably higher binding to GGA3 than GDP-bound *Pf*Arf1. Just like *Hs*Arf6 in the reverse assay format, *Pf*Arf6 binding to JIP4, and to a lesser extent GGA3, was considerably higher than that obtained for *Pf*Arf1.

The *in vitro* assay setups involved N-terminally truncated Arf-GTPase proteins, which can fold properly (Goldberg, 1998) and have been shown to be soluble when expressed (previous chapter), but just as the myristoylated N-terminal helix displays a regulatory role in the lipid modification abilities of Arfs, the helix conformational shift as it binds a membrane or sequence identifiers in the helix itself may also play a regulatory role in how effectors distinguish between Arf GTPase subfamily members as well. The feature that the effectors still produce significant binding to Arf6-GDP could be related to the relatively high Arf6 fluorescence readings during GDP preloading, which in turn could be due to the unique nature of endogenous Arf6 in cells. Human Arf6-GDP has recently been shown to be membrane bound along with Arf6-GTP (Kosciuk *et al*., 2020), in contrast to other Arf GTPases where the GDP form is cytosolic. This suggests that Arf6-GDPs play a more complex role than simply an 'inactive' switch (Macia *et al*., 2004). This unique feature of Arf6-GDP might imply that it shares a more similar active conformation with Arf6-GTP, in contrast to Arf1-GDP and Arf1-GTP. This could in turn can result in the invariant tryptophan residue of Arf6-GDP to be partially exposed, which would generate higher tryptophan fluorescence readings that would be expected based on Arf1-GDP. Membrane bound Arf6-GDP may thus also interact with more effector proteins compared to other cytosolic Arf subfamily member bound to GDP. If this is the case, then it would also be a way of identifying Arf6 homologues compared to other Arf isoforms, in the *in vitro* plate assay formats described in this chapter. GDP-bound Arf6 homologues should produce higher effector binding readings than other Arf subfamily members

bound to GDP, which should generate absorbance readings closer to zero. As these were preliminary findings, the repetition of these assays would paint a more accurate picture of whether the Arf6-GDP effector binding readings were due to a higher similarity of their structures to Arf6-GTP, or due to possible ineffective GDP loading as the Arf6-GDP fluorescence values were higher in comparison to the Arf1-GDP values.

The high-throughput assay nature of this assay format would also benefit from being repeated with a purified His-tagged *Pf*Arf6 showing stability longer than just 3-5 days, as suggested by the results in this chapter, as expressing new *Pf*Arf6 frequently would be logistically cumbersome and would not promote the reproducibility of these assays. This might entail investigating alternative storage buffers and conditions for the purified protein (as discussed in previous chapter), using tryptophan fluorescence and the effector binding assays as a means of monitoring protein stability over time. When screening for potential Arf-effector interaction inhibitors, the assay would need to be repeated with a serial dilution of any flagged compounds from future drug libraries. Future studies should include more Arf effectors, in conjunction to GGA3 and JIP4, to attempt to increase the *in vitro* accuracy of distinguishing Arf GTPase subfamily members. As with GGA3 being known to bind all Arf subfamily members (control effector), other effectors known to bind both Arf1 and Arf6 are: the lipid modifying enzymes PLD and PIP5K, which are involved in PIP_2 and PA production at the Golgi and plasma membrane (Honda *et al*., 1999; Donaldson & Jackson, 2000); ARHGAP21 (or ARHGAP10), which is involved in F-actin dynamics (Dubois *et al*., 2005; Chavrier & Ménétrey, 2010). Other possible Arf6 specific effectors to include are: FIP3/4 and MKLP1, which are involved in endosome targeting to the cleavage furrow during cytokinesis (Schonteich *et al*., 2007; Makyio *et al*., 2012); AP-1B, which localises to recycling endosomes and helps mediate sorting of cargo to the plasma membrane (Shteyn *et al*., 2011). As Arf GAPS can function as Arf effectors, it would also be beneficial to include: SMAP1 - which is involved in Arf6-mediated receptor endocytosis (Tanabe *et al*., 2005; Kon *et al*., 2008); ASAP1 - (or AMAP1), which is involved in the premetastatic ability of uveal melanoma and invadopodia formation (Bowden *et al*., 1999; Yoo *et al*., 2019); ARAP3 - which is involved in invadopodia-dependent MT1-MMP recycling (Loskutov *et al*., 2014); and EPI64B – a Rab35 GAP involved in CIE (Chesneau *et al*., 2012). Including Arf6 (QS) and Arf1 (MXXE) mutants may help distinguish Arf6 and Arf1 effector specificity *in vitro*. With the GGA3 JIP4 signals being greater on the Ni-NTA and glutathione plates, respectively, using both assay formats for each new effector would be needed.

The applications of these *in vitro* immobilised assay systems can also extend to detecting the activation and deactivation of Arfs using GEFs and GAPs, as has been explored with Arf1 (Swart *et al*., 2020). Preloaded Arf-GDP and Arf-GTP mixtures could be incubated with the regulatory Sec7 and GAP domains, respectively, before being added to the Ni-NTA or glutathione plate. In this regard, potential inhibitors for the Arf activation cycle could also be screened for. The overall goal of the interaction assay experiments was to determine if *in vitro* binding of Arf proteins to the Arf-binding domains of GGA3 and JIP4 can be used to distinguish between *Pf*Arf1 and *Pf*Arf6 and whether *Pf*Arf6 correlated more with human Arf6 than Arf1. The preliminary results obtained from the experiments performed was that *Pf*Arf6 was able to bind to both GGA3 and JIP4, that *Pf*Arf6 was distinguishable from *Pf*Arf1 and, despite the higher sequence similarity between *Pf*Arf6 and human Arf1 compared to Arf6, the preliminary data shows that *Pf*Arf6 is an Arf6 homologue.

Chapter 4: Detection of regulator mediated Arf-GTPase activity using NDPK and luciferase.

4.1. Introduction

The intrinsic GTPase activity of small GTPases, including Arfs, is notoriously slow, so Arf-GTPase regulators are implemented in cells to mediate faster and tightly controlled GTP/GDP cycling (Kahn & Gilman, 1986). Arf GEFs activate Arfs by catalysing the exchange of bound GDP for GTP (Goldberg, 1998), whereas Arf GAPs deactivate Arfs by stimulating the hydrolysis of the bound GTP to GDP. It is specifically the Sec7 and GAP domains of Arf GEFs and GAPs, respectively, that mediate these functions and are conserved amongst all Arf GEFs and GAPs (Donaldson & Jackson, 2000). Sec7 domains contain a hydrophobic surface groove that binds the nucleotide binding site of Arf GTPases, which exposes conserved residues that insert into the GTPase active site to sterically and electrostatically expel GDP (Beraud-Dufour *et al*., 1998; Renault *et al*., 2003). GAP domains contain a zinc finger motif, with a conserved arginine residue, which is inserted into the nucleotide binding site to stabilise the transition state of the GTP hydrolysis reaction (Ismail *et al*., 2010; Cherfils & Zeghouf, 2013). Due to their high conservation and importance in cellular upkeep, Arf GTPase regulators are able to mediate the activity of more than one Arf isoform (Donaldson & Jackson, 2000). The exact specificity of regulators for a particular Arf subfamily member is debatable, especially when comparing *in vitro* and *in vivo* experiments. In the cell most GEFs and GAPs share subcellular localisations with their respective Arfs, such as the GEF and GAP ARNO (cytohesin-2) and ArfGAP1 being found in the vicinity of Arf6 and Arf1 at the plasma membrane and Golgi apparatus, respectively (Frank *et al*., 1998; Hernández-Deviez *et al*., 2004; Liu *et al*., 2005). However, *in vitro* studies have shown that the Sec7 domain of the cytohesin family of GEFS can activate all Arf subfamily members, and that the GAP domain of ArfGAP1 could deactivate both Arf1 and Arf6 (Knorr *et al*., 2000; Ogasawara *et al*., 2000; Macia *et al*., 2001; Bai *et al*., 2011).

Simple, robust GTPase activity assays are not readily available, particularly assays which can be carried out in microtiter plates and are thus amenable to the screening of compound libraries for Arf inhibitors. These assays have usually involved: coupling to NADPH reduction, the use of radioactive GTP substrates, or GTP/GDP-bound GTPase specific antibodies (Self & Hall, 1995; Eberth & Ahmadian, 2009). Overall, these assays are labour intensive, expensive, and are relatively inaccurate due to high background signals (Marshall *et al*., 2012). In general, assay methods involving bioluminescence have been shown to be more accurate, cost effective, and simple to perform in a high-throughput format (Karamohamed *et al*., 1999). Nucleoside diphosphate kinases (NDPKs) balance the nucleoside triphosphate (NTP) pools within the cell, in order to maintain cell homeostasis, and are highly conserved between prokaryotes and eukaryotes (Chakrabarty, 1998). They are able to reversibly transfer the γ-

phosphate of NTPs to other nucleoside diphosphates (NDPs), thus producing specific NTPs and NDPs for various cellular mechanisms. Within all NDPKs are the conserved invariant residues HGSD, whereby the histidine (H) at position 117 is phosphorylated and is involved in nucleotide binding (Almaula *et al*., 1995). It is through this phosphorylated enzyme intermediate that NDPK is able to reversibly transfer terminal phosphates (Chakrabarty, 1998). NTPs bind free NDPK, whereas NDPs bind, albeit with a lower affinity, to the phosphorylated (His117) enzyme (Lascu & Gonin, 2000). The relative cellular pools of available NDPs and NTPs dictate the direction of the NDPK kinase reaction. In mammalian cells, ATP is in abundance compared to other NTPs so is often a donor in NDPK reactions, whereas in lower organisms including *E. coli* and bacteria it is all dependent on cellular location and if the conversion reaction is at equilibrium (Lascu & Gonin, 2000; Yu *et al*., 2017). Thus, according to Le Chatelier's principle, the kinase reaction can be manipulated to force GTP to ATP conversion, using ADP as a substrate, which enables ATP detection using firefly luciferase. In this chapter, an *in vitro* Arf-GTPase activity assay was designed that incorporates both Arf and NDPK in a coupled bioluminescence format. The assay was performed in three separate steps: firstly an Arf-GTPase incubation (with or without the regulatory GEF and GAP domains) in the presence of GTP, followed by conversion of residual GTP to ATP by NDPK, and finally the ATP detection by firefly luciferase-mediated bioluminescence (**Figure 15**).

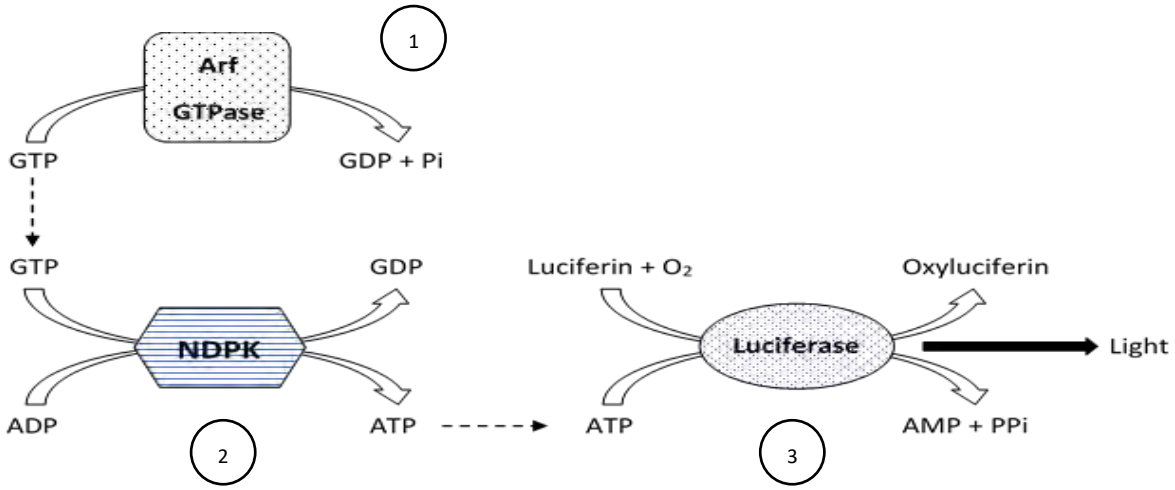

Figure 15: Schematic diagram representing the Arf-NDPK coupled bioluminescence assay principle.

Step 1: Arf-GTPase incubation containing Arf-GTPase (*Hs*Arf1; *Hs*Arf6; or *Pf*Arf1), Arf regulators (ARNO^{Sec7} (GEF) and/or GAP1^{GAP}), and GTP are carried out in a 96-well plate. Step 2: NDPK incubation, where an NDPK reaction mixture (NDPK, molar excess ADP) is added to each Arf-GTPase reaction well, converting any GTP left in the mixture to ATP. Step 3: Luciferase incubation, where the addition of luciferin and firefly luciferase converts any ATP in the well to AMP + PPi, oxyluciferin, and a photon. The luminescence is recorded in a plate reader (more GTP consumed/used by Arf-GTPase = less GTP converted to ATP by NDPK = less light produced by luciferase).

4.2. Aims & objectives

The overall intent for the Arf-NDPK bioluminescence assays was to determine whether the use of NDPK could detect Arf-GTPase activity *in vitro*. As intrinsic GTPase activity is slow, the Sec7 and GAP domains of ARNO and ArfGAP1, respectively, were introduced to determine whether NDPK could detect regulator stimulated Arf-GTPase activity *in vitro*. To achieve these aims, the following objectives were pursued using techniques and resources detailed in Chapter 5 (Methods and materials):

- Confirm that the luciferase-based ATP Bioluminescence Assay Kit (Sigma-Aldrich) could detect ATP linearly within a nanomolar to micromolar range (1 nM – 1 μM).
- Determine whether the expressed and purified NDPK (Chapter 3) was active and could convert GTP to ATP successfully.
- Determine whether the NDPK could convert a serial dilution of GTP to ATP in a linearly detected manner.
- Determine whether the intrinsic activity of *Hs*Arf1 could be detected, using NDPK, after an incubation with GTP.
- Determine whether the GTPase activity of *Hs*Arf1 could be stimulated by the addition of either the GAP domain of ArfGAP1 (promote GTP hydrolysis), or the Sec7 domain of ARNO (promote GDP/GTP exchange), or a combination of both.
- Determine whether the addition of either the Sec7 or GAP domains or a combination of both could stimulate *Hs*Arf6 or *Pf*Arf1 GTPase activity.

4.3. Results

4.3.1. NDPK GTP-to-ATP conversion activity

To find out whether the expressed His-tagged NDPK could convert nucleotide triphosphates, cellular amounts of ATP had to first be detected linearly in the presence of assay associated proteins. In a 96-well plate, a three-fold serial dilution of ATP (1 nM – 1 µM) was prepared in Arf assay buffer containing 1 µM *Hs*Arf1 and 20 nM NDPK. A luciferase containing ATP detection reagent (Sigma-Aldrich) was added to each ATP mixture, in a 1:1 volume ratio. The ATP standard curve generated was corrected for an ATP free background control, and with an R^2 value of 0.9979 (i.e. > 0.99), ATP detection proved linear (**Figure 16A**). As 1 nM ATP could be detected in the presence of *Hs*Arf1 and NDPK, a two-fold serial dilution of NDPK (1 nM – 100 nM) was prepared to determine whether NDPK could convert GTP to ATP, and the lower limit of NDPK needed to generate a linear GTP signal. NDPK reaction mixtures all contained 1 µM GTP as well as 5 µM ADP (molar excess) and were incubated for 10 min before the detection reagent was added in a 1:1 ratio. All NDPK mixtures generated a high luminescence signal after being corrected for GTP-free background control, containing 100 nM NDPK and 5 µM ADP, confirming GTP to ATP conversion by NDPK (**Figure 16B**). Luminescence values tended to be the highest between 12.25 and 25 nM NDPK, though the 25 nM value was not significantly different from 1 nM NDPK ($p = 0.17$).

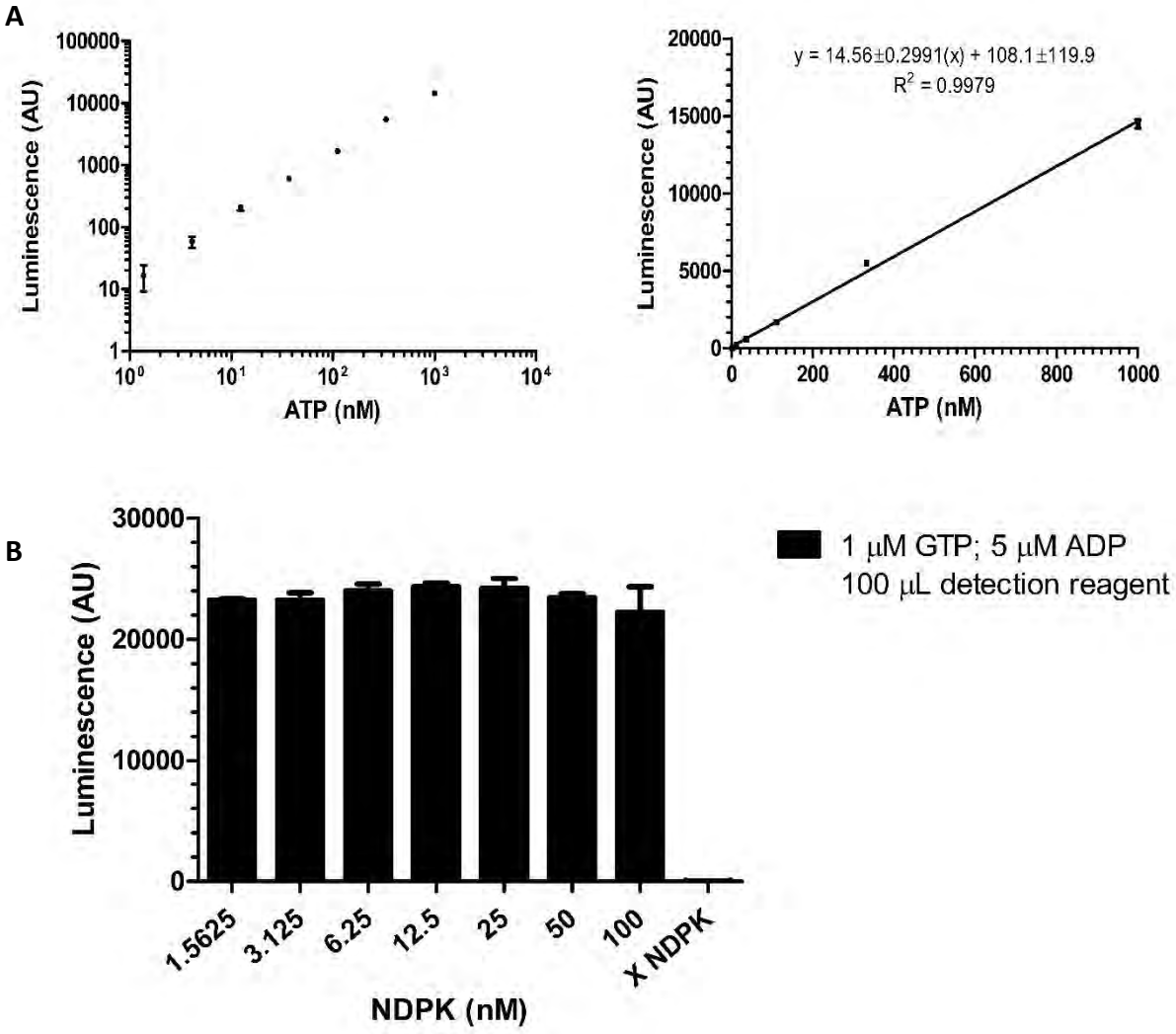

Figure 16: ATP standard curve (1 nM – 1 μM) and use of NDPK to detect GTP. (Left) Logarithmic scale; (Right) Linear scale showing line of best fit equation and R^2. **(A)** An ATP three-fold serial dilution (1.37 nm to 1 μM) was prepared in Arf assay buffer supplemented with *Hs*Arf1 and 20 nM NDPK, and added into a white 96-well plate. To each well, an equal volume of luciferase detection reagent was added (1:1 reaction mixture: detection reagent) and luminescence (AU) measured after a 5 min incubation. All values were corrected for background luminescence from an ATP free reaction mixture. **(B)** A two-fold serial dilution (1.56 nM – 100 nM) of NDPK was prepared in Arf assay buffer, and aliquoted into a white-walled 96-well plate. Each well contained a final concentration of 1 μM GTP and 5 μM ADP, and the plate was incubated for 10 min at room temperature. To each well an equal volume (100 μL) of luciferase detection reagent was added (1:1 reaction mixture: detection reagent) and luminescence measured, after a 5 min incubation. Each point represents the mean and standard deviation of triplicate readings.

Two three-fold serial dilutions of GTP (10 nM – 10 μM; 1 nM – 1 μM) were prepared in Arf assay buffer, with 20 nM NDPK and 5 μM ADP, to ascertain the linear GTP to ATP conversion range of NDPK (**Figure 17A – B**). Luciferase detection reagent was added to both mixtures, in a 1:1 ratio, after the NDPK incubation. The 10 μM GTP serial dilution displayed the upper range limit for linear GTP detection, as the line plateaued between 1 and 10 μM GTP, indicating NDPK incompletely converted GTP to ATP. This was supported by the generated R^2 value (0.8553) being below the 0.99 threshold (**Figure 17A**). The 1 μM GTP serial dilution, however, was converted to ATP in a more 'linear' fashion, as the R^2 value was 0.9971 (**Figure 17B**). NDPK conversion of 1 nM GTP to ATP was detectable, even after being corrected for a GTP free background control mixture. The 1 nM – 1 μM GTP serial dilution was repeated but using 50 μL detection reagent, instead of 100 μL, to establish whether a 2:1 ratio of reaction mixture to detection reagent would still produce a linear correlation. The measured GTP to ATP conversion by NDPK also appeared linear as the generated R^2 value (0.9875) met the 0.99 threshold (**Figure 17C**).

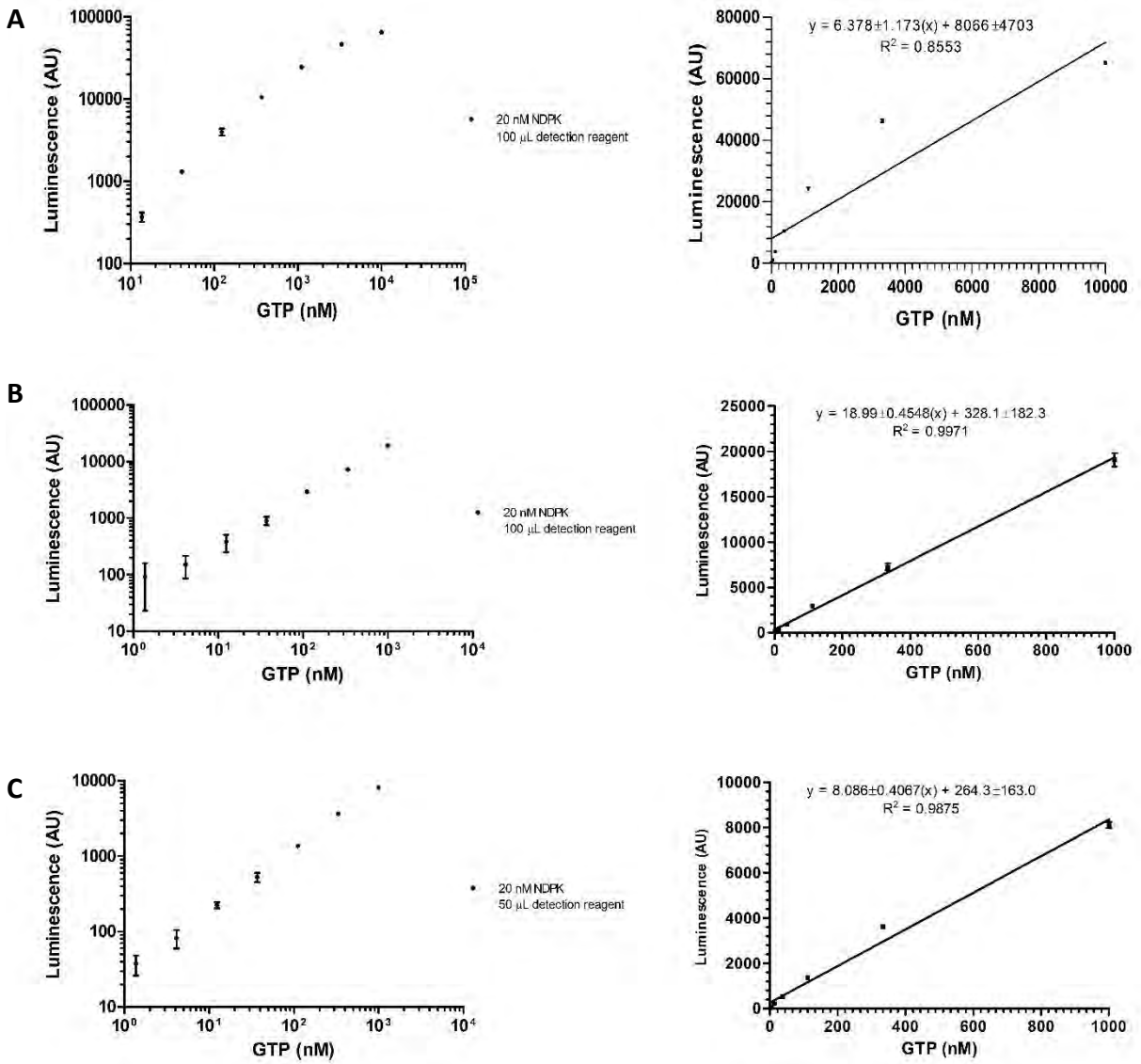

Figure 17: Optimisation of GTP-to-ATP conversion activity of NDPK. (Left) Logarithmic scale; (Right) Linear scale showing line of best fit equation and R^2. A series of GTP three-fold serial dilutions were prepared in Arf assay buffer, and were aliquoted into a white-walled 96-well plate: **(A)** 20 nM NDPK and GTP (13.7 nM – 10 µM); **(B – C)** 20 nM NDPK and GTP (1.37 nM – 1 µM). Each well contained 5 µM ADP and the plate was incubated for 10 minutes at room temperature, before a volume of luciferase detection reagent was added: **(A – B)** 100 µL (1:1 reaction mixture: detection reagent); **(C)** 50 µL (2:1 reaction mixture: detection reagent). Luminescence was measured after a 5 min incubation at room temperature and all values were corrected for background luminescence from a GTP free reaction mixture. Each point represents the mean and standard deviation of triplicate readings.

4.3.2. Arf-NDPK coupled reaction

Arf-GTPases have extremely slow intrinsic GTPase activity, thus their full GTPase capacities are only seen when in the presence of their GTPase regulators, namely guanine nucleotide exchange factors (GEFs) and GTPase-activating proteins (GAPs). Thus, to determine whether NDPK could detect Arf-GTPase activity, the regulators would presumably have to be included. ARNO^{Sec7} and GAP1^{GAP} display *in vitro* GEF and GAP activity, respectively, on *Hs*Arf1 (Swart *et al*., 2020). Thus, the initial GTPase activity assay was tested with *Hs*Arf1 in conjunction with ARNO^{Sec7} and GAP1^{GAP}. *Hs*Arf1 (1 µM) reaction mixtures, with/without ARNO^{Sec7} and/or GAP1^{GAP} (0.2 µM), were prepared in Arf assay buffer and allowed to incubate for 60 or 120 min (room temperature; gentle agitation), before the standard NDPK reaction mixture (20 nM NDPK; 5 µM ADP final concentrations) was added to each Arf mixture (**Figure 18**). After the NDPK incubation the luciferase containing detection reagent was added, in a 1:1 ratio, to each Arf-NDPK reaction mixture. Negative control reaction mixtures were also prepared, containing: ARNO^{Sec7}, GAP1^{GAP} or ARNO^{Sec7} and GAP1^{GAP}; as well as assay buffer alone, to show that the regulatory proteins themselves did not display any GTPase activity. Each reaction contained 2 µM GTP, so the buffer only control indicated the total amount of input GTP, whereas the *Hs*Arf1 only mixture served as the intrinsic GTPase activity control. The *Hs*Arf1 + GAP1^{GAP} experimental mixtures displayed a significant decrease in light output (i.e significant increase in GTP hydrolysed (%), see **Figure 15**) after 60 and 120 min, namely 1.6 % ($p = 0.042$) and 16.3 % ($p = 0.019$), respectively, when compared to the GAP1^{GAP} control. The *Hs*Arf1 + GAP1^{GAP} + ARNO^{Sec7} experimental mixtures were similar, displaying 2.4 % ($p = 0.0049$) and 10.0 % ($p = 0.0070$) GTP hydrolysed after 60 and 120 min, respectively, when compared to the GAP1^{GAP} + ARNO^{Sec7} control. The *Hs*Arf1 + ARNO^{Sec7} experimental mixtures displayed no significant change in light output after 120 min.

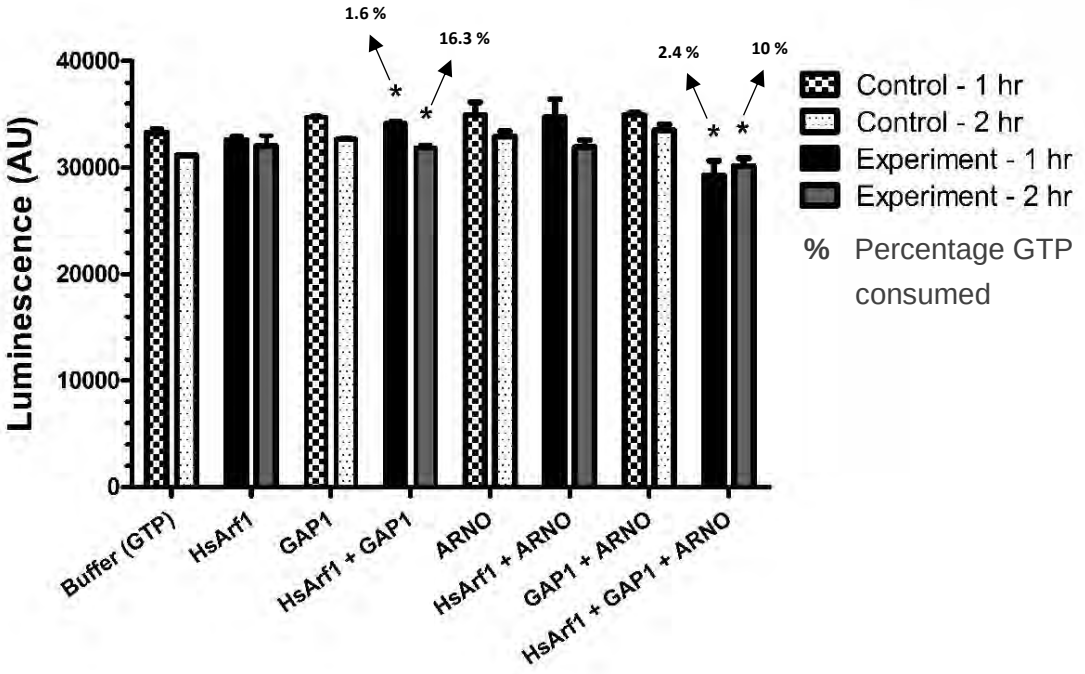

Figure 18: Initial attempt to detect regulator mediated *Hs*Arf1 activity using NDPK. Arf GTPase reaction mixtures were prepared (*Hs*Arf1 in the presence of $GAP1^{GAP}$ and/or $ARNO^{Sec7}$; each protein on their own as controls) in assay buffer, and added into a white-walled 96-well plate wells. The plate was incubated for 60 or 120 min at room temperature, with gentle agitation, before a NDPK reaction mixture was added to each well (100 µL Arf-NDPK reaction mixture: 1 µM *Hs*Arf1, 2 µM GTP, 0.1 µM $ARNO^{Sec7}$ and/or 0.1 µM $GAP1^{GAP}$; 20 nM NDPK, 5 µM ADP). The plate was incubated for 10 min at room temperature, before a volume of luciferase detection reagent was added (1:1 – Arf-NDPK reaction mixture: detection reagent). Luminescence was recorded, using a Spectramax M3 (Molecular Devices) plate reader, immediately after a 5 min luciferase incubation. Arf assay buffer consisted of 15 mM HEPES, pH 7.4, 150 mM KCl, 1 mM $MgCl_2$,1 mM DTT. Each point represents the mean and standard deviation of triplicate readings. (*) = p-value < 0.05, when comparing an experimental mixture to its respective control.

The above assay method was adjusted slightly in order to obtain a more quantifiable amount of GTP hydrolysis (i.e. a greater decrease in light output compared to the respective controls). First, the total Arf-NDPK reaction mixture was doubled in volume, while maintaining the volume of detection reagent (i.e. now a 2:1 reaction mixture to detection reagent ratio). This change in total reaction volume prompted the 1 µM – 1 nM GTP serial dilution with 20 nM NDPK, using 50 µL detection reagent (**Figure 17C**). The generated R^2 value of 0.9875 just met the 0.99 threshold, confirming a 2:1 reaction mixture to detection reagent ration could still detect 1 nM - 1 µM GTP. Along with the total reaction volume change, the Arf-GTPase incubation time (now 90/180 minutes), as well as the GTP and $ARNO^{Sec7}$/$GAP1^{GAP}$ concentrations (now 1 µM and 0.5 µM, respectively) were increased. Lastly the Arf-GTPase incubation step (90/180 min) was first conducted in round-bottom plates, before being transferred to white-walled plates, to improve the mixing of small reagent volumes added to the

reaction. The adjusted *Hs*Arf1-NDPK assay method resulted in a larger decrease in light generated, i.e. an increased amount of input GTP was hydrolysed (**Figure 19**). A significant amount of GTP was consumed (light decrease) as observed in the *Hs*Arf1 + GAP1^{GAP} experimental mixtures, namely 25.5 % ($p = 0.000071$) and 31.6 % ($p = 0.000072$) after 90 and 180 min, respectively when compared to the GAP1^{GAP} control. The *Hs*Arf1 + GAP1^{GAP} + ARNO^{Sec7} experimental mixtures registered greater amounts of consumed GTP after 90 and 180 minutes, namely 31.9 % ($p = 0.00024$) and 59.7 % ($p = 0.00015$), respectively, when compared to the GAP1^{GAP} + ARNO^{Sec7} control. No significant change in luminescence, when compared to the ARNO^{Sec7} control, was observed for the *Hs*Arf1 + ARNO^{Sec7} experimental mixtures after 90 and 180 min. Slight intrinsic GTPase activity was observed, after 180 min for *Hs*Arf1 compared to buffer only (input GTP) control, of 8.2 % ($p = 0.0088$) (**Figure 19**).

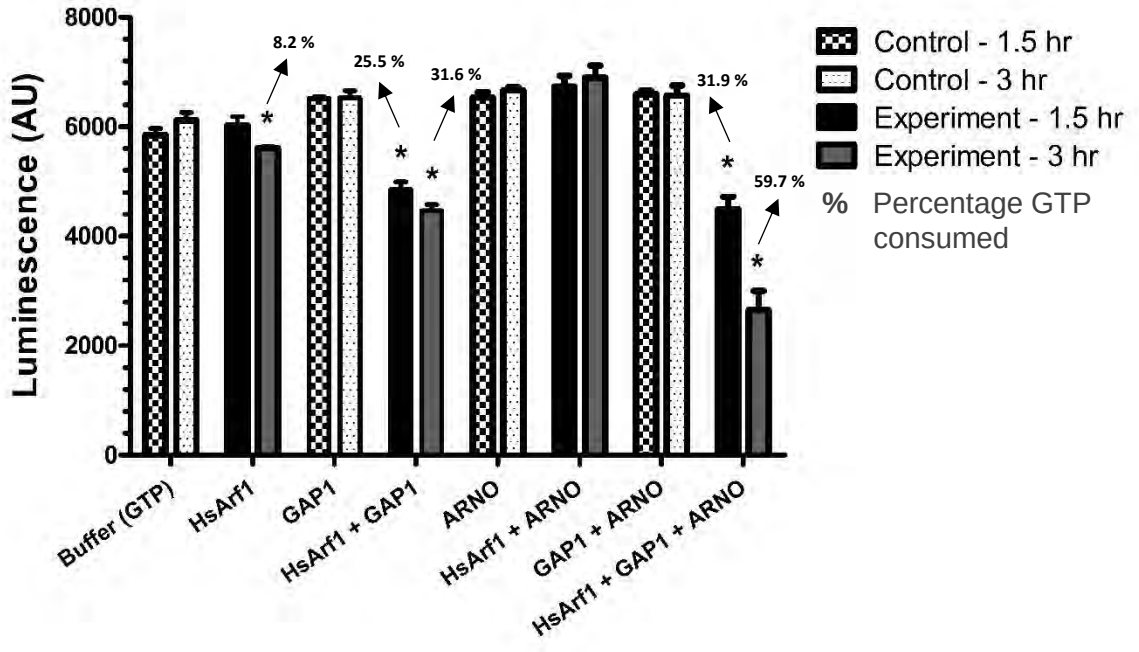

Figure 19: Detection of regulator mediated *Hs*Arf1 GTPase activity. Arf GTPase reaction mixtures were prepared (*Hs*Arf1 in the presence of GAP1^{GAP} and/or ARNO^{Sec7}; each protein on their own as controls) in assay buffer and added into a round-bottom 96-well plate wells. The plate was incubated for 90 or 180 min at room temperature, with gentle agitation, before being transferred to a white-walled 96-well plate. A NDPK reaction mixture was added to each well (200 µL Arf-NDPK reaction mixture: 1 µM *Hs*Arf1, 1 µM GTP, 0.5 µM ARNO^{Sec7} and/or 0.5 µM GAP1^{GAP}; 20 nM NDPK, 5 µM ADP). The plate was incubated for 10 min at room temperature, before a volume of luciferase detection reagent (half of Arf-NDPK mixture volume) was added (2:1 – reaction mixture: detection reagent). Luminescence was recorded, using a Spectramax M3 (Molecular Devices) plate reader, immediately after a 5-minute luciferase incubation. Arf assay buffer consisted of 15 mM HEPES, pH 7.4, 150 mM KCl, 1 mM $MgCl_2$,1 mM DTT. Each point represents the mean and standard deviation of triplicate readings. (*) = p-value < 0.05, when comparing an experimental mixture to its respective control.

As GAP1^{GAP} + ARNO^{Sec7} stimulated *Hs*Arf1-GTPase activity was detected, the same Arf-NDPK assay protocol was repeated with *Hs*Arf6 and *Pf*Arf1, using the same GTPase regulators (**Figure 20**). No intrinsic GTPase activity was observed after 90 or 180 min for *Hs*Arf6 and *Pf*Arf1, respectively. For *Hs*Arf6, the significant amount of GTP consumed (light decrease) in the *Hs*Arf6 + GAP1^{GAP} + ARNO^{Sec7} reaction mixture was 49.4 % ($p = 0.0057$) and 77.3 % ($p = 0.000018$) after 90 and 180 min, respectively, whereas for the *Hs*Arf6 + GAP1^{GAP} reaction mixture it was 27.7 % ($p = 0.011$) and 37.6 % ($p = 0.00031$), respectively, when compared to the GAP1^{GAP} + ARNO^{Sec7} and GAP1^{GAP} controls. The *Hs*Arf6 + ARNO^{Sec7} reaction mixture, on the other hand, lead to no significant change in light generated after 90 or 180 min (**Figure 20A**). For *Pf*Arf1, the significant amount of GTP consumed (light decrease) in the *Pf*Arf1 + GAP1^{GAP} + ARNO^{Sec7} reaction mixture was 16.5 % ($p = 0.0014$) and 27.8 % ($p = 0.000090$) after 90 and 180 min, respectively, whereas for the *Pf*Arf1 + GAP1^{GAP} reaction mixture it was only 8.3 % ($p = 0.014$) and 13.6 % ($p = 0.0043$), respectively, when compared to the GAP1^{GAP} + ARNO^{Sec7} and GAP1^{GAP} controls. Unexpectedly, the *Pf*Arf1 + ARNO^{Sec7} reaction mixture generated a substantial 42.1 % ($p = 0.0020$) and 36.2 % ($p = 0.000025$) increase in light generated after 90 and 180 min, respectively, when compared to the ARNO^{Sec7} control (**Figure 20B**). Both experimental setups were repeated in the exact same manner, except in an adjusted assay buffer (adapted from Mondal *et al*, 2015) intended to promote Arf-GTPase activity. However, this produced less GTPase activity than the Arf assay buffer used here and the results are shown in the Appendix (**Figures A3 – A5**).

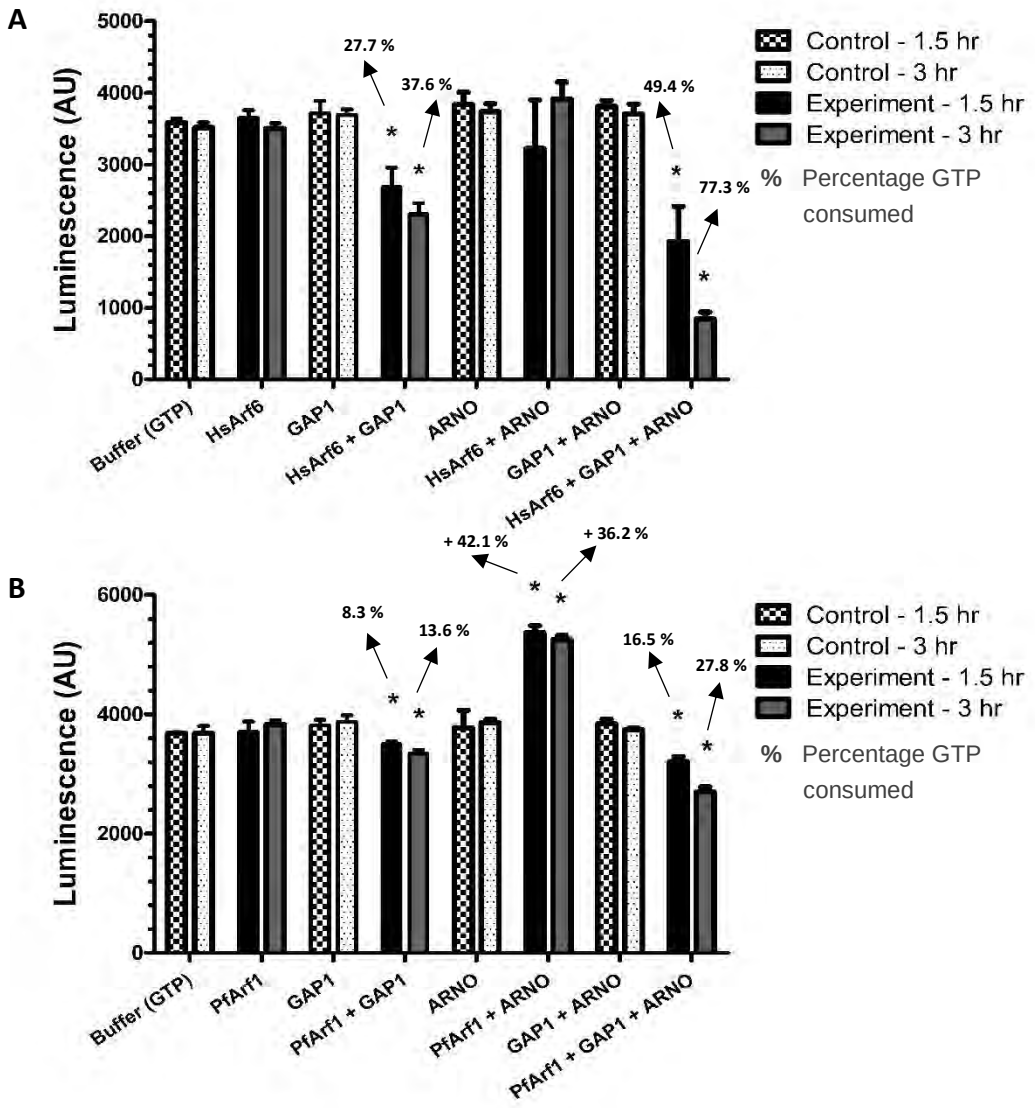

Figure 20: Detection of *Hs*Arf6 and *Pf*Arf1 GTPase activity, using *Hs*Arf1 regulators. Arf GTPase reaction mixtures were prepared (**(A)** *Hs*Arf6; or **(B)** *Pf*Arf1, in the presence of $GAP1^{GAP}$ and/or $ARNO^{Sec7}$; each protein on their own as controls) in assay buffer added into a round-bottom 96-well plate wells. The plate was incubated for 90 or 180 min at room temperature, with gentle agitation, before being transferred in a white-walled 96-well plate. A NDPK reaction mixture was added to each well (Arf-NDPK reaction mixture: 1 µM **(A)** *Hs*Arf6; or **(B)** *Pf*Arf1, 1 µM GTP, 0.5 µM $ARNO^{Sec7}$ and/or 0.5 µM $GAP1^{GAP}$; 20 nM NDPK, 5 µM ADP). The plate was incubated for 10 min at room temperature, before a volume of detection reagent was added (2:1 – reaction mixture: detection reagent). Luminescence was recorded, using a Spectramax M3 (Molecular Devices) plate reader, immediately after a 5-minute luciferase incubation. The Arf assay buffer consisted of 15 mM HEPES, pH 7.4, 150 mM KCl, 1 mM $MgCl_2$,1 mM DTT. Each point represents the mean and standard deviation of triplicate readings. (*) = p-value < 0.05, when comparing an experimental mixture to its respective control.

4.4. Discussion

As for most small GTPases, Arfs, as well as their regulators, have been implicated in human disease and their roles in many pathologies continue to be discovered. With Arf GTPase known to display little to no intrinsic activity, their activity is tightly regulated by pools of GEFs and GAPs (Kahn & Gilman, 1986). The alterations in diseases such as the majority of cancers, include the amplification of Arf GEFs and GAPs. The amplified pool of available active Arf GTPases and their regulators is thought to be how the increased level of demand is met for cancer cell homeostasis (Li *et al*., 2014; Qi *et al*., 2017; Li *et al*., 2017). In malaria and host RBC infection, vesicle-mediated trafficking of *Plasmodium* proteins and the endocytosis of surrounding RBC cytoplasm are key processes. During this intraerythrocytic stage of the parasite life cycle, trafficking machinery including Arf GTPases are of considerable importance (Cook *et al*., 2010; Ebrahimzadeh *et al*., 2018). Thus, the ability to screen for inhibitors of the full Arf GTPase cycle in a simple, high-throughput manner, would prove highly beneficial in an *in vitro* setting.

The NDPK expressed from *E. coli* was able to convert 1 µM GTP to ATP, and the conversion was not dependent on NDPK concentration over the range of 100 nM to 1.56 nM enzyme. To compensate for possible degradation of NDPK during storage between experiments, 20 nM NDPK was used for all subsequent assays. NDPK was shown to covert GTP to ATP efficiently in a linear fashion over the range of 1 µM to 1.37 nM GTP. The initial *Hs*Arf1-NDPK assay format was able to detect a statistically significant percentage of GTP consumption after 60 and 120 min, respectively, albeit very low. A study performed by Mondal *et al*. (2015), utilised a similar GTPase and NDPK bioluminescence assay system with Ras GTPases, however the GTPase incubation times with regulators were between 90 and 180 min, the amount of GTP added was lower, and the concentration of regulators used was higher. The adjusted assay conditions led to more quantifiable GTP consumption (i.e. decrease in light output) by *Hs*Arf1. With these changes, the adjusted *Hs*Arf1-NDPK assay was able to generate a significant decrease in luminescence, i.e. a more robustly quantifiable amount of GTPase activity was detected (more suitable for future inhibition screening). According to the adjusted *Hs*Arf1-NDPK assay:luciferase detection reagent volume ratios, NDPK was shown to convert 1.37 nM to ATP and was detected by firefly luciferase in a linear fashion, thus the NDPK/luciferase component of the assay setup was still able to detect slight changes in input GTP. In the study performed by Mondal *et al*. (2015), their NDPK/luciferase assay components were screened with the LOPAC library (1280 pharmacologically active compound), of which only two compounds showed any interference. These two compounds, luciferase inhibitors, only reduced the luminescence signal by 20 - 25 %, and no compound affected NDPK activity. Thus, in future drug screening using this assay system, it increases the possibility that any hit causing a reduced signal would be from inhibition of the GTPase activity

cycle and not from an interference of the NDPK/luciferase components, although this would still need to be controlled for. GAP1^{GAP} stimulated *Hs*Arf1 GTPase activity, which was stimulated even further by the addition of ARNO^{Sec7}, was expected as they have been shown to act on Arf1 *in vitro* (Ogasawara *et al*., 2000; Macia *et al*., 2001).

After 180 min, *Hs*Arf6 displayed the greatest GAP1^{GAP} stimulated GTP consumption of 38 %, followed by *Hs*Arf1 and *Pf*Arf1 with 32 % and 14 %, respectively. Total GTP consumption after 180 min with the full set of regulators (including GAP1^{GAP} + ARNO^{Sec7}) displayed a similar order with 77 %, 60 %, and 28 % input GTP being hydrolysed by *Hs*Arf6, *Hs*Arf1, and *Pf*Arf1, respectively. *Hs*Arf6 displaying greater GAP1^{GAP} stimulated GTPase activity than *Hs*Arf1 was unexpected as ArfGAP1 is mostly known as an Arf1 GAP *in vivo*. The greater amount of input GTP consumed by *Hs*Arf6 in the presence of GAP1^{GAP} and ARNO^{Sec7}, may be due to ARNO being known as an Arf6 GEF *in vivo* (Frank *et al*., 1998; Liu *et al*., 2005). Whereas there was slight intrinsic *Hs*Arf1 GTPase activity observed of 8.24 %, neither *Hs*Arf6 nor *Pf*Arf1 displayed any detectable intrinsic GTPase activity after 180 min, respectively, which was to be expected (Kahn & Gilman, 1986). The ARNO^{Sec7} stimulated *Hs*Arf1 and *Hs*Arf6 experimental wells displayed no significant change in light output after 180 min, which was to be expected as the continuous tryptophan fluorescence figures implied that the His-tagged Arfs were purified in predominantly GTP-bound form (previous chapter). Unexpectedly though, the ARNO^{Sec7} stimulated *Pf*Arf1 experimental wells displayed a 42 % and 36 % increase in light output after 60 and 180 min, respectively. The reason(s) for this phenomenon are not known and may require further investigation, such as whether the combination of proteins stimulates the activity of firefly luciferase. The same assay format was not performed on *Pf*Arf6, due to the questionable stability of the protein under the storage conditions used (Chapter 3). *Pf*Arf1 is highly homologous to *Hs*Arf1, sharing 78.66 % sequence identity. GAP and Sec7 regulatory domains have been shown to stimulate the activity of *Pf*Arf1 *in vitro* using plate immobilisation assays (Swart *et al*., 2020), so even with GAP1^{GAP} and ARNO^{Sec7} present, the overall GTPase activity of *Pf*Arf1 may be lower than that of $^{N\Delta17}$*Hs*Arf1 and *Hs*Arf6. However, it should be noted that GAP and Sec7 domains from human ArfGAP1 and ARNO, respectively, were used this study. Unlike with mammalian cells, the *P. falciparum* genome only encodes for one GEF and two GAPs (Baumgartner *et al*., 2008; Cook *et al*., 2011). Malarial Arf GTPase activity assays in future would benefit from using the Sec7 and GAP domain of these malarial regulators. Inhibition screening would then focus on the entire malarial Arf GTPase cycle, and thus may prove more efficient in stimulating *Pf*Arf1 activity. These malarial regulators could also be compared to the GEF and GAP activity of other regulators

Just as the inclusion of a *P. falciparum* Sec7 and GAP would benefit in screening for malarial inhibitors, so would the inclusion of other specific Sec7 and GAP domains, especially used with *Hs*Arf6, promote the screening for cancer therapeutics. Expression of ARNO is upregulated in colon and liver cancer (Xu *et al*., 2013; Pan *et al*., 2014). Other Arf6 GEFs utilised in the progression of various cancers are

BRAG2, general receptor for phosphoinositides-1 (GRP1/cytohesin-3), and EFA6. BRAG2 is upregulated in breast, lung, and pancreatic cancer, whereas GRP1 is upregulated in liver cancer (Morishige *et al*., 2007; Menju *et al*., 2011; Xie *et al*., 2012; Fu *et al*., 2014). EFA6 is upregulated in glioma and renal cell carcinoma (Li *et al*., 2006; Hashimoto *et al*., 2016), however, it is also downregulated in breast, brain, and ovarian cancer (Pils *et al*., 2005; van den Boom *et al*., 2006; Zangari *et al*., 2014). The Sec7 domain of ARNO and EFA6 only share 30 % sequence identity (Franco *et al*., 1999), thus the addition of the EFA6 Sec7 domain would also contribute towards determining Arf GEF specificity towards Arfs *in vitro*. An *in vitro* study performed by Macia *et al*., (2001), suggested that the specificity of EFA6 and ARNO for Arf6 and Arf1, respectively, is determined by their Sec7 domains. The inclusion of Arf6 specific GAPs that are involved in cancer, such as GIT1/2, ASAP1, SMAP1, and ARAP3 would also promote cancer therapeutic screening. GIT1 and ASAP1 are both highly expressed in multiple types of cancers including breast, colon, head and neck, liver, melanoma, and renal cell carcinoma (Ehlers *et al*., 2005; Onodera *et al*., 2005; Müller *et al*., 2010; Peng *et al*., 2013; Chan *et al*., 2014; Sato *et al*., 2014; Lu *et al*., 2016). However, GIT2, SMAP1, and ARAP3 have been shown to be downregulated in breast, colon, and gastric cancer, respectively (Yagi *et al*., 2011; Sangar *et al*., 2013; Sirirattanakul *et al*., 2015). As some of the GEFs and GAPs are downregulated in particular cancers, screening for compounds that would enhance their GEF/GAP activity on Arf6 may also prove useful as a therapeutic tool.

Optimisation of the assay protocol, whereby closer to 100 % of the input GTP is consumed, would serve as very useful high-throughput screening platform for inhibitors of the regulation of Arf GTPase activity. Serial dilutions of the assay components (GEF/GAP concentration; GTP concentration) would shed more light on the concentration of components needed to consume all the input GTP, so as to increase the detection window for GTPase activity inhibition in future drug screening. By serially diluting Arf, one would be able to obtain apparent Km (Michaelis constant) values, thus generating Arf GTPase activity profiles for particular Sec7 and GAP domains. The assays could also be performed with a serial dilution of either the Sec7 or GAP domain and determine specific concentrations of the regulator domains required to stimulate half-maximal Arf activity (EC_{50}), which would provide a more accurate picture of the GEF and GAP specificity of each Arf GTP *in vitro*. In addition to manipulating the concentration of assay components, there are various types of mutations of the Arfs GTPases themselves that could be used to improve the interpretation of the assays. Using constitutively active (GTP-bound), constitutively inactive (GDP-bound), and fast cycling Arf GTPase mutants may serve as controls for inhibitor screening (Macia *et al*., 2004; Montagnac *et al*., 2011; Mondal *et al*., 2015). Arf GTPase chimera mutations, whereby the interswitch region of an Arf is swapped for the interswitch of other Arf GTPases, may also be used. It was the *in vivo* use of Arf chimeras like this that identified the QS motif adjacent to the switch I region, which is used as a signature to identify Arf6 homologues (Al-Awar *et al*., 2000). Combining the activity mutations with the chimeras may contribute towards

determining GEF and GAP specificity towards Arfs *in vitro* (Bhatt *et al*., 2019; Quilty *et al*., 2018). SecinH3 and QS11 are known Arf GEF and GAP inhibitors, respectively, which have been used in our research group before. SecinH3 has been shown to inhibit cytohesin family and BRAG2 GEF activity (Hafner *et al*., 2006; Grossmann *et al*., 2013), whereas QS11 is the only reported inhibitor of ArfGAP1 (Zhang *et al*., 2007). These inhibitors could be incorporated into the assay setup, in a serial dilution to obtain the required concentration of SecinH3/QS11 to inhibit Arf GEF and GAP activity by half (IC_{50}). The IC_{50} values for each inhibitor on a particular Sec7 or GAP domain may be used to compare with future screened hits.

These data would prove invaluable to the effector binding specificity assays as an orthogonal activity assay at the very least. As suggested in the possible applications of the immobilisation assays in the previous chapter, preloaded Arf-GDP could be incubated with GTP and a Sec7 domain, and preloaded Arf-GTP could be incubated with a GAP domain, before being added onto the nickel or glutathione coated plates. The effector binding signals with Arf-GDP and Arf-GTP only would thus serve as controls for the activity of the Sec7 or GAP domains. The *in vitro* specificity of the Sec7 and GAP domains of other Arf GEFs and GAPs, determined using serial dilutions, may also help distinguish between Arf1 and Arf6 homologues. For example, if a particular Sec7 or GAP domain is found to be more active on human Arf6 than Arf1 and shares a similar profile with the malarial proteins may also help distinguish whether the *Pf*Arf6 Arf protein correlates more to an Arf6 or Arf1 homologue. Overall, the goal was to establish a novel *in vitro* Arf GTPase activity. Regulator stimulated Arf GTPase activity was eventually detectable, and to varying degrees, owing to the Arf specificity of the $GAP1^{GAP}$ and $ARNO^{Sec7}$ domains used. The groundwork for a simple, high-throughput assay system has been laid for the detection of the full Arf GTPase activity cycle, as well as a means of determining Arf GTPase specificity for regulators (and vice versa) *in vitro*.

Chapter 5: Methods and materials

5.1. Constructs

Plasmid constructs used in this study were: pET-28a-*Hs*Arf1$^{N\Delta17}$ and pET-28a-*Pf*Arf1$^{N\Delta17}$ (donated by T. Swart, PhD thesis), pET-28a-*Hs*Arf6$^{N\Delta13}$ and pET-28a-*Pf*Arf6$^{N\Delta17}$ (donated by F. Khan, Masters dissertation), pET-28a-*Ec*NDPK, pET-28a-ARNO^{Sec7}, pET-28a-ArfGAP1^{GAP}, pGEX-4T-2-hGGA3^{GAT} and pGEX-4T-1-JIP4^{LZII}.

The coding sequences of $^{N\Delta17}$*Pf*Arf1 (PlasmoDB ID PF3D7-1020900) and $^{N\Delta17}$ *Pf*Arf6 (PlasmoDB ID PF3D7-1034700) had previously been PCR amplified from templates containing the codon-optimised sequences for human expression (supplied by GensScript, Hong Kong) and sub-cloned into the *Nhe*I/*Bam*HI restriction sites of pET-28a. The $^{N\Delta17}$*Hs*Arf1 and $^{N\Delta13}$*Hs*Arf6 sequences were amplified from pArf1-CFP-N1 and pArf6-CFP-N1 (Addgene plasmids 11381 and 11382; gifts from Joel Swanson) and respectively sub-cloned between the *Nhe*I/*Bam*HI and *Bam*HI/*Xho*I sites of pET-28a (T. Swart, F. Khan). These constructs were used to produce the respective N-terminally His-tagged Arf GTPase proteins, minus their N-terminal amphipathic helix, in *E. coli*. Hereafter, these proteins were referred to as *Hs*Arf1, *Hs*Arf6, *Pf*Arf1, and *Pf*Arf6.

pET-28a-*Ec*NDPK, pET-28a-ARNO^{Sec7} and pET-28a-ArfGAP1^{GAP} were used to produce His-tagged *E. coli* NDPK (GenBank KXG98239.1), the Sec7 domain (amino acids 51 – 253) of human ARNO (NP_004219.3) and the GAP domain (amino acids 1 – 140) of human ArfGAP1 (NP_060679.1), respectively. In all cases the coding sequences were optimised for *E. coli* expression, cloned between the *Nhe*I/*Bam*HI restriction sites of pET-28a and supplied by GenScript. Hereafter, these proteins were referred to as NDPK, ARNO^{Sec7} and ArfGAP1^{GAP}.

pGEX-4T-2-hGGA3^{GAT} and pGEX-4T-1-JIP4^{LZII} constructs were used to produce GST-fusion proteins with the binding domains of Arf GTPase effector proteins in *E. coli*. The pGEX-4T-2-hGGA3^{GAT} construct, a gift from Kazuhisa Nakayama (Addgene construct # 79436), contained the code for the GAT domain (amino acids 107 – 286) of human GGA3. The coding sequence of the leucin zipper (LZII) domain (amino acids 381 - 475) of human JIP4 (NP_001124000.1) were codon-optimised for expression in *E. coli*, cloned into the *Bam*HI/*Xho*I sites of pGEX-4T-1 and supplied by GenScript (Hong Kong). Hereafter, these proteins were referred to as GGA3^{GAT} and JIP4^{LZII}.

5.2. Transformed *E. coli* stock solution preparation

5.2.1. Preparation of competent *E. coli* cells

The various *E. coli* cells used in this study were T7 Express lysY/Iq (New England Biolabs), XL-10 Gold (Stratagene), and Rosetta (DE3) cells (Novagen). Untransformed *E. coli* cells were grown overnight at 37°C in 5 mL Luria broth with shaking, from either a colony on a plate or from a frozen glycerol stock. The 5 mL of untransformed *E. coli* was split equally into 100 mL Luria broth each (1 in 40 inoculum) and incubated at 37°C, with shaking, until a 0.6 – 0.8 OD_{600nm} reading was reached. The cells were centrifuged at approximately 2000 *g* for 10 min at 4°C, with the pellets kept on ice afterwards. The two pellets were resuspended in 4 mL ice-cold RF-1 buffer (100 mM KCl, 50 mM $MnCl_2$, 30 mM potassium acetate, 10 mM $CaCl_2$, 15 % (v/v) glycerol) each, then incubated on ice for 20 min. The suspensions were centrifuged at approximately 1500 *g* for 10 min at 4°C, and the pellets re-suspended in 3 mL ice-cold RF-2 buffer (10 mM HEPES, 10 mM KCl, 75 mM $CaCl_2$, 15 % (v/v) glycerol) each.

5.2.2. Transformation of competent cells

To 50 µL of competent *E. coli* cells, thawed on ice, 0.1-1 µg of pure plasmid was added and mixed gently before being incubated on ice for 30 min. The cells were subjected to heat-shock by incubation at 42.5°C for 1 min in a heating block, then incubated on ice for 5 min. To each transformation sample, 500 µL of Luria broth was added, followed by an incubation at 37°C for 60 min. Approximately 50 µL of each transformation sample was plated on LB-agar-KAN plates (containing 50 $\mu g.mL^{-1}$ kanamycin) or LB-agar-AMP plates (containing 50 $\mu g.mL^{-1}$ ampicillin) and allowed to dry. The plates were then inverted and incubated overnight at 37°C. Autoclaved pipette tips were used to remove a single colony from each plate and placed into respective McCartney bottles containing 3 mL of LB broth and 20 µL of 10 $mg.mL^{-1}$ kanamycin/ampicillin. After being incubated overnight at 37 °C, 850 µL of each overnight culture was added to 150 µL of glycerol and stored at -80 °C.

5.2.3. Alkaline lysis plasmid miniprep

To obtain plasmid minipreps for diagnostic restriction digests, scrapings from *E. coli* glycerol stocks were added to 5 mL Luria broth (containing 50 $\mu g.mL^{-1}$ kanamycin) and incubated overnight at 37°C, with shaking. Overnight cultures were pelleted in a microfuge at approximately 3000 *g* for 3 min and the *E. coli* pellets re-suspended in 100 µL GTE buffer (25 mM Tris, pH 8.0, 30 mM glucose, 10 mM EDTA, 10 $\mu g.mL^{-1}$ RNase). A 200 µL cell lysis solution (0.2 N NaOH, 1% (w/v) SDS) was added to the re-suspensions, with vigorous shaking, followed by termination using 150 µL of a 5 M potassium

acetate solution (pH 4.8). The solutions were centrifuged in a microfuge, at approximately 17 000 *g* for 5 min to pellet the precipitate and 400 µL of supernatant extracted from each solution. To precipitate and then pellet the plasmid DNA, 850 µL of absolute ethanol was added to the extracted supernatants, followed by centrifugation in a microfuge at approximately 17 000 *g* for 6 min, where after the supernatant was removed. The pellets were washed in a 1 mL of 70 % (v/v) ethanol solution, air-dried and dissolved in 50 µL water after all the ethanol was removed. Alkaline lysis minipreps were stored at -20°C.

5.2.4. Diagnostic restriction digestion

To digest plasmid from the alkaline lysis miniprep, the following digest mixture was prepared (41 µL): 30 µL molecular biology grade water, 6 µL of plasmid minprep, 4 µL of 10 × Thermoscientific Fast Digest buffer, and 0.5 µL of each Thermoscientific FastDigest restriction enzyme required for the plasmid (*Xho*I and *Nhe*I for pET-NDPK). Digest mixtures were incubated at 37 °C for 3 h and stored at -20°C until further use.

5.2.5. Agarose gel electrophoresis

Agarose gels (0.8 %) were prepared by heating 0.4 g agarose (Seakam LE) in 50 mL of 1X TBE buffer (100 mM Tris, 100 mM boric acid, 2 mM EDTA) until it was fully dissolved. Once the gel had cooled slightly 12 µL of 1 $mg.mL^{-1}$ ethidium bromide was added and the solution poured into a casting tray to set for 1 hour, before being submerged in 1 × TBE buffer within a gel buffer tank. A sample loading buffer (7 mL of 1 × TBE buffer, 3 mL of glycerol, 0.025 % bromophenol blue) was prepared and 7 µL added to each plasmid miniprep restriction digest mixture (41 µL), after which, 30 µL was loaded into the gel sample wells. The ladder well was loaded with 5 µL of the DNA ladder sample solution (5 µL 1kb DNA ladder (Promega, G571A), 15 µL water, 3.5 µL sample loading buffer). Diagnostic gels were run at 100 V for 1 h and then photographed under UV light using the ChemiDoc XRS+ gel documentation system (Bio-Rad).

5.3. Protein expression and purification

5.3.1. Analytical scale expression

Transformed T7 Express lysY/Iq (New England Biolabs) or Rosetta (DE3) (Novagen) *E. coli* cells were grown overnight, with shaking at 37°C, in Luria broth containing 50 μg.mL^{-1} kanamycin or ampicillin (pET constructs – kanamycin; pGEX constructs – ampicillin). Two vials of 8 mL Luria broth, containing 50 μg.mL^{-1} kanamycin or ampicillin, were each inoculated with 400 μL (1 in 20 inoculum) overnight culture and incubated at 37°C, with shaking, until OD_{600nm} readings reached between 0.5 – 0.9. Expression was induced (I) in one of the cultures using a final concentration of 0.1, 0.4, or 1 mM IPTG (Sigma-Aldrich), while the other culture was left uninduced (U) as a control. Induced expression incubations were conducted mostly at 37°C for 4 h (adapted from Zerbs *et al*., 2014), but also at 30°C for 6 h or 25°C for 12 h, with shaking. Both I and U expression cultures were centrifuged at approximately 5000 *g* for 10 min at 4°C, supernatants discarded, and pellets stored at -80°C. From this point onwards, all steps were conducted on ice using ice-cold buffers. The frozen pellets were thawed on ice for 10 min before being resuspended in 1 mL wash buffer (50 mM Tris-HCl, pH 8.0). The resuspended pellets were then lysed by adding 100 μL of 10 mg.mL^{-1} lysozyme and incubated on ice for 30 min with periodic swirling. Suspensions were then sonicated twice for 45 seconds at 60 Hz, with 1 min incubation on ice between sonication steps. The cell lysates were centrifuged at 5000 g for 10 min at 4°C, in order to separate the soluble and insoluble fractions. The insoluble fractions (pellets) were resuspended in 1 mL wash buffer. Samples from each fraction were taken and stored at -20°C until used for SDS-PAGE analysis.

5.3.2. Preparative scale expression

A scraping, from the relevant transformed *E. coli* glycerol stock, was added to 5 mL Luria broth containing 50 μg.mL^{-1} kanamycin or ampicillin (pET constructs – kanamycin; pGEX constructs – ampicillin) and cultured overnight at 37°C with shaking. 2.5 mL of the overnight culture was added (1 in 100 inoculum) to 250 mL Luria broth, containing 50 μg.mL^{-1} kanamycin or ampicillin, and incubated at 37°C, with shaking, until OD_{600nm} readings reached between 0.5 – 0.9. Protein expression was induced by adding 0.1 or 1 mM IPTG to the expression culture, followed by incubation at 37°C for 4 h, with shaking (or at modified incubation temperature and duration, depending on the analytical scale expression analyses). The cells were centrifuged at approximately 5000 *g* at 4°C for 10 min, with the pellet being resuspended in 20 mL of Ni-NTA equilibration buffer (50 mM Tris-HCl, pH 8.0, 20 mM imidazole) or glutathione equilibration buffer (1 × PBS-T (phosphate-buffered saline containing 0.2 % (v/v) Triton X-100), 1 mM PMSF) for His-tagged and GST-tagged fusion proteins, respectively. The

resuspended pellet was centrifuged at approximately 5000 g at 4°C for 10 min, the supernatant discarded, and the pellet stored at -80°C overnight before cell lysis.

5.3.3. Cell lysis

Lysis was performed on ice using ice-cold filter sterilised buffers. The stored frozen pellet, from the preparative scale expression protocol, was thawed on ice for 30 min, before being resuspended in 10 mL Ni-NTA equilibration buffer (His-tagged proteins) or glutathione equilibration buffer (GST-tagged proteins). The resuspended cells were incubated on ice for 30 min with 2 $mg.mL^{-1}$ lysozyme, before immediately being sonicated twice for 1 min at 60 Hz, with 1 min on ice between sonication steps. The cell lysate was centrifuged at approximately 14000 g at 4°C for 30 min to separate the soluble (supernatant) and insoluble (pellet) fractions. The soluble cell lysate fraction was kept on ice until purification.

5.3.4. Preparation of Ni-NTA and glutathione agarose columns

A Ni-NTA SuperFlow column (Qiagen) was used to purify oligo His-tagged fusion proteins. Columns were stored at 4°C in storage solution (50% ethanol). Just before a purification, after the storage solution was allowed to run-through, the column was washed with a full volume of water before being conditioned with two full volumes of Ni-NTA equilibration buffer (50 mM Tris-HCl, pH 8.0, 20 mM imidazole). After a purification, the column was recharged (nickel restored) before another purification could took place. After the storage solution was run through, full volumes of various filter sterilised liquids were run through the column in the following order: water, stripping buffer (20 mM sodium phosphate, 500 mM NaCl, 50 mM EDTA, pH 7.4), water, nickel sulphate solution (0.1 M $NiSO_4$), Ni-NTA equilibration buffer, water, then stored in a half volume storage solution at 4°C (lid closed and tip sealed).

Lyophilised glutathione agarose powder (Sigma-Aldrich, Germany) was hydrated (70 mg agarose in 14 mL water) overnight at 4°C, in a repurposed Ni-NTA column. The agarose beads were washed in 10 volumes of water and stored in glutathione storage buffer (2 mM NaCl, 1 mM NaN_3) at 4°C until further use. Just before a purification, after the storage solution was allowed to run-through, the column was washed with a full volume of water before being conditioned with two full volumes of glutathione equilibration buffer (1 × PBS-T (phosphate-buffered saline containing 0.2 % (v/v) Triton X-100), 1 mM PMSF). After a purification, the column was washed before another purification could took place. After the storage solution was run through, full volumes of various filter sterilised liquids were run through the column in the following order: water twice, cleansing buffer 1 (0.1 M borate, pH 8.5 (NaOH), 0.5

M NaCl), water, cleansing buffer 2 (0.1 M acetate, pH 4.5 (acetic acid), 0.5 M NaCl), water, then stored in a half volume glutathione storage buffer at 4°C (lid closed and tip sealed).

5.3.5. Ni-NTA affinity chromatography

The Ni-NTA column was kept at 4°C and the liquids run through it were all ice-cold and filter sterilised. The soluble fraction (from preparative scale production) was filtered through a 0.2 µm filter and stored on ice. A 60 µL sample of the filtered lysate (whole soluble fraction) was collected and stored on ice for subsequent SDS-PAGE analysis. The filtered lysate was applied to the conditioned Ni-NTA column and a 60 µL sample of the flow-through was collected and stored on ice for subsequent SDS-PAGE analysis. The column was washed twice in 5 mL Ni-NTA equilibration buffer (50 mM Tris-HCl, pH 8.0, 20 mM imidazole), with 60 µL samples of the flow-through from each wash being taken and stored on ice for subsequent SDS-PAGE analysis. His-tagged protein bound to the column was then eluted out with 3 mL elution buffer (50 mM Tris-HCl, pH 8.0, 500 mM imidazole), with a 60 µl sample of the eluate taken and stored on ice for subsequent SDS-PAGE analysis. The eluate was kept on ice until application to a desalting column.

5.3.6. Glutathione affinity chromatography

The glutathione agarose column was kept at 4°C and the liquids run through it were all ice-cold and filter sterilised. The soluble fraction (from large scale expression) was filtered through a 0.2 µm filter and stored on ice. A 60 µL sample of the filtered lysate (whole soluble fraction) was collected and stored on ice for subsequent SDS-PAGE analysis. The filtered lysate was applied to the conditioned glutathione agarose column and a 60 µL sample of the flow-through was collected and stored on ice for subsequent SDS-PAGE analysis. The column was washed twice in 5 mL glutathione equilibration buffer (1 × PBS-T (phosphate-buffered saline containing 0.2 % (v/v) Triton X-100), 1 mM PMSF), with 60 µL samples of the flow-through from each wash being taken and stored on ice for subsequent SDS-PAGE analysis. GST-tagged protein bound to the column was then eluted out with 3 mL glutathione elution buffer (50 mM Tris-HCl, pH 9.0, 10 mM reduced glutathione), with a 60 µl sample of the eluate taken and stored on ice for subsequent SDS-PAGE analysis. The eluate was kept on ice until application to a desalting column.

5.3.7. Desalting (Buffer exchange)

A PD-10 Sephadex G-25 M desalting column (GE Healthcare) was used to exchange the buffer, at 4°C, to remove excess imidazole/reduced glutathione from the eluted His/GST-tagged protein. The desalting

column was conditioned with 5 full volumes of assay buffer (NDPK assay buffer according to Matsuura *et al.,* (2016) – 50 mM Tris, pH 7.6, 5 mM $MgCl_2$); (Arf assay buffer – 25 mM HEPES, pH 7.4, 150 mM KCl, 1 mM $MgCl_2$, 1 mM DTT). Subsequently 2.5 mL of the Ni-NTA or glutathione eluate was applied to the column to penetrate the resin. Purified protein was eluted from the column, 1 mL at a time into Eppendorf tubes, using 4 mL assay buffer in total. The column was washed with filter sterilised water and stored in 50 % ethanol at room temperature.

5.3.8. Protein concentration and storage

The protein $Abs_{260/280nm}$ feature of the NanoDrop 2000/2000c spectrophotometer (Thermo Scientific) was used to determine the concentration, in $mg.mL^{-1}$, of all four 1 mL tubes of desalted protein in quintuplicate. Arf assay buffer (buffer used to elute proteins from the desalting column) was used to blank all readings. The three tubes with the highest average concentration were then combined (3 mL desalted protein). A 60 µL sample of the combined desalted protein was taken and stored on ice for subsequent SDS-PAGE analysis. Purified, desalted proteins were stored at -20°C in 50 % (v/v) glycerol (6 mL total). The protein concentrations of the final combined protein samples were recorded in quintuplicate again, with the average taken as the stored concentration in $mg.mL^{-1}$.

5.4. SDS-PAGE and Western blotting analysis

5.4.1. SDS-PAGE

To each of the 60 µL purification samples (collected from the affinity chromatography and desalting steps), 20 µL of 4 × SDS sample loading buffer (0.25 M Tris, pH 6.8, 4.2 % (w/v) SDS, 40 % (v/v) glycerol, 4 % (v/v) β-mercaptoethanol, 1 % (w/v) bromophenol blue in water) was added, and samples placed in boiling water for 5 minutes. Proteins were resolved through a 12 or 15 % acrylamide resolving gel (0.38 M Tris, pH 8.8, 0.1% (w/v) SDS, 12/15 % (w/v) acrylamide, 0.32/0.40 % (w/v) bis-acrylamide, 0.0035 % (w/v) ammonium persulphate, 0.0007 % (v/v) TEMED in water). A 4 % stacking gel (0.125 M Tris, pH 6.8, 0.1 % (w/v) SDS, 4 % (w/v) acrylamide, 0.1 % (w/v) bis-acrylamide, 0.05 % (w/v) ammonium persulphate, 0.0012 % (v/v) TEMED in water) was used. Loading volumes for the gel were 20 µL protein sample and 5 µL protein standard (unstained protein standard, broad range (10-200 kDa, New England Biolabs); blue prestained protein standard, broad range (11-250 kDa, New England Biolabs); Precision Plus all blue prestained protein standard (10-250 kDa, Bio-Rad)). Gels were run at 25 mA for 90 min in 1 × SDS running buffer (25 mM Tris, pH 8.3-8.5, 192 mM glycine,

0.1 % (w/v) SDS in water) and stained in Coomassie stain (0.25 % (w/v) Coomassie blue R-250, 45 % (v/v) methanol, 10 % (v/v) acetic acid in water) overnight at room temperature, or for 3 h at 37°C. Stained gels were submerged in destain solution (40 % (v/v) methanol, 10 % (v/v) acetic acid in water) until bands became visible. Gels were photographed using a Chemidoc XRS+ gel documentation system and software (Bio-Rad). (Methods adapted from Laemmli, 1970).

5.4.2. Western blotting

After running an SDS-PAGE gel, the Coomassie staining step was omitted. Instead, the gel was removed from the gel sandwich and incubated in transblot buffer (25 mM Tris, 192 mM glycine, 20 % (v/v) methanol in water) for 15 min. A Bio-Rad Mini-PROTEAN II transblot sandwich was prepared, containing the gel and an Amersham Hybond-ECL nitrocellulose blotting membrane, and transblotted at 90 V for 1 h submerged in transblot buffer. The membrane was then rinsed in water before being subjected to antigen staining.

5.4.3. Detection of His-tagged proteins

The Hybond membrane was blocked in 20 mL incubation buffer (0.1 % (v/v) Tween-20, 1 % (w/v) BSA, 10 mM imidazole in TBS (20 mM Tris, pH 7.4, 0.15 M NaCl in water)) overnight at 4°C. HisDetector Nickel-HRP (SeraCare) was used to probe the membrane, in a 1:5000 dilution, for 1 h at ambient temperature. The membrane was then washed in three volumes of wash buffer (0.1 % (v/v) Tween-20, 10 mM imidazole in TBS), before being covered in small volume of TMB membrane peroxidase substrate (SeraCare) and rinsed in water after bands became visible on the membrane.

5.4.4. Detection of GST-tagged proteins

The Hybond membrane was blocked in 20 mL in incubation buffer (0.1 % (v/v) Tween 20, 1 % (w/v) BSA, 10 mM reduced glutathione in TBS (Tris-buffered saline)) for 40 min at room temperature, then probed with a 1:1000 dilution of rabbit anti-GST primary antibodies (Sigma-Aldrich) overnight at 4°C. The membrane was then washed in three volumes of wash buffer (0.1 % (v/v) Tween-20, 10 mM reduced glutathione in TBS) and incubated in 1:5000 dilution of goat-anti-rabbit HRP conjugated secondary antibodies (SeraCare) for 1 h at room temperature. Three volumes of wash buffer were used again, after which TMB membrane peroxidase substrate (SeraCare) was used to cover the membrane, which was rinsed in water after the bands became visible.

2.5. Immobilised Arf-effector interaction assays

2.5.1. Nucleotide exchange and intrinsic tryptophan fluorescence

To preload human Arf GTPase proteins (*Hs*Arf1 and *Hs*Arf6) with GTP or GDP, each protein was added to Arf assay buffer in black 96-well plates, at a final concentration of 5 µM, together with 20 mM EDTA and 50 µM GTP/GDP. The load mixtures were incubated at 25°C for 60 min, with gentle agitation, after which $MgCl_2$ was added to a final concentration of 30 mM before being incubated for a further 10 minutes with gentle agitation at ambient temperature. Intrinsic tryptophan fluorescence was measured, either continuously or as end-point readings, at an excitation wavelength of 297 nm and an emission wavelength of 340 nm in a SpectraMax M3 (Molecular Devices) plate reader. Each biological replicate was conducted in technical triplicate. Loading of malarial Arf GTPase (*Pf*Arf1 and *Pf*Arf6) was performed in the same manner as human Arf GTPase, except for 2 mM EDTA and 3 mM $MgCl_2$ being used instead of 20 mM and 30 mM, respectively. The GTP/GDP incubation for *Pf*Arf6 was performed for 120 min.

2.5.2. Ni-NTA immobilised Arf-effector-GST interaction assay

To a pre-blocked Pierce clear, 96-well, nickel coated plate (Thermo Scientific), 2 µM of GTP/GDP-loaded Arf GTPase (*Hs*Arf1, *Hs*Arf6, *Pf*Arf1, or *Pf*Arf6) was aliquoted in triplicate (50 µL per well) in Arf assay buffer with 1 % (w/v) bovine serum albumin (BSA).The plate was incubated for 30 min at 4°C with gentle agitation, before 50 µL of 2 µM GST-JIP4^{LZII}/GGA3^{GAT}, also in 1 % (w/v) BSA supplemented Arf assay buffer was added to each well (100 µL total reaction mixture, with final concentrations of 1 µM Arf-GTP/GDP; 1 µM effector). Incubation at 4°C, with gentle agitation, was continued for a further 120 min before the protein solutions were aspirated. The wells were first washed once in wash buffer 1 (200 µL of Arf assay buffer with 0.1 % (v/v) Tween-20) and then twice in wash buffer 2 (2 × 200 µL of Arf assay buffer without DTT). A GST substrate master mix (2 mM reduced L-glutathione and 1mM 1-chloro-2,4-dinitrobenzene (CDNB) in phosphate-buffered saline (1X PBS), pH 7.4), pre-equilibrated to room temperature, was added (200 µL) to each well and the plate was incubated at room temperature for 30 min. The absorbance of each well was read at 340 nm in a Spectramax M3 plate reader. Background absorbance readings were also recorded in triplicate wells incubated with GST-JIP4^{LZII}/GGA3^{GAT} only (i.e. without immobilised Arf GTPase proteins), with the mean absorbance being subtracted from their corresponding experimental GST-JIP4^{LZII}/GGA3^{GAT} well absorbance values.

2.5.3. Glutathione immobilised effector-Arf-GST interaction assay

The wells of a Pierce glutathione coated plate (Thermo Scientific) were washed in two volumes (200 µL per wash, per well) of wash buffer (Arf assay buffer without DTT, with 0.1 % Tween-20). Blocking buffer (Arf assay buffer without DTT, with 1 % (w/v) BSA) was added to each well (200 µL), followed by an incubation for 20 min at 25°C with gentle agitation. GST-JIP4^{LZII}/GGA3^{GAT}, diluted to final concentration of 1 µM in Arf assay buffer supplemented with 0.1 % BSA, was added in triplicate to the plate (100 µL), and incubated for 30 min at 25°C, with gentle agitation. The glutathione plate was subsequently washed again in two volumes of wash buffer. Preloaded Arf-GTP/GDP (*Hs*Arf1, *Hs*Arf6, *Pf*Arf1, and *Pf*Arf6) was diluted to final concentration of 1 µM in Arf assay buffer supplemented with 0.1% BSA, when added to each respective well (100 µL). The plate was incubated for 60 min at 25°C, with gentle agitation, before being washed twice in wash buffer. A HisDetector Nickel-HRP solution was prepared (HisDetector Nickel-HRP (Sera Care) diluted 1: 10 000 in Arf assay buffer with 1 % (w/v) BSA) and 200 µL pipetted into each well. The plate was incubated with His-tag buffer for 60 min at 25°C, with gentle agitation, followed by two washes with wash buffer. The plate was subsequently incubated in SureBlue Reserve HRP substrate (Sera Care), pre-equilibrated to room temperature, for 30 min at 25°C (200 µL per well), and the absorbance values at 650 nm were recorded in a Spectramax M3 plate reader. Wells incubated with preloaded Arf-GTP and Arf-GDP only, in the absence of immobilised GST-tagged effector proteins, were used to record background absorbance readings in triplicate, with the mean absorbance being subtracted from their corresponding experimental Arf-GTP/GDP well absorbance values.

2.6. Coupled bioluminescence assay

2.6.1. ATP detection using luciferase

Into a white-walled 96-well plate, 100 µL of a three-fold serial dilution of ATP (1.37 nM – 1 µM) in Arf assay buffer (15 mM HEPES, pH 7.4, 150 mM KCl, 1 mM $MgCl_2$,1 mM DTT) was aliquoted in triplicate. Each 100 µL aliquot contained 1 µM *Hs*Arf1 and 20 nM NDPK. The luciferase containing detection reagent from the ATP Assay Kit (Sigma), was prepared according to the kit protocol. To each 100 µL reaction mixture, 100 µL of detection reagent was added followed by an incubation for 5 min at room temperature (200 µL total reaction mixture). End-point luminescence was recorded immediately after incubation using a Spectramax M3 (Molecular Devices) plate reader. An ATP free background control was also aliquoted in triplicate, with the mean luminescence being subtracted from corresponding experimental ATP values.

2.6.2. NDPK-luciferase coupled reaction

Into a white-walled 96-well plate, 100 µL of a two-fold serial dilution of NDPK (1.56 nM – 100 nM) in Arf assay buffer was aliquoted in triplicate. Each well contained 1 µM GTP and 5 µM ADP. The plate was incubated for 10 min at room temperature immediately after the NDPK was added. To each NDPK reaction mixture, 100 µL of luciferase ATP detection reagent was added (200 µL total reaction mixture). The luminescence was recorded, using a Spectramax M3 (Molecular Devices) plate reader, after the 5 min luciferase incubation.

Into a white-walled 96-well plate, 100 µL of a three-fold serial dilution of GTP (13.70 nM – 10 µM; 1.37 nM – 1 µM) in Arf assay buffer was aliquoted in triplicate. Each aliquot contained 20 nM NDPK and 5 µM ADP. The plate was incubated for 10 min at room temperature immediately after the GTP was added. To each NDPK reaction mixture, 100 µL of luciferase ATP detection reagent was added (200 µL total reaction mixture), with the luminescence being recorded, using a Spectramax M3 (Molecular Devices) plate reader, after the 5 min luciferase incubation. The three-fold serial dilution of GTP (1.37 nM – 1 µM) was repeated twice with two respective condition changes. The first change involved using 1 nM NDPK (instead of 20 nM), and the second involved using 50 µL detection reagent (instead of 100 µL; 150 µL total reaction mixture). A GTP free background control was also aliquoted in triplicate, with the mean luminescence being subtracted from corresponding experimental GTP values.

2.6.3. Arf-NDPK coupled bioluminescence assay

2.6.3.1. 1:1 Arf-NDPK mixture to ATP detection reagent

Into a white-walled 96-well plate, stimulated *Hs*Arf1 GTPase reaction mixtures (*Hs*Arf1 + $GAP1^{GAP}$; *Hs*Arf1 + $ARNO^{Sec7}$; *Hs*Arf1 + $GAP1^{GAP}$ + $ARNO^{Sec7}$) were prepared in Arf assay buffer and aliquoted in triplicate (50 µL per well). Each respective well contained 4 µM GTP, 2 µM *Hs*Arf1, 0.2 µM $ARNO^{Sec7}$ and/or $GAP1^{GAP}$. Negative control wells were prepared containing Arf, the regulators, or assay buffer alone and plated in triplicate, each containing 4 µM GTP. Immediately after the GTP was added, the plate was incubated for 60 or 120 min at room temperature, with gentle agitation. A 50 µL NDPK reaction mixture (40 nM NDPK; 10 µM ADP) was added to each well (100 µL Arf-NDPK reaction mixture final concentrations: 2 µM GTP, 1 µM *Hs*Arf1, 0.1 µM $ARNO^{Sec7}$ and/or $GAP1^{GAP}$; 20 nM NDPK, 5 µM ADP). The plate was incubated for 10 min at room temperature, before 100 µL luciferase ATP detection reagent was added (1:1 – reaction mixture: detection reagent). Luminescence was recorded, using a Spectramax M3 (Molecular Devices) plate reader, immediately after the 5 min luciferase incubation. The above-mentioned protocol was repeated exactly as stated, except in a

different assay buffer, adapted from Mondal *et al.* (2015), and the GloMax Discover System Technical Manual #TM397 (Promega). The buffer was referred to as adjusted-Arf assay buffer for convenience (50 mM Tris-HCl, pH 7.5,50 mM NaCl, 10 mM $CaCl_2$, 10 mM $MgCl_2$, 1 mM EDTA).

2.6.3.2. 2:1 Arf-NDPK mixture to ATP detection reagent

Into a round-bottom 96-well plate, stimulated Arf GTPase reaction mixtures (Arf + $GAP1^{GAP}$; Arf + $ARNO^{Sec7}$; Arf + $GAP1^{GAP}$ + $ARNO^{Sec7}$) were prepared in Arf assay buffer and aliquoted in triplicate (100 µL per well). Each respective well contained 2 µM GTP, 2 µM Arf, 1 µM $ARNO^{Sec7}$ and/or $GAP1^{GAP}$. Negative control wells were prepared containing Arf, the regulators, or assay buffer alone and plated in triplicate, each containing 2 µM GTP. Immediately after the GTP was added, the plate was incubated for 90 or 180 min at room temperature, with gentle agitation, with each respective well being transferred to their corresponding well in a white-walled 96-well plate. A 100 µL NDPK reaction mixture (40 nM NDPK; 10 µM ADP) was added to each well (200 µL Arf-NDPK reaction mixture final concentrations: 1 µM GTP, 1 µM Arf, 0.5 µM $ARNO^{Sec7}$ and/or $GAP1^{GAP}$; 20 nM NDPK, 5 µM ADP). The plate was incubated for 10 min at room temperature, before 100 µL luciferase ATP detection reagent was added (2:1 – reaction mixture: detection reagent). Luminescence was recorded, using a Spectramax M3 (Molecular Devices) plate reader, immediately after the 5-minute luciferase incubation. The above-mentioned protocol was repeated exactly as stated, except in the adjusted-Arf assay buffer. This method was used for *Hs*Arf1, *Hs*Arf6, as well as *Pf*Arf1.

2.7. Statistical analysis

The non-linear regression feature on GraphPad Prism5 was used to find line of best fit, with an R^2 value above 0.99 taken to be 'linear'. Paired t-tests were performed to ascertain differences in mean and standard deviation (SD), with a p-value less than 0.05 taken as significant.

Appendix

Figure A1: Sequence alignment of truncated human and malarial Arf-GTPases. MEGA was used to generate a multiple pairwise alignment of the N-terminally truncated Arf sequences (*Hs*Arf1, *Hs*Arf6, *Pf*Arf1, *Pf*Arf6), and the alignment was viewed using Jalview software. The two- and four-residue regions highlighted in black represent the Arf6 (QS) and Arf1 (MXXE) specific motifs, respectively. The single residue region coloured black represents the conserved tryptophan (W) residue used to monitor nucleotide exchange by fluorescence.

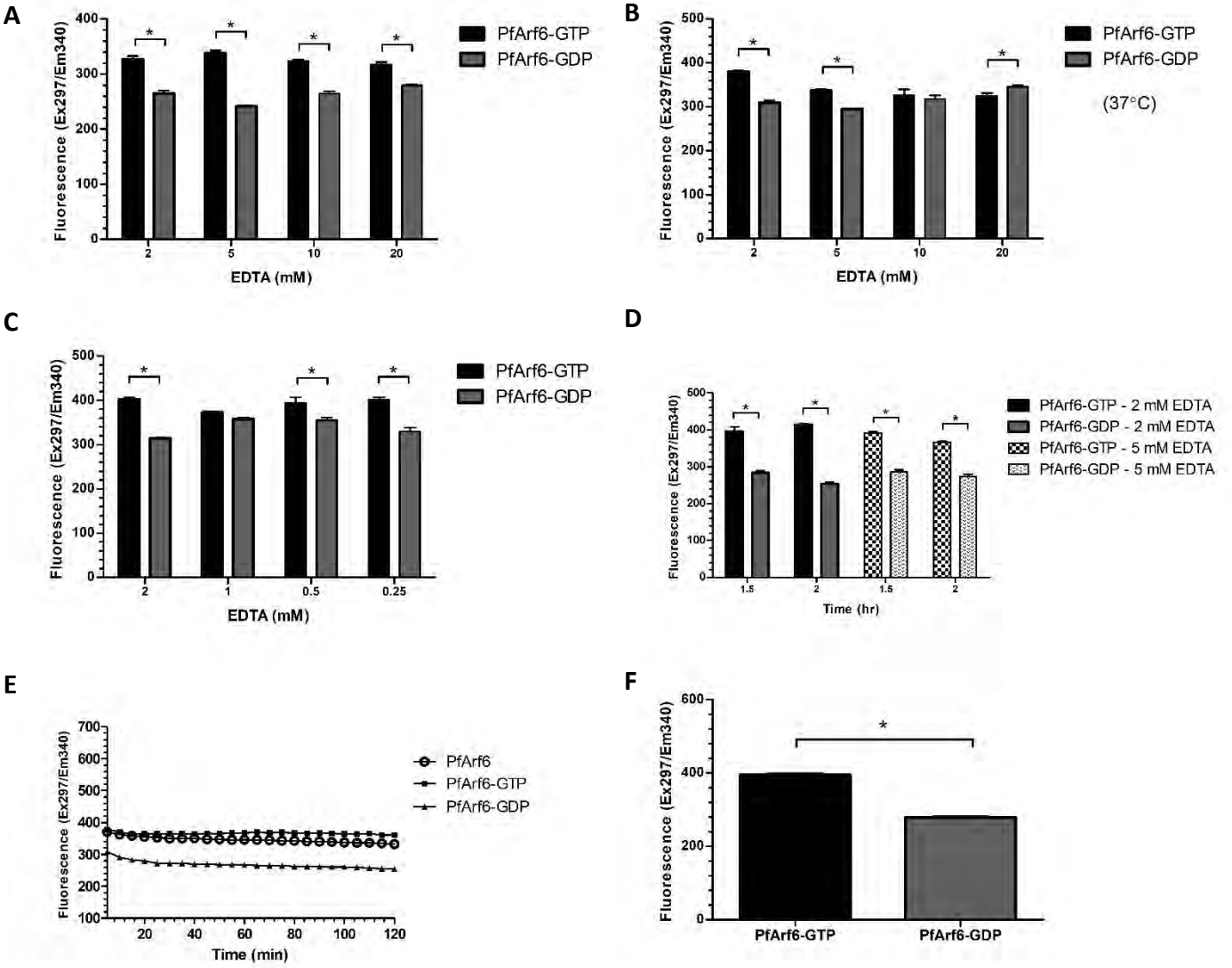

Figure A2: Using tryptophan fluorescence to help determine more favourable nucleotide exchange conditions for *Pf*Arf6. **(A)** older *Pf*Arf6. **(B – D)** newly purified *Pf*Arf6. Nucleotide exchange was performed by incubating 5 µM *Pf*Arf GTPase with 50 µM GTP/GDP, under varying EDTA (mM), time (h), and temperature (°C) conditions. The *Pf*Arf-GTP and *Pf*Arf-GDP complexes were stabilised after a 10 min incubation, after 3 mM $MgCl_2$ was added, with gentle agitation, and tryptophan fluorescence was measured as an end-point reading (Ex_{297}/Em_{340}). **(A)** EDTA (2, 5, 10, 20 mM), for 60 min at 25°C; **(B)** EDTA (2, 5, 10, 20 mM), for 60 min at 37°C; **(C)** EDTA (2, 1, 0.5, 0.25 mM), for 60 min at 25°C; **(D)** 2/5 mM EDTA, for 90 or 120 min at 25°C. **(E – F)** Five µM *Pf*Arf GTPase, in the presence of 50 µM GTP/GDP and 2 mM EDTA, was incubated for 120 min at 25°C, with gentle agitation. A continuous reading of tryptophan fluorescence (Ex_{297}/Em_{340}), including *Pf*Arf own its own, was measured every 5 min for 120 min **(E)**; or as an end-point **reading (F)** using a Spectramax M3 (Molecular Devices) plate reader. Each point represents the mean and standard deviation of triplicate readings. (*) = p-value < 0.05.

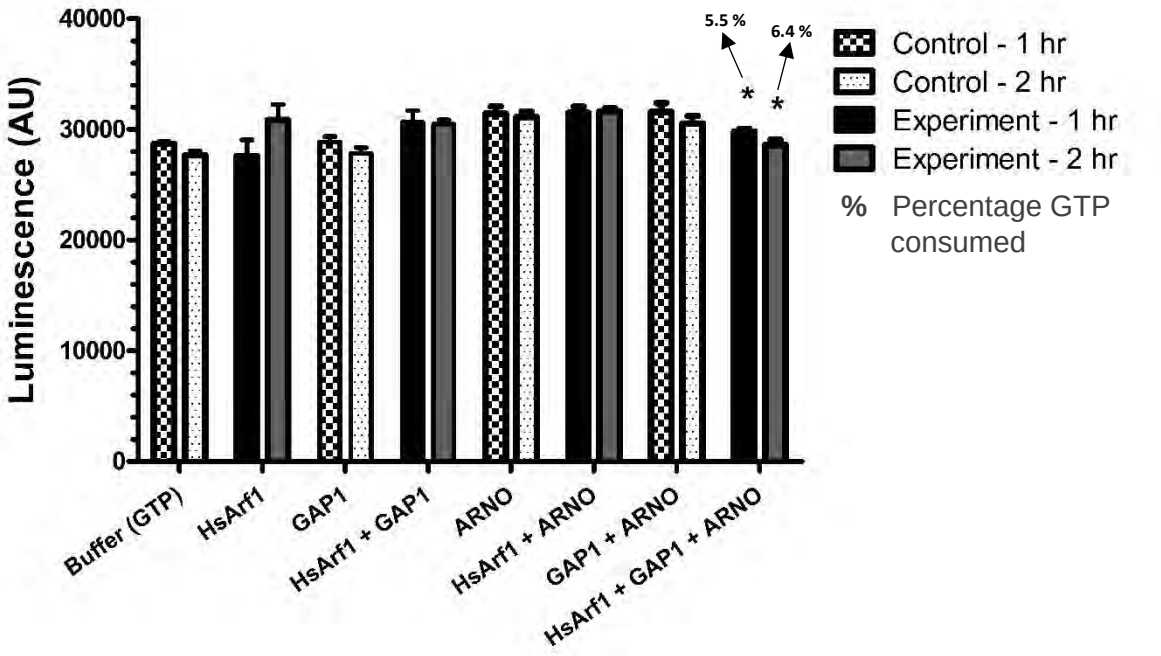

Figure A3: Initial attempt to detect regulator mediated *Hs*Arf1 activity using NDPK and an adjusted assay buffer. Arf GTPase reaction mixtures were prepared (*Hs*Arf1 in the presence of $GAP1^{GAP}$ and/or $ARNO^{Sec7}$; each protein on their own as controls) in assay buffer, and added into a white-walled 96-well plate wells. The plate was incubated for 60 or 120 min at room temperature, with gentle agitation, before a NDPK reaction mixture was added to each well (Arf-NDPK reaction mixture: 1 µM *Hs*Arf1, 2 µM GTP, 0.1 µM $ARNO^{Sec7}$ and/or 0.1 µM $GAP1^{GAP}$; 20 nM NDPK, 5 µM ADP). The plate was incubated for 10 min at room temperature, before a volume of luciferase detection reagent was added (1:1 – Arf-NDPK reaction mixture: detection reagent). Luminescence was recorded, using a Spectramax M3 (Molecular Devices) plate reader, immediately after a 5-minute luciferase incubation. Adjusted assay buffer consisted of 50 mM Tris-HCl, pH 7.5, 50 mM NaCl, 10 mM $CaCl_2$, 10 mM $MgCl_2$, 1 mM EDTA. Each point represents the mean and standard deviation of triplicate readings. (*) = p-value < 0.05, when comparing an experimental mixture to its respective control.

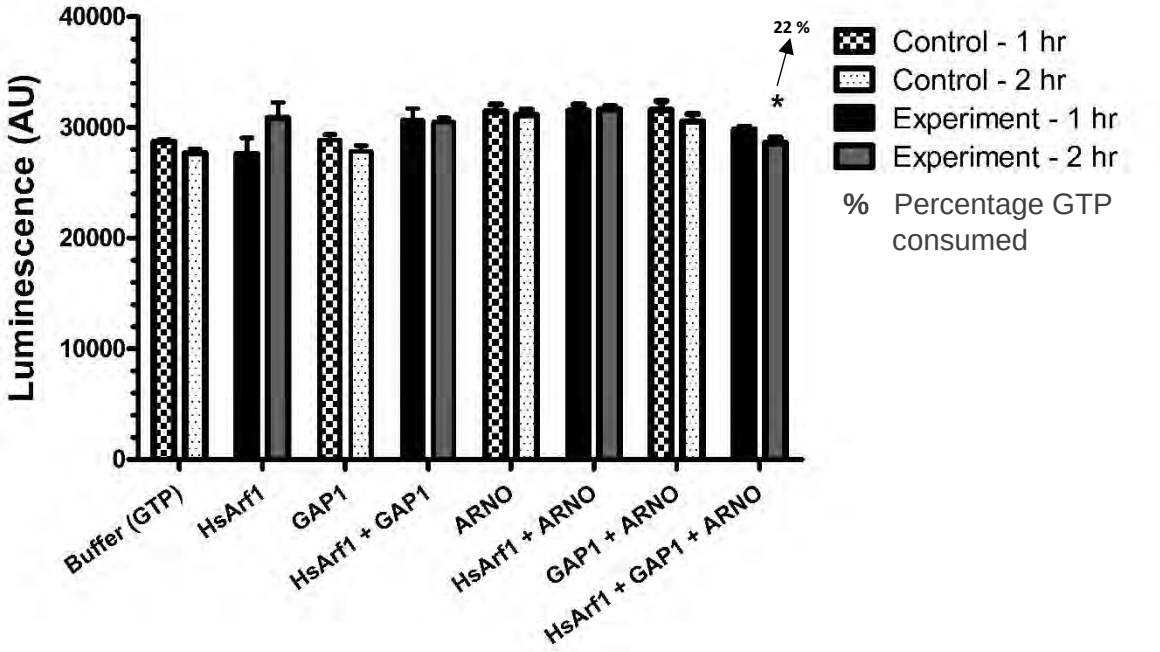

Figure A4: Detection of regulator mediated *Hs*Arf1 GTPase activity using an adjusted assay buffer. Arf GTPase reaction mixtures were prepared (*Hs*Arf1 in the presence of $GAP1^{GAP}$ and/or $ARNO^{Sec7}$; each protein on their own as controls) in assay buffer and added into a round-bottom 96-well plate wells. The plate was incubated for 90 or180 min at room temperature, with gentle agitation, before being transferred to a white-walled 96-well plate. A NDPK reaction mixture was added to each well (Arf-NDPK reaction mixture: 1 µM *Hs*Arf1, 1 µM GTP, 0.5 µM $ARNO^{Sec7}$ and/or 0.5 µM $GAP1^{GAP}$; 20 nM NDPK, 5 µM ADP). The plate was incubated for 10 min at room temperature, before a volume of luciferase detection reagent (half of Arf-NDPK mixture volume) was added (2:1 – reaction mixture: detection reagent). Luminescence was recorded, using a Spectramax M3 (Molecular Devices) plate reader, immediately after a 5 min luciferase incubation. Adjusted assay buffer consisted of 50 mM Tris-HCl, pH 7.5, 50 mM NaCl, 10 mM $CaCl_2$, 10 mM $MgCl_2$, 1 mM EDTA. Each point represents the mean and standard deviation of triplicate readings. (*) = p-value < 0.05, when comparing an experimental mixture to its respective control.

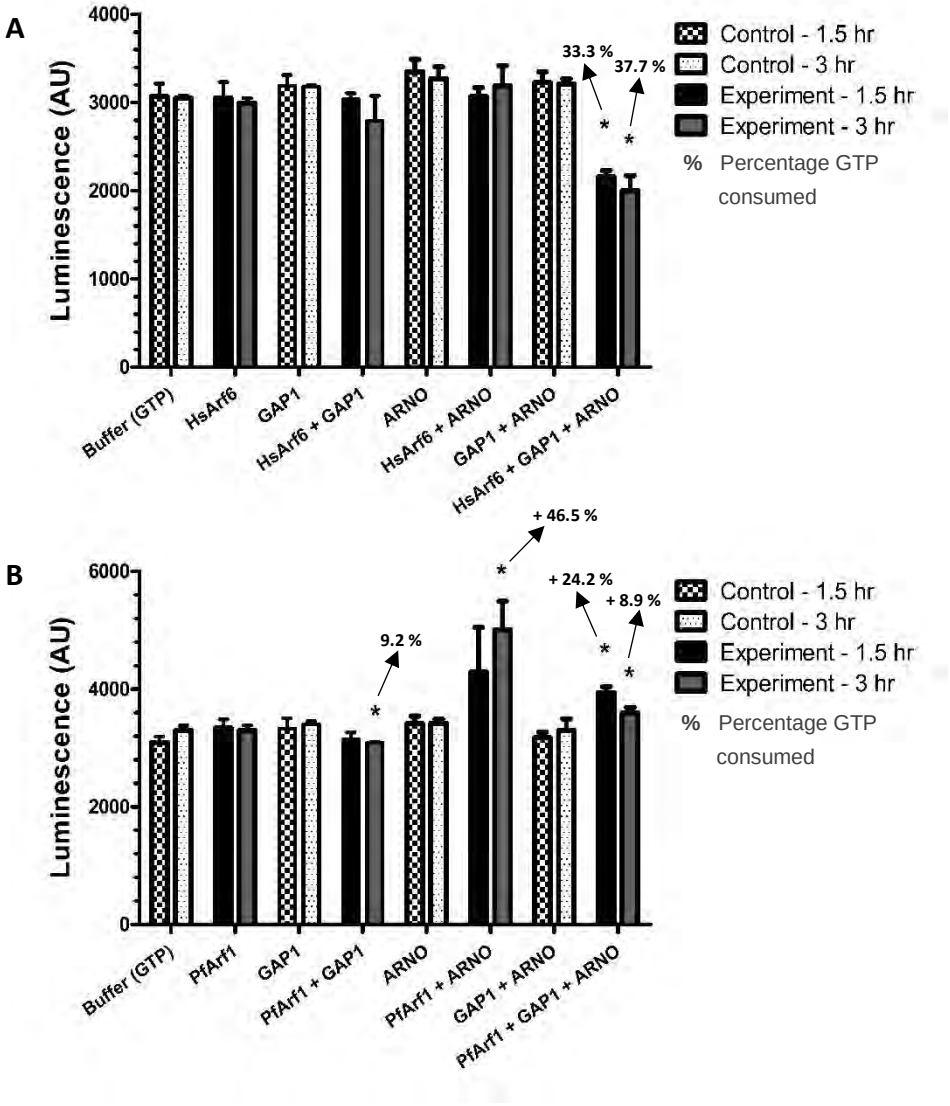

Figure A5: Detection of *Hs*Arf6 and *Pf*Arf1 GTPase activity, using *Hs*Arf1 regulators in an adjusted assay buffer. Arf GTPase reaction mixtures were prepared (**(A)** *Hs*Arf6; or **(B)** *Pf*Arf1, in the presence of $GAP1^{GAP}$ and/or $ARNO^{Sec7}$; each protein on their own as controls) in assay buffer added into a round-bottom 96-well plate wells. The plate was incubated for 90 or 180 min at room temperature, with gentle agitation, before being transferred in a white-walled 96-well plate. A NDPK reaction mixture was added to each well (Arf-NDPK reaction mixture: 1 µM **(A)** *Hs*Arf6; or **(B)** *Pf*Arf1, 1 µM GTP, 0.5 µM $ARNO^{Sec7}$ and/or 0.5 µM $GAP1^{GAP}$; 20 nM NDPK, 5 µM ADP). The plate was incubated for 10 min at room temperature, before a volume of detection reagent was added (2:1 – reaction mixture: detection reagent). Luminescence was recorded, using a Spectramax M3 (Molecular Devices) plate reader, immediately after a 5 min luciferase incubation. Adjusted assay buffer consisted of 50 mM Tris-HCl, pH 7.5, 50 mM NaCl, 10 mM $CaCl_2$, 10 mM $MgCl_2$, 1 mM EDTA. Each point represents the mean and standard deviation of triplicate readings. (*) = p-value < 0.05, when comparing an experimental mixture to its respective control.

References

Abraham, S., Kogata, N., F ssler, R. and Adams, R., 2008. Integrin β1 Subunit Controls Mural Cell Adhesion, Spreading, and Blood Vessel Wall Stability. *Circulation Research*, 102(5), 562-570.

Ahmadian, M., Stege, P., Scheffzek, K. and Wittinghofer, A., 1997. Confirmation of the arginine-finger hypothesis for the GAP-stimulated GTP-hydrolysis reaction of Ras. *Nature Structural Biology*, 4(9), 686-689.

Aikawa, M., Hepler, P., Huff, C. and Sprinz, H., 1966. The Feeding Mechanism of Avian Malarial Parasites. *Journal of Cell Biology*, 28(2), 355-373.

Aizel, K., Biou, V., Navaza, J., Duarte, L., Campanacci, V., Cherfils, J. and Zeghouf, M., 2013. Integrated Conformational and Lipid-Sensing Regulation of Endosomal ArfGEF BRAG2. *PLoS Biology*, 11(9), e1001652.

Alano, P., 2007. Plasmodium falciparum gametocytes: still many secrets of a hidden life. *Molecular Microbiology*, 66(2), 291-302.

Al-Awar, O., Radhakrishna, H., Powell, N. and Donaldson, J., 2000. Separation of Membrane Trafficking and Actin Remodeling Functions of ARF6 with an Effector Domain Mutant. *Molecular and Cellular Biology*, 20(16), 5998-6007.

Albertson, R., Riggs, B. and Sullivan, W., 2005. Membrane traffic: a driving force in cytokinesis. *Trends in Cell Biology*, 15(2), 92-101.

Almaula, N., Lu, Q., Delgado, J., Belkin, S. and Inouye, M., 1995. Nucleoside diphosphate kinase from Escherichia coli. *Journal of bacteriology*, 177(9), 2524-2529.

Altschuler, Y., Liu, S., Katz, L., Tang, K., Hardy, S., Brodsky, F., Apodaca, G. and Mostov, K., 1999. Adp-Ribosylation Factor 6 and Endocytosis at the Apical Surface of Madin-Darby Canine Kidney Cells. *Journal of Cell Biology*, 147(1), 7-12.

Amor, J., Harrison, D., Kahn, R. and Ringe, D., 1994. Structure of the human ADP-ribosylation factor 1 complexed with GDP. *Nature*, 372(6507), 704-708.

Antonny, B., Beraud-Dufour, S., Chardin, P. and Chabre, M., 1997. N-Terminal Hydrophobic Residues of the G-Protein ADP-Ribosylation Factor-1 Insert into Membrane Phospholipids upon GDP to GTP Exchange†. *Biochemistry*, 36(15), 4675-4684.

Attar, M., Salem, J., Pursel, H. and Santy, L., 2012. CNK3 and IPCEF1 produce a single protein that is required for HGF dependent Arf6 activation and migration. *Experimental Cell Research*, 318(3), 228-237.

Baca, A. and Hol, W., 2000. Overcoming codon bias: A method for high-level overexpression of Plasmodium and other AT-rich parasite genes in Escherichia coli. *International Journal for Parasitology*, 30(2), 113-118.

Bach, A., Enjalbert, S., Comunale, F., Bodin, S., Vitale, N., Charrasse, S. and Gauthier-Rouvière, C., 2010. ADP-Ribosylation Factor 6 Regulates Mammalian Myoblast Fusion through Phospholipase D1 and Phosphatidylinositol 4,5-Bisphosphate Signaling Pathways. *Molecular Biology of the Cell*, 21(14), 2412-2424.

Baghban, R., Roshangar, L., Jahanban-Esfahlan, R., Seidi, K., Ebrahimi-Kalan, A., Jaymand, M., Kolahian, S., Javaheri, T. and Zare, P., 2020. Tumor microenvironment complexity and therapeutic implications at a glance. *Cell Communication and Signaling*, 18(1).

Bai, M., Gad, H., Turacchio, G., Cocucci, E., Yang, J., Li, J., Beznoussenko, G., Nie, Z., Luo, R., Fu, L., Collawn, J., Kirchhausen, T., Luini, A. and Hsu, V., 2011. ARFGAP1 promotes AP-2-dependent endocytosis. *Nature Cell Biology*, 13(5), 559-567.

Bakar, N., Klonis, N., Hanssen, E., Chan, C. and Tilley, L., 2010. Digestive-vacuole genesis and endocytic processes in the early intraerythrocytic stages of Plasmodium falciparum. *Journal of Cell Science*, 123(3), 441-450.

Balasubramanian, N., Scott, D., Castle, J., Casanova, J. and Schwartz, M., 2007. Arf6 and microtubules in adhesion-dependent trafficking of lipid rafts. *Nature Cell Biology*, 9(12), 1381-1391.

Basu, A., Li, X. and Leong, S., 2011. Refolding of proteins from inclusion bodies: rational design and recipes. *Applied Microbiology and Biotechnology*, 92(2), 241-251.

Baumgartner, F., Wiek, S., Paprotka, K., Zauner, S. and Lingelbach, K., 2001. A point mutation in an unusual Sec7 domain is linked to brefeldin A resistance in a Plasmodium falciparum line generated by drug selection. *Molecular Microbiology*, 41(5), 1151-1158.

Beemiller, P., Hoppe, A. and Swanson, J., 2006. A Phosphatidylinositol-3-Kinase-Dependent Signal Transition Regulates ARF1 and ARF6 during Fcγ Receptor-Mediated Phagocytosis. *PLoS Biology*, 4(6), e162.

Beemiller, P., Zhang, Y., Mohan, S., Levinsohn, E., Gaeta, I., Hoppe, A. and Swanson, J., 2010. A Cdc42 Activation Cycle Coordinated by PI 3-Kinase during Fc Receptor-mediated Phagocytosis. *Molecular Biology of the Cell*, 21(3), 470-480.

Bell, M., Engleka, M., Malik, A. and Strickler, J., 2013. To fuse or not to fuse: What is your purpose? *Protein Science*, 22(11), 1466-1477.

Beraud-Dufour, S., Robineau, S., Chardin, P., Paris, S., Chabre, M., Cherfils, J. and Antonny, B., 1998. A glutamic finger in the guanine nucleotide exchange factor ARNO displaces Mg2+ and the beta -phosphate to destabilize GDP on ARF1. *The EMBO Journal*, 17(13), 3651-3659.

Berg, O. and Silva, P., 1997. Codon bias in Escherichia coli: the influence of codon context on mutation and selection. *Nucleic Acids Research*, 25(7), 1397-1404.

Bhatt, J., Hancock, W., Meissner, J., Kaczmarczyk, A., Lee, E., Viktorova, E., Ramanadham, S., Belov, G. and Sztul, E., 2019. Promiscuity of the catalytic Sec7 domain within the guanine nucleotide exchange factor GBF1 in ARF activation, Golgi homeostasis, and effector recruitment. *Molecular Biology of the Cell*, 30(12), 1523-1535.

Bigay, J., Casella, J., Drin, G., Mesmin, B. and Antonny, B., 2005. ArfGAP1 responds to membrane curvature through the folding of a lipid packing sensor motif. *The EMBO Journal*, 24(13), 2244-2253.

Birnbaum, J., Flemming, S., Reichard, N., Soares, A., Mesén-Ramírez, P., Jonscher, E., Bergmann, B. and Spielmann, T., 2017. A genetic system to study Plasmodium falciparum protein function. *Nature Methods*, 14(4), 450-456.

Birnbaum, J., Scharf, S., Schmidt, S., Jonscher, E., Hoeijmakers, W., Flemming, S., Toenhake, C., Schmitt, M., Sabitzki, R., Bergmann, B., Fröhlke, U., Mesén-Ramírez, P., Blancke Soares, A., Herrmann, H., Bártfai, R. and Spielmann, T., 2020. A Kelch13-defined endocytosis pathway mediates artemisinin resistance in malaria parasites. *Science*, 367(6473), 51-59.

Boman, A., Zhang, C., Zhu, X. and Kahn, R., 2000. A Family of ADP-Ribosylation Factor Effectors That Can Alter Membrane Transport through thetrans-Golgi. *Molecular Biology of the Cell*, 11(4), 1241-1255.

Boshans, R., Szanto, S., van Aelst, L. and D'Souza-Schorey, C., 2000. ADP-Ribosylation Factor 6 Regulates Actin Cytoskeleton Remodeling in Coordination with Rac1 and RhoA. *Molecular and Cellular Biology*, 20(10), 3685-3694.

Botelho, R., Teruel, M., Dierckman, R., Anderson, R., Wells, A., York, J., Meyer, T. and Grinstein, S., 2000. Localized Biphasic Changes in Phosphatidylinositol-4,5-Bisphosphate at Sites of Phagocytosis. *Journal of Cell Biology*, 151(7), 1353-1368.

Bowden, E., Barth, M., Thomas, D., Glazer, R. and Mueller, S., 1999. An invasion-related complex of cortactin, paxillin and PKCμ associates with invadopodia at sites of extracellular matrix degradation. *Oncogene*, 18(31), 4440-4449.

Brown, H., Gutowski, S., Moomaw, C., Slaughter, C. and Sternwels, P., 1993. ADP-ribosylation factor, a small GTP-dependent regulatory protein, stimulates phospholipase D activity. *Cell*, 75(6), 1137-1144.

Brown, F., Rozelle, A., Yin, H., Balla, T. and Donaldson, J., 2001. Phosphatidylinositol 4,5-bisphosphate and Arf6-regulated membrane traffic. *Journal of Cell Biology*, 154(5), 1007-1018.

Bushell, E., Gomes, A., Sanderson, T., Anar, B., Girling, G., Herd, C., Metcalf, T., Modrzynska, K., Schwach, F., Martin, R., Mather, M., McFadden, G., Parts, L., Rutledge, G., Vaidya, A., Wengelnik, K., Rayner, J. and Billker, O., 2017. Functional Profiling of a Plasmodium Genome Reveals an Abundance of Essential Genes. *Cell*, 170(2), 260-272.

Campa, F., Yoon, H., Ha, V., Szentpetery, Z., Balla, T. and Randazzo, P., 2009. A PH Domain in the Arf GTPase-activating Protein (GAP) ARAP1 Binds Phosphatidylinositol 3,4,5-Trisphosphate and Regulates Arf GAP Activity Independently of Recruitment to the Plasma Membranes. *Journal of Biological Chemistry*, 284(41), 28069-28083.

Carmeliet, P. and Jain, R., 2011. Molecular mechanisms and clinical applications of angiogenesis. *Nature*, 473(7347), 298-307.

Casanova, J., 2007. Regulation of Arf Activation: the Sec7 Family of Guanine Nucleotide Exchange Factors. *Traffic*, 8(11), 1476-1485.

Cauvin, C., Rosendale, M., Gupta-Rossi, N., Rocancourt, M., Larraufie, P., Salomon, R., Perrais, D. and Echard, A., 2016. Rab35 GTPase Triggers Switch-like Recruitment of the Lowe Syndrome Lipid Phosphatase OCRL on Newborn Endosomes. *Current Biology*, 26(1), 120-128.

Chabu, C., Li, D. and Xu, T., 2017. EGFR/ARF6 regulation of Hh signalling stimulates oncogenic Ras tumour overgrowth. *Nature Communications*, 8(1).

Chakrabarty, A., 1998. Nucleoside diphosphate kinase: role in bacterial growth, virulence, cell signalling and polysaccharide synthesis. *Molecular Microbiology*, 28(5), 875-882.

Chan, S., Huang, W., Chang, J., Chang, K., Kuo, W., Wang, M., Lin, K., Uen, Y., Hou, M., Lin, C., Jang, T., Tu, C., Lee, Y., Lee, Y., Tien, M. and Wang, L., 2014. MicroRNA-149 targets GIT1 to suppress integrin signaling and breast cancer metastasis. *Oncogene*, 33(36), 4496-4507.

Chardin, P., Paris, S., Antonny, B., Robineau, S., Béraud-Dufour, S., Jackson, C. and Chabre, M., 1996. A human exchange factor for ARF contains Sec7- and pleckstrin-homology domains. *Nature*, 384(6608), 481-484.

Chavrier, P. and Goud, B., 1999. The role of ARF and Rab GTPases in membrane transport. *Current Opinion in Cell Biology*, 11(4), 466-475.

Chavrier, P. and Ménétrey, J., 2010. Toward a Structural Understanding of Arf Family: Effector Specificity. *Structure*, 18(12), 1552-1558.

Chen, P., Jian, X., Yoon, H. and Randazzo, P., 2013. ARAP2 Signals through Arf6 and Rac1 to Control Focal Adhesion Morphology*. *Journal of Biological Chemistry*, 288(8), 5849-5860.

Chen, P., Luo, R., Jian, X. and Randazzo, P., 2014. The Arf6 GTPase-activating Proteins ARAP2 and ACAP1 Define Distinct Endosomal Compartments That Regulate Integrin α5β1 Traffic. *Journal of Biological Chemistry*, 289(44), 30237-30248.

Cherfils, J. and Chardin, P., 1999. GEFs: structural basis for their activation of small GTP-binding proteins. *Trends in Biochemical Sciences*, 24(8), 306-311.

Cherfils, J. and Zeghouf, M., 2013. Regulation of Small GTPases by GEFs, GAPs, and GDIs. *Physiological Reviews*, 93(1), 269-309.

Chesneau, L., Dambournet, D., Machicoane, M., Kouranti, I., Fukuda, M., Goud, B. and Echard, A., 2012. An ARF6/Rab35 GTPase Cascade for Endocytic Recycling and Successful Cytokinesis. *Current Biology*, 22(2), 147-153.

Chou, W., Lee, P., Tan, Y., Lin, H., Yang, C., Chen, K. and Chuang, C., 2017. An integrative transcriptomic analysis reveals bisphenol A exposure-induced dysregulation of microRNA expression in human endometrial cells. *Toxicology in Vitro*, 41, 133-142.

Cockcroft, S., Thomas, G., Fensome, A., Geny, B., Cunningham, E., Gout, I., Hiles, I., Totty, N., Truong, O. and Hsuan, J., 1994. Phospholipase D: a downstream effector of ARF in granulocytes. *Science*, 263(5146), 523-526.

Collins, B., Watson, P. and Owen, D., 2003. The Structure of the GGA1-GAT Domain Reveals the Molecular Basis for ARF Binding and Membrane Association of GGAs. *Developmental Cell*, 4(3), 321-332.

Conner, S. and Schmid, S., 2003. Regulated portals of entry into the cell. *Nature*, 422(6927), 37-44.

Cook, W., Smith, C., Senkovich, O., Holder, A. and Chattopadhyay, D., 2010. Structure of Plasmodium falciparum ADP-ribosylation factor 1. *Acta Crystallographica Section F Structural Biology and Crystallization Communications*, 66(11), 1426-1431.

Cook, W., Senkovich, O. and Chattopadhyay, D., 2011. Structure of the catalytic domain of Plasmodium falciparum ARF GTPase-activating protein (ARFGAP). *Acta Crystallographica Section F Structural Biology and Crystallization Communications*, 67(11), 1339-1344.

Coppolino, M., Dierckman, R., Loijens, J., Collins, R., Pouladi, M., Jongstra-Bilen, J., Schreiber, A., Trimble, W., Anderson, R. and Grinstein, S., 2002. Inhibition of Phosphatidylinositol-4-phosphate 5-

Kinase Iα Impairs Localized Actin Remodeling and Suppresses Phagocytosis. *Journal of Biological Chemistry*, 277(46), 43849-43857.

Cronin, T., DiNitto, J., Czech, M. and Lambright, D., 2004. Structural determinants of phosphoinositide selectivity in splice variants of Grp1 family PH domains. *The EMBO Journal*, 23(19), 3711-3720.

Dalal, S. and Klemba, M., 2015. Amino acid efflux by asexual blood-stage Plasmodium falciparum and its utility in interrogating the kinetics of hemoglobin endocytosis and catabolism in vivo. *Molecular and Biochemical Parasitology*, 201(2), 116-122.

Dambournet, D., Machicoane, M., Chesneau, L., Sachse, M., Rocancourt, M., El Marjou, A., Formstecher, E., Salomon, R., Goud, B. and Echard, A., 2011. Rab35 GTPase and OCRL phosphatase remodel lipids and F-actin for successful cytokinesis. *Nature Cell Biology*, 13(8), 981-988.

Davidson, A., Humphreys, D., Brooks, A., Hume, P. and Koronakis, V., 2015. The Arf GTPase-Activating Protein Family Is Exploited by Salmonella enterica Serovar Typhimurium To Invade Nonphagocytic Host Cells. *mBio*, 6(1), e02253-02264.

de Bernardez Clark, E., 1998. Refolding of recombinant proteins. *Current Opinion in Biotechnology*, 9(2), 157-163.

de Marco, A., 2009. Strategies for successful recombinant expression of disulfide bond-dependent proteins in Escherichia coli. *Microbial Cell Factories*, 8(1).

de Niz, M., Meibalan, E., Mejia, P., Ma, S., Brancucci, N., Agop-Nersesian, C., Mandt, R., Ngotho, P., Hughes, K., Waters, A., Huttenhower, C., Mitchell, J., Martinelli, R., Frischknecht, F., Seydel, K., Taylor, T., Milner, D., Heussler, V. and Marti, M., 2018. Plasmodium gametocytes display homing and vascular transmigration in the host bone marrow. *Science Advances*, 4(5), eaat3775.

Dell'Angelica, E., Puertollano, R., Mullins, C., Aguilar, R., Vargas, J., Hartnell, L. and Bonifacino, J., 2000. Ggas. *Journal of Cell Biology*, 149(1), 81-94.

Demain, A. and Vaishnav, P., 2009. Production of recombinant proteins by microbes and higher organisms. *Biotechnology Advances*, 27(3), 297-306.

DiNitto, J., Cronin, T. and Lambright, D., 2003. Membrane Recognition and Targeting by Lipid-Binding Domains. *Science Signaling*, 2003(213), re16.

Dodonova, S., Aderhold, P., Kopp, J., Ganeva, I., Röhling, S., Hagen, W., Sinning, I., Wieland, F. and Briggs, J., 2017. 9Å structure of the COPI coat reveals that the Arf1 GTPase occupies two contrasting molecular environments. *eLife*, 6.

Doherty, G. and McMahon, H., 2009. Mechanisms of Endocytosis. *Annual Review of Biochemistry*, 78(1), 857-902.

Donaldson, J., 2003. Multiple Roles for Arf6: Sorting, Structuring, and Signaling at the Plasma Membrane. *Journal of Biological Chemistry*, 278(43), 41573-41576.

Donaldson, J. and Jackson, C., 2000. Regulators and effectors of the ARF GTPases. *Current Opinion in Cell Biology*, 12(4), 475-482.

Donaldson, J. and Jackson, C., 2011. ARF family G proteins and their regulators: roles in membrane transport, development and disease. *Nature Reviews Molecular Cell Biology*, 12(6), 362-375.

Donovan, R., Robinson, C. and Glick, B., 1996. Review: Optimizing inducer and culture conditions for expression of foreign proteins under the control of thelac promoter. *Journal of Industrial Microbiology*, 16(3), 145-154.

Drin, G., Casella, J., Gautier, R., Boehmer, T., Schwartz, T. and Antonny, B., 2007. A general amphipathic α-helical motif for sensing membrane curvature. *Nature Structural & Molecular Biology*, 14(2), 138-146.

D'Souza-Schorey, C., Boshans, R., McDonough, M., Stahl, P. and Van Aelst, L., 1997. A role for POR1, a Rac1-interacting protein, in ARF6-mediated cytoskeletal rearrangements. *The EMBO Journal*, 16(17), 5445-5454.

D'Souza-Schorey, C. and Chavrier, P., 2006. ARF proteins: roles in membrane traffic and beyond. *Nature Reviews Molecular Cell Biology*, 7(5), 347-358.

D'Souza-Schorey, C. and Clancy, J., 2012. Tumor-derived microvesicles: shedding light on novel microenvironment modulators and prospective cancer biomarkers. *Genes & Development*, 26(12), 1287-1299.

D'Souza-Schorey, C., Li, G., Colombo, M. and Stahl, P., 1995. A regulatory role for ARF6 in receptor-mediated endocytosis. *Science*, 267(5201), 1175-1178.

Dubois, T., Paléotti, O., Mironov, A., Fraisier, V., Stradal, T., De Matteis, M., Franco, M. and Chavrier, P., 2005. Golgi-localized GAP for Cdc42 functions downstream of ARF1 to control Arp2/3 complex and F-actin dynamics. *Nature Cell Biology*, 7(4), 353-364.

Dunphy, J., Moravec, R., Ly, K., Lasell, T., Melancon, P. and Casanova, J., 2006. The Arf6 GEF GEP100/BRAG2 Regulates Cell Adhesion by Controlling Endocytosis of β1 Integrins. *Current Biology*, 16(3), 315-320.

Dutta, D. and Donaldson, J., 2015. Sorting of Clathrin-Independent Cargo Proteins Depends on Rab35 Delivered by Clathrin-Mediated Endocytosis. *Traffic*, 16(9), 994-1009.

Ebrahimzadeh, Z., Mukherjee, A. and Richard, D., 2018. A map of the subcellular distribution of phosphoinositides in the erythrocytic cycle of the malaria parasite Plasmodium falciparum. *International Journal for Parasitology*, 48(1), 13-25.

Eberth, A. and Ahmadian, M., 2009. In Vitro GEF and GAP Assays. *Current Protocols in Cell Biology*, Chapter 14, unit 14.9.

Egami, Y., Fujii, M., Kawai, K., Ishikawa, Y., Fukuda, M., and Araki, N., 2015. Activation-Inactivation Cycling of Rab35 and ARF6 Is Required for Phagocytosis of Zymosan in RAW264 Macrophages. *Journal of Immunology Research*, 2015, 1-12.

Egami, Y., Fukuda, M. and Araki, N., 2011. Rab35 regulates phagosome formation through recruitment of ACAP2 in macrophages during FcγR-mediated phagocytosis. *Journal of Cell Science*, 124(21), 3557-3567.

Ehlers, J., Worley, L., Onken, M. and Harbour, J., 2005. DDEF1 Is Located in an Amplified Region of Chromosome 8q and Is Overexpressed in Uveal Melanoma. *Clinical Cancer Research*, 11(10), 3609-3613.

El Azreq, M., Garceau, V., and Bourgoin, S., 2011. Cytohesin-1 regulates fMLF-mediated activation and functions of the β2 integrin Mac-1 in human neutrophils. Journal of Leukocyte Biology. 89(6), 823-836.

Elliott, D., McIntosh, M., Hosgood, H., Chen, S., Zhang, G., Baevova, P. and Joiner, K., 2008. Four distinct pathways of hemoglobin uptake in the malaria parasite Plasmodium falciparum. *Proceedings of the National Academy of Sciences*, 105(7), 2463-2468.

Feng, X., Degese, M., Iglesias-Bartolome, R., Vaque, J., Molinolo, A., Rodrigues, M., Zaidi, M., Ksander, B., Merlino, G., Sodhi, A., Chen, Q. and Gutkind, J., 2014. Hippo-Independent Activation of YAP by the GNAQ Uveal Melanoma Oncogene through a Trio-regulated Rho GTPase Signaling Circuitry. *Cancer Cell*, 25(6), 831-845.

Fielding, A., Schonteich, E., Matheson, J., Wilson, G., Yu, X., Hickson, G., Srivastava, S., Baldwin, S., Prekeris, R. and Gould, G., 2005. Rab11-FIP3 and FIP4 interact with Arf6 and the Exocyst to control membrane traffic in cytokinesis. *The EMBO Journal*, 24(19), 3389-3399.

Fölsch, H., 2005. The building blocks for basolateral vesicles in polarized epithelial cells. *Trends in Cell Biology*, 15(4), 222-228.

Francis, S., Sullivan, D. and Goldberg, A., 1997. Hemoglobin metabolism in the malaria parasite Plasmodium falciparum. *Annual Review of Microbiology*, 51(1), 97-123.

Francis, D. and Page, R., 2010. Strategies to Optimize Protein Expression in E. coli. *Current Protocols in Protein Science*, 61(1).

Franco, M., Boretto, J., van Donselaar, E., Neri, A., D'Souza-Schorey, C, and Chavrier, P., 1999. EFA6, a sec7 domain-containing exchange factor for ARF6, coordinates membrane recycling and actin cytoskeleton organization. *The EMBO Journal*, 18(6), 1480-1491.

Frank, S. and Hansen, S., 2008. The PIX–GIT complex: A G protein signaling cassette in control of cell shape. *Seminars in Cell & Developmental Biology*, 19(3), 234-244.

Frank, S., Hatfield, J. and Casanova, J., 1998. Remodeling of the Actin Cytoskeleton Is Coordinately Regulated by Protein Kinase C and the ADP-Ribosylation Factor Nucleotide Exchange Factor ARNO. *Molecular Biology of the Cell*, 9(11), 3133-3146.

Fu, Y., Li, J., Feng, M., Yang, X., Wang, Y., Zhang, Y., Qin, W., Xia, Q., and Zhang, Z., 2014. Cytohesin-3 is upregulated in hepatocellular carcinoma and contributes to tumor growth and vascular invasion. *International Journal of Clinical and Experimental Pathology*, 7(5), 2123-2132.

Galindo, A., Soler, N., McLaughlin, S., Yu, M., Williams, R. and Munro, S., 2016. Structural Insights into Arl1-Mediated Targeting of the Arf-GEF BIG1 to the trans-Golgi. *Cell Reports*, 16(3), 839-850.

Gallop, J. and McMahon, H., 2005. BAR domains and membrane curvature: bringing your curves to the BAR. *Biochemical Society Symposia*, 72, 223-231.

Gardner, M., Hall, N., Fung, E., White, O., Berriman, M., Hyman, R., Carlton, J., Pain, A., Nelson, K., Bowman, S., Paulsen, I., James, K., Eisen, J., Rutherford, K., Salzberg, S., Craig, A., Kyes, S., Chan, M., Nene, V., Shallom, S., Suh, B., Peterson, J., Angiuoli, S., Pertea, M., Allen, J., Selengut, J., Haft, D., Mather, M., Vaidya, A., Martin, D., Fairlamb, A., Fraunholz, M., Roos, D., Ralph, S., McFadden, G., Cummings, L., Subramanian, G., Mungall, C., Venter, J., Carucci, D., Hoffman, S., Newbold, C., Davis, R., Fraser, C. and Barrell, B., 2002. Genome sequence of the human malaria parasite Plasmodium falciparum. *Nature*, 419(6906), 498-511.

Gillingham, A. and Munro, S., 2007. The Small G Proteins of the Arf Family and Their Regulators. *Annual Review of Cell and Developmental Biology*, 23(1), 579-611.

Glotzer, M., 2005. The Molecular Requirements for Cytokinesis. *Science*, 307(5716), 1735-1739.

Goldberg, J., 1998. Structural Basis for Activation of ARF GTPase. *Cell*, 95(2), 237-248.

Goldenring, J., 2015. Recycling endosomes. *Current Opinion in Cell Biology*, 35, 117-122.

Gong, Q., Weide, M., Huntsman, C., Xu, Z., Jan, L. and Ma, D., 2007. Identification and Characterization of a New Class of Trafficking Motifs for Controlling Clathrin-independent Internalization and Recycling. *Journal of Biological Chemistry*, 282(17), 13087-13097.

González-Montalbán, N., García-Fruitós, E. and Villaverde, A., 2007. Recombinant protein solubility—does more mean better? *Nature Biotechnology*, 25(7), 718-720.

Grant, B. and Donaldson, J., 2009. Pathways and mechanisms of endocytic recycling. *Nature Reviews Molecular Cell Biology*, 10(9), 597-608.

Gräslund, S., Nordlund, P., Weigelt, J., Hallberg, B., Bray, J., Gileadi, O, Knapp, S., Oppermann, U., Arrowsmith, C., Hui, R., Ming, J., dhe-Paganon, S., Park, H., Savchenko, A., Yee, A., Edwards, A., Vincentelli, R., Cambillau, C., Kim, R., Kim, S., Rao, S., Shi, Y., Terwilliger, T., Kim, C., Hung, L., Waldo, G., Peleg, Y., Albeck, S., Unger, T., Dym, O., Prilusky, J., Sussman, J., Stevens, R., Lesley, S., Wilson, I., Joachimiak, A., Collart, F., Dementieva, I., Donnelly, M., Eschenfeldt, W., Kim, Y., Stols, L., Wu, R., Zhou, M., Burley, S., Emtage, J., Sauder, J., Thompson, D., Bain, K., Luz, J., Gheyi, T., Zhang, F., Atwell, S., Almo, S., Bonanno, J., Fiser, A., Swaminathan, S., Studier, F., Chance, M., Sali, A., Acton, T., Xiao, R., Zhao, L., Ma, C., Hunt, J., Tong, L., Cunningham, K., Inouye, M., Anderson, S., Janjua, H., Shastry, R., Ho, C., Wang, D., Wang, H., Jiang, M., Montelione, G., Stuart, D., Owens, R., Daenke, S., Schütz, A., Heinemann, U., Yokoyama, S., Büssow, K., and Gunsalus, K., 2008. Protein production and purification. *Nature Methods*, 5(2), 135-146.

Grossmann, A., Yoo, J., Clancy, J., Sorensen, L., Sedgwick, A., Tong, Z., Ostanin, K., Rogers, A., Grossmann, K., Tripp, S., Thomas, K., D'Souza-Schorey, C., Odelberg, S. and Li, D., 2013. The Small GTPase ARF6 Stimulates β-Catenin Transcriptional Activity During WNT5A-Mediated Melanoma Invasion and Metastasis. *Science Signaling*, 6(265), ra14.

Grüring, C., Heiber, A., Kruse, F., Ungefehr, J., Gilberger, T. and Spielmann, T., 2011. Development and host cell modifications of Plasmodium falciparum blood stages in four dimensions. *Nature Communications*, 2(1), 165.

Gutiérrez-González, M., Farías, C., Tello, S., Pérez-Etcheverry, D., Romero, A., Zúñiga, R., Ribeiro, C., Lorenzo-Ferreiro, C. and Molina, M., 2019. Optimization of culture conditions for the expression of three different insoluble proteins in Escherichia coli. *Scientific Reports*, 9(1).

Guttery, D., Holder, A. and Tewari, R., 2012. Sexual Development in Plasmodium: Lessons from Functional Analyses. *PLoS Pathogens*, 8(1), e1002404.

Hafner, M., Schmitz, A., Grüne, I., Srivatsan, S., Paul, B., Kolanus, W., Quast, T., Kremmer, E., Bauer, I. and Famulok, M., 2006. Inhibition of cytohesins by SecinH3 leads to hepatic insulin resistance. *Nature*, 444(7121), 941-944.

Hanono, A., Garbett, D., Reczek, D., Chambers, D. and Bretscher, A., 2006. EPI64 regulates microvillar subdomains and structure. *Journal of Cell Biology*, 175(5), 803-813.

Hanssen, E., Knoechel, C., Dearnley, M., Dixon, M., Le Gros, M., Larabell, C. and Tilley, L., 2012. Soft X-ray microscopy analysis of cell volume and hemoglobin content in erythrocytes infected with asexual and sexual stages of Plasmodium falciparum. *Journal of Structural Biology*, 177(2), 224-232.

Hashimoto, S., Furukawa, S., Hashimoto, A., Tsutaho, A., Fukao, A., Sakamura, Y., Parajuli, G., Onodera, Y., Otsuka, Y., Handa, H., Oikawa, T., Hata, S., Nishikawa, Y., Mizukami, Y., Kodama, Y., Murakami, M., Fujiwara, T., Hirano, S. and Sabe, H., 2019. ARF6 and AMAP1 are major targets of KRAS and TP53 mutations to promote invasion, PD-L1 dynamics, and immune evasion of pancreatic cancer. *Proceedings of the National Academy of Sciences*, 116(35), 17450-17459.

Hashimoto, S., Mikami, S., Sugino, H., Yoshikawa, A., Hashimoto, A., Onodera, Y., Furukawa, S., Handa, H., Oikawa, T., Okada, Y., Oya, M. and Sabe, H., 2016. Lysophosphatidic acid activates Arf6 to promote the mesenchymal malignancy of renal cancer. *Nature Communications*, 7(1), 10656.

Hernández-Deviez, D., Roth, M., Casanova, J. and Wilson, J., 2004. ARNO and ARF6 Regulate Axonal Elongation and Branching through Downstream Activation of Phosphatidylinositol 4-Phosphate 5-Kinase α. *Molecular Biology of the Cell*, 15(1), 111-120.

Hiester, K. and Santy, L., 2013. The Cytohesin Coiled-Coil Domain Interacts with Threonine 276 to Control Membrane Association. *PLoS ONE*, 8(11), e82084.

Higashijima, T., Ferguson, K., Sternweis, P., Ross, E., Smigel, M. and Gilman, A., 1987. The effect of activating ligands on the intrinsic fluorescence of guanine nucleotide-binding regulatory proteins. *Journal of Biological Chemistry*, 262(2), 752-756.

Hiller, N., Bhattacharjee, S., van Ooij, C., Liolios, K., Harrison, T., Lopez-Estraño, C. and Haldar, K., 2004. A Host-Targeting Signal in Virulence Proteins Reveals a Secretome in Malarial Infection. *Science*, 306(5703), 1934-1937.

Hiroi, T., Someya, A., Thompson, W., Moss, J. and Vaughan, M., 2006. GEP100/BRAG2: Activator of ADP-ribosylation factor 6 for regulation of cell adhesion and actin cytoskeleton via E-cadherin and α-catenin. *Proceedings of the National Academy of Sciences*, 103(28), 10672-10677.

Hisaeda, H., Yasutomo, K. and Himeno, K., 2005. Malaria: immune evasion by parasites. *The International Journal of Biochemistry & Cell Biology*, 37(4), 700-706.

Hoefen, R. and Berk, B., 2006. The multifunctional GIT family of proteins. *Journal of Cell Science*, 119(8), 1469-1475.

Honda, A., Nogami, M., Yokozeki, T., Yamazaki, M., Nakamura, H., Watanabe, H., Kawamoto, K., Nakayama, K., Morris, A., Frohman, M. and Kanaho, Y., 1999. Phosphatidylinositol 4-Phosphate 5-

Kinase α Is a Downstream Effector of the Small G Protein ARF6 in Membrane Ruffle Formation. *Cell*, 99(5), 521-532.

Honda, A., Al-Awar, O., Hay, J. and Donaldson, J., 2005. Targeting of Arf-1 to the early Golgi by membrin, an ER-Golgi SNARE. *Journal of Cell Biology*, 168(7), 1039-1051.

Hongu, T. and Kanaho, Y., 2014. Activation machinery of the small GTPase Arf6. *Advances in Biological Regulation*, 54, 59-66.

Hongu, T., Yamauchi, Y., Funakoshi, Y., Katagiri, N., Ohbayashi, N. and Kanaho, Y., 2016. Pathological functions of the small GTPase Arf6 in cancer progression: Tumor angiogenesis and metastasis. *Small GTPases*, 7(2), 47-53.

Horgan, C., Hanscom, S., Jolly, R., Futter, C. and McCaffrey, M., 2010. Rab11-FIP3 links the Rab11 GTPase and cytoplasmic dynein to mediate transport to the endosomal-recycling compartment. *Journal of Cell Science*, 123(2), 181-191.

Hotary, K., Li, X., Allen, E., Stevens, S. and Weiss, S., 2006. A cancer cell metalloprotease triad regulates the basement membrane transmigration program. *Genes & Development*, 20(19), 2673-2686.

Howe, R., Kelly, M., Jimah, J., Hodge, D. and Odom, A., 2012. Isoprenoid Biosynthesis Inhibition Disrupts Rab5 Localization and Food Vacuolar Integrity in Plasmodium falciparum. *Eukaryotic Cell*, 12(2), 215-223.

Hu, Z., Du, J., Yang, L., Zhu, Y., Yang, Y., Zheng, D., Someya, A., Gu, L. and Lu, X., 2012. GEP100/Arf6 Is Required for Epidermal Growth Factor-Induced ERK/Rac1 Signaling and Cell Migration in Human Hepatoma HepG2 Cells. *PLoS ONE*, 7(6), e38777.

Hu, Z., Xu, R., Liu, J., Zhang, Y., Du, J., Li, W., Zhang, W., Li, Y., Zhu, Y. and Gu, L., 2013. GEP100 regulates epidermal growth factor-induced MDA-MB-231 breast cancer cell invasion through the activation of Arf6/ERK/uPAR signalling pathway. *Experimental Cell Research*, 319(13), 1932-1941.

Huang, Y. and Sidney, W., 2010. GIT1 Act As GAP For Arf6 Downstream Integrin Outside-In Signaling During Platelet Aggregation. *The FASEB Journal*, 24(S1), 867.2.

Humphreys, D., Davidson, A., Hume, P., Makin, L. and Koronakis, V., 2013. Arf6 coordinates actin assembly through the WAVE complex, a mechanism usurped by Salmonella to invade host cells. *Proceedings of the National Academy of Sciences*, 110(42), 16880-16885.

Isabet, T., Montagnac, G., Regazzoni, K., Raynal, B., Khadali, F., England, P., Franco, M., Chavrier, P., Houdusse, A. and Ménétrey, J., 2009. The structural basis of Arf effector specificity: the crystal structure of ARF6 in a complex with JIP4. *The EMBO Journal*, 28(18), 2835-2845.

Ismail, S., Vetter, I., Sot, B. and Wittinghofer, A., 2010. The Structure of an Arf-ArfGAP Complex Reveals a Ca2+ Regulatory Mechanism. *Cell*, 141(5), 812-821.

Jackson, C. and Casanova, J., 2000. Turning on ARF: the Sec7 family of guanine-nucleotide-exchange factors. *Trends in Cell Biology*, 10(2), 60-67.

Jang, S., Jang, S. and Ko, J., 2012. Regulation of ADP-ribosylation factor 4 expression by small leucine zipper protein and involvement in breast cancer cell migration. *Cancer Letters*, 314(2), 185-197.

Jian, X., Brown, P., Schuck, P., Gruschus, J., Balbo, A., Hinshaw, J. and Randazzo, P., 2009. Autoinhibition of Arf GTPase-activating Protein Activity by the BAR Domain in ASAP1. *Journal of Biological Chemistry*, 284(3), 1652-1663.

Jian, X., Gruschus, J., Sztul, E. and Randazzo, P., 2012. The Pleckstrin Homology (PH) Domain of the Arf Exchange Factor Brag2 Is an Allosteric Binding Site. *Journal of Biological Chemistry*, 287(29), 24273-24283.

Jian, X., Tang, W., Zhai, P., Roy, N., Luo, R., Gruschus, J., Yohe, M., Chen, P., Li, Y., Byrd, R., Xia, D. and Randazzo, P., 2015. Molecular Basis for Cooperative Binding of Anionic Phospholipids to the PH Domain of the Arf GAP ASAP1. *Structure*, 23(11), 1977-1988.

Jones, D., Morris, J., Morgan, C., Kondo, H., Irvine, R. and Cockcroft, S., 2000. Type I Phosphatidylinositol 4-Phosphate 5-Kinase Directly Interacts with ADP-ribosylation Factor 1 and Is Responsible for Phosphatidylinositol 4,5-Bisphosphate Synthesis in the Golgi Compartment. *Journal of Biological Chemistry*, 275(18), 13962-13966.

Jonscher, E., Flemming, S., Schmitt, M., Sabitzki, R., Reichard, N., Birnbaum, J., Bergmann, B., Höhn, K. and Spielmann, T., 2019. PfVPS45 Is Required for Host Cell Cytosol Uptake by Malaria Blood Stage Parasites. *Cell Host & Microbe*, 25(1), 166-173.e5.

Kahn, R., Cherfils, J., Elias, M., Lovering, R., Munro, S. and Schurmann, A., 2006. Nomenclature for the human Arf family of GTP-binding proteins: ARF, ARL, and SAR proteins. *Journal of Cell Biology*, 172(5), 645-650.

Kahn, R., Bruford, E., Inoue, H., Logsdon, J., Nie, Z., Premont, R., Randazzo, P., Satake, M., Theibert, A., Zapp, M. and Cassel, D., 2008. Consensus nomenclature for the human ArfGAP domain-containing proteins. *Journal of Cell Biology*, 182(6), 1039-1044.

Kam, J., Miura, K., Jackson, T., Gruschus, J., Roller, P., Stauffer, S., Clark, J., Aneja, R. and Randazzo, P., 2000. Phosphoinositide-dependent Activation of the ADP-ribosylation Factor GTPase-activating Protein ASAP1. *Journal of Biological Chemistry*, 275(13), 9653-9663.

Karamohamed, S., Nordström, T. and Nyrén, P., 1999. Real-Time Bioluminometric Method for Detection of Nucleoside Diphosphate Kinase Activity. *BioTechniques*, 26(4), 728-734.

Karandur, D., Nawrotek, A., Kuriyan, J. and Cherfils, J., 2017. Multiple interactions between an Arf/GEF complex and charged lipids determine activation kinetics on the membrane. *Proceedings of the National Academy of Sciences*, 114(43), 11416-11421.

Kawasaki, M., Nakayama, K. and Wakatsuki, S., 2005. Membrane recruitment of effector proteins by Arf and Rab GTPases. *Current Opinion in Structural Biology*, 15(6), 681-689.

Kelkar, N., Standen, C. and Davis, R., 2005. Role of the JIP4 Scaffold Protein in the Regulation of Mitogen-Activated Protein Kinase Signaling Pathways. *Molecular and Cellular Biology*, 25(7), 2733-2743.

Khan, A. and Ménétrey, J., 2013. Structural Biology of Arf and Rab GTPases' Effector Recruitment and Specificity. *Structure*, 21(8), 1284-1297.

Kirkwood, J., Hargreaves, D., O'Keefe, S. and Wilson, J., 2015. Analysis of crystallization data in the Protein Data Bank. *Acta Crystallographica Section F Structural Biology Communications*, 71(10), 1228-1234.

Kobayashi, H. and Fukuda, M., 2012. Rab35 regulates Arf6 activity through centaurin-β2 (ACAP2) during neurite outgrowth. *Journal of Cell Science*, 125(9), 2235-2243.

Kobayashi, H. and Fukuda, M., 2013. Rab35 establishes the EHD1-association site by coordinating two distinct effectors during neurite outgrowth. *Journal of Cell Science*, 126(11), 2424-2435.

Kon, S., Tanabe, K., Watanabe, T., Sabe, H. and Satake, M., 2008. Clathrin dependent endocytosis of E-cadherin is regulated by the Arf6GAP isoform SMAP1. *Experimental Cell Research*, 314(7), 1415-1428.

Koronakis, V., Hume, P., Humphreys, D., Liu, T., Horning, O., Jensen, O. and McGhie, E., 2011. WAVE regulatory complex activation by cooperating GTPases Arf and Rac1. *Proceedings of the National Academy of Sciences*, 108(35), 14449-14454.

Kosciuk, T., Price, I., Zhang, X., Zhu, C., Johnson, K., Zhang, S., Halaby, S., Komaniecki, G., Yang, M., DeHart, C., Thomas, P., Kelleher, N., Fromme, J. and Lin, H., 2020. NMT1 and NMT2 are lysine myristoyltransferases regulating the ARF6 GTPase cycle. *Nature Communications*, 11(1).

Kouranti, I., Sachse, M., Arouche, N., Goud, B. and Echard, A., 2006. Rab35 Regulates an Endocytic Recycling Pathway Essential for the Terminal Steps of Cytokinesis. *Current Biology*, 16(17), 1719-1725.

Knorr, T., Nagel, W. and Kolanus, W., 2000. Phosphoinositides determine specificity of the guanine-nucleotide exchange activity of cytohesin-1 for ADP-ribosylation factors derived from a mammalian expression system. *European Journal of Biochemistry*, 267(12), 3784-3791.

Krugliak, M., Zhang, J. and Ginsburg, H., 2002. Intraerythrocytic Plasmodium falciparum utilizes only a fraction of the amino acids derived from the digestion of host cell cytosol for the biosynthesis of its proteins. *Molecular and Biochemical Parasitology*, 119(2), 249-256.

Kwiatkowski, D. and Nowak, M., 1991. Periodic and chaotic host-parasite interactions in human malaria. *Proceedings of the National Academy of Sciences*, 88(12), 5111-5113.

Lascu, I. and Gonin, P., 2000. The catalytic mechanism of nucleoside diphosphate kinases. *Journal of Bioenergetics and Biomembranes*, 32(3), 237-246.

Lauer, S., 1997. A Membrane Network for Nutrient Import in Red Cells Infected with the Malaria Parasite. *Science*, 276(5315), 1122-1125.

Lazarus, M., Schneider, T. and Taraschi, T., 2008. A new model for hemoglobin ingestion and transport by the human malaria parasite Plasmodium falciparum. *Journal of Cell Science*, 121(11), 1937-1949.

Lee, S., Yang, J., Hong, W., Premont, R. and Hsu, V., 2005. ARFGAP1 plays a central role in coupling COPI cargo sorting with vesicle formation. *Journal of Cell Biology*, 168(2), 281-290.

Lew, V., Tiffert, T. and Ginsburg, H., 2003. Excess hemoglobin digestion and the osmotic stability ofPlasmodium falciparum–infected red blood cells. *Blood*, 101(10), 4189-4194.

Li, Y., Kelly, W., Logsdon, J., Schurko, A., Harfe, B., Hill-Harfe, K. and Kahn, R., 2004. Functional genomic analysis of the ADP-ribosylation factor family of GTPases: phylogeny among diverse eukaryotes and function in C. elegans. *The FASEB Journal*, 18(15), 1834-1850.

Li, J., Malaby, A., Famulok, M., Sabe, H., Lambright, D. and Hsu, V., 2012. Grp1 Plays a Key Role in Linking Insulin Signaling to Glut4 Recycling. *Developmental Cell*, 22(6), 1286-1298.

Li, M., Ng, S., Wang, J., Lai, L., Yi Leung, S., Franco, M., Peng, Y., He, M., Kung, H. and Lin, M., 2006. EFA6A Enhances Glioma Cell Invasion through ADP Ribosylation Factor 6/Extracellular Signal–Regulated Kinase Signaling. *Cancer Research*, 66(3), 1583-1590.

Li, R., Peng, C., Zhang, X., Wu, Y., Pan, S. and Xiao, Y., 2017. Roles of Arf6 in cancer cell invasion, metastasis and proliferation. *Life Sciences*, 182, 80-84.

Li, M., Tian, L., Yao, H., Lu, J., Ge, J., Guo, Y., Liu, M. and Xiao, H., 2014. ASAP1 mediates the invasive phenotype of human laryngeal squamous cell carcinoma to affect survival prognosis. *Oncology Reports*, 31(6), 2676-2682.

Li, M., Wang, J., Ng, S., Chan, C., He, M., Yu, F., Lai, L., Shi, C., Chen, Y., Yew, D., Kung, H. and Lin, M., 2009. Adenosine diphosphate-ribosylation factor 6 is required for epidermal growth factor-induced glioblastoma cell proliferation. *Cancer*, 115(21), 4959-4972.

Liang, J. and Kornfeld, S., 1998. Comparative activity of ADP-ribosylation factor family members in the early steps of coated vesicle formation on rat liver Golgi membranes. *Journal of Biological Chemistry*, 272(7), 4141-4148.

Liang, C., Qin, Y., Zhang, B., Ji, S., Shi, S., Xu, W., Liu, J., Xiang, J., Liang, D., Hu, Q., Ni, Q., Yu, X. and Xu, J., 2017. ARF6, induced by mutant Kras, promotes proliferation and Warburg effect in pancreatic cancer. *Cancer Letters*, 388, 303-311.

Liu, B., Blanch, A., Namvar, A., Carmo, O., Tiash, S., Andrew, D., Hanssen, E., Rajagopal, V., Dixon, M. and Tilley, L., 2019. Multimodal analysis of Plasmodium knowlesi-infected erythrocytes reveals large invaginations, swelling of the host cell, and rheological defects. *Cellular Microbiology*, 21(5), e13005.

Liu, W., Duden, R., Phair, R. and Lippincott-Schwartz, J., 2005. ArfGAP1 dynamics and its role in COPI coat assembly on Golgi membranes of living cells. *Journal of Cell Biology*, 168(7), 1053-1063.

Liu, J., Istvan, E., Gluzman, I., Gross, J. and Goldberg, D., 2006. Plasmodium falciparum ensures its amino acid supply with multiple acquisition pathways and redundant proteolytic enzyme systems. *Proceedings of the National Academy of Sciences*, 103(23), 8840-8845.

Liu, Y., Kahn, R. and Prestegard, J., 2010. Dynamic structure of membrane-anchored Arf•GTP. *Nature Structural & Molecular Biology*, 17(7), 876-881.

Liu, Z., Miao, J., and Cui, L., 2011. Gametocytogenesis in malaria parasite: commitment, development, and regulation. *Future Microbiology*, 6(11), 1351–1369.

Lichty, J., Malecki, J., Agnew, H., Michelson-Horowitz, D. and Tan, S., 2005. Comparison of affinity tags for protein purification. *Protein Expression and Purification*, 41(1), 98-105.

Loovers, H., Kortholt, A., de Groote, H., Whitty, L., Nussbaum, R., and van Haastert, P., 2007. Regulation of Phagocytosis in Dictyostelium by the Inositol 5-Phosphatase OCRL Homolog Dd5P4. *Traffic*, 8(5), 618-628.

Loskutov, Y., Kozyulina, P., Kozyreva, V., Ice, R., Jones, B., Roston, T., Smolkin, M., Ivanov, A., Wysolmerski, R. and Pugacheva, E., 2014. NEDD9/Arf6-dependent endocytic trafficking of matrix metalloproteinase 14: a novel mechanism for blocking mesenchymal cell invasion and metastasis of breast cancer. *Oncogene*, 34(28), 3662-3675.

Lu, X., Wan, F., Zhang, H., Shi, G. and Ye, D., 2016. ITGA2B and ITGA8 are predictive of prognosis in clear cell renal cell carcinoma patients. *Tumour biology*, 37(1), 253-262.

Lundmark, R., Doherty, G., Vallis, Y., Peter, B. and McMahon, H., 2008. Arf family GTP loading is activated by, and generates, positive membrane curvature. *Biochemical Journal*, 414(2), 189-194.

Luse, S. and Miller, L., 1971. Plasmodium Falciparum Malaria. *The American Journal of Tropical Medicine and Hygiene*, 20(5), 655-660.

Lyon, J., and Haynes, J., 1986. Plasmodium falciparum antigens synthesized by schizonts and stabilized at the merozoite surface when schizonts mature in the presence of protease inhibitors. *Journal of Immunology*, 136(6), 2245-2251.

Ma, L., Umasankar, P., Wrobel, A., Lymar, A., McCoy, A., Holkar, S., Jha, A., Pradhan-Sundd, T., Watkins, S., Owen, D. and Traub, L., 2016. Transient Fcho1/2·Eps15/R·AP-2 Nanoclusters Prime the AP-2 Clathrin Adaptor for Cargo Binding. *Developmental Cell*, 37(5), 428-443.

Macia, E., Chabre, M. and Franco, M., 2001. Specificities for the Small G Proteins ARF1 and ARF6 of the Guanine Nucleotide Exchange Factors ARNO and EFA6. *Journal of Biological Chemistry*, 276(27), 24925-24930.

Macia, E., Luton, F., Partisani, M., Cherfils, J., Chardin, P. and Franco, M., 2004. The GDP-bound form of Arf6 is located at the plasma membrane. *Journal of Cell Science*, 117(11), 2389-2398.

Makyio, H., Ohgi, M., Takei, T., Takahashi, S., Takatsu, H., Katoh, Y., Hanai, A., Ueda, T., Kanaho, Y., Xie, Y., Shin, H., Kamikubo, H., Kataoka, M., Kawasaki, M., Kato, R., Wakatsuki, S. and Nakayama, K., 2012. Structural basis for Arf6-MKLP1 complex formation on the Flemming body responsible for cytokinesis. *The EMBO Journal*, 31(11), 2590-2603.

Malaby, A., van den Berg, B. and Lambright, D., 2013. Structural basis for membrane recruitment and allosteric activation of cytohesin family Arf GTPase exchange factors. *Proceedings of the National Academy of Sciences*, 110(35), 14213-14218.

Manolea, F., Chun, J., Chen, D., Clarke, I., Summerfeldt, N., Dacks, J. and Melançon, P., 2010. Arf3 Is Activated Uniquely at the trans-Golgi Network by Brefeldin A-inhibited Guanine Nucleotide Exchange Factors. *Molecular Biology of the Cell*, 21(11), 1836-1849.

Mantel, P., Hoang, A., Goldowitz, I., Potashnikova, D., Hamza, B., Vorobjev, I., Ghiran, I., Toner, M., Irimia, D., Ivanov, A., Barteneva, N. and Marti, M., 2013. Malaria-Infected Erythrocyte-Derived Microvesicles Mediate Cellular Communication within the Parasite Population and with the Host Immune System. *Cell Host & Microbe*, 13(5), 521-534.

Marchesin, V., Castro-Castro, A., Lodillinsky, C., Castagnino, A., Cyrta, J., Bonsang-Kitzis, H., Fuhrmann, L., Irondelle, M., Infante, E., Montagnac, G., Reyal, F., Vincent-Salomon, A. and Chavrier, P., 2015. ARF6–JIP3/4 regulate endosomal tubules for MT1-MMP exocytosis in cancer invasion. *Journal of Cell biology*, 211(2), 339-358.

Marshall, C., Meiri, D., Smith, M., Mazhab-Jafari, M., Gasmi-Seabrook, G., Rottapel, R., Stambolic, V. and Ikura, M., 2012. Probing the GTPase cycle with real-time NMR: GAP and GEF activities in cell extracts. *Methods*, 57(4), 473-485.

Mart nez-Alonso, M., Gonz lez-Montalb n, N., Garc a-Fruit s, E. and Villaverde, A., 2008. The Functional Quality of Soluble Recombinant Polypeptides Produced in Escherichia coli Is Defined by a Wide Conformational Spectrum. *Applied and Environmental Microbiology*, 74(23), 7431-7433.

Matsumoto, Y., Sakurai, H., Kogashiwa, Y., Kimura, T., Matsumoto, Y., Shionome, T., Asano, M., Saito, K. and Kohno, N., 2016. Inhibition of epithelial–mesenchymal transition by cetuximab via the EGFR-GEP100-Arf6-AMAP1 pathway in head and neck cancer. *Head & Neck*, 39(3), 476-485.

Matsuura, M., Shaw, R., Moses, J., Kim, H., Kim, M., Kim, M., Hoshika, S., Karalkar, N. and Benner, S., 2016. Assays To Detect the Formation of Triphosphates of Unnatural Nucleotides: Application to Escherichia coli Nucleoside Diphosphate Kinase. *ACS Synthetic Biology*, 5(3), 234-240.

Maxfield, F. and McGraw, T., 2004. Endocytic recycling. *Nature Reviews Molecular Cell Biology*, 5(2), 121-132.

Mayor, S. and Pagano, R., 2007. Pathways of clathrin-independent endocytosis. *Nature Reviews Molecular Cell Biology*, 8(8), 603-612.

Mayor, S., Parton, R. and Donaldson, J., 2014. Clathrin-Independent Pathways of Endocytosis. *Cold Spring Harbor Perspectives in Biology*, 6(6), a016758-a016758.

Meissner, J., Bhatt, J., Lee, E., Styers, M., Ivanova, A., Kahn, R. and Sztul, E., 2018. The ARF guanine nucleotide exchange factor GBF1 is targeted to Golgi membranes through a PIP-binding domain. *Journal of Cell Science*, 131(3).

Ménétrey, J., Macia, E., Pasqualato, S., Franco, M. and Cherfils, J., 2000. Structure of Arf6-GDP suggests a basis for guanine nucleotide exchange factors specificity. *Nature Structural Biology*, 7(6), 466-469.

Menju, T., Hashimoto, S., Hashimoto, A., Otsuka, Y., Handa, H., Ogawa, E., Toda, Y., Wada, H., Date, H. and Sabe, H., 2011. Engagement of Overexpressed Her2 with GEP100 Induces Autonomous Invasive Activities and Provides a Biomarker for Metastases of Lung Adenocarcinoma. *PLoS ONE*, 6(9), e25301.

Merithew, E., Hatherly, S., Dumas, J., Lawe, D., Heller-Harrison, R. and Lambright, D., 2001. Structural Plasticity of an Invariant Hydrophobic Triad in the Switch Regions of Rab GTPases Is a Determinant of Effector Recognition. *Journal of Biological Chemistry*, 276(17), 13982-13988.

Michalakis Y., Renaud F., 2009. Malaria: Evolution in vector control. *Nature*, 462(7271), 298-300.

Milani, K., Schneider, T. and Taraschi, T., 2015. Defining the Morphology and Mechanism of the Hemoglobin Transport Pathway in Plasmodium falciparum-Infected Erythrocytes. *Eukaryotic Cell*, 14(4), 415-426.

Miura, Y., Hongu, T., Yamauchi, Y., Funakoshi, Y., Katagiri, N., Ohbayashi, N. and Kanaho, Y., 2016. ACAP3 regulates neurite outgrowth through its GAP activity specific to Arf6 in mouse hippocampal neurons. *Biochemical Journal*, 473(17), 2591-2602.

Mondal, S., Hsiao, K. and Goueli, S., 2015. A Homogenous Bioluminescent System for Measuring GTPase, GTPase Activating Protein, and Guanine Nucleotide Exchange Factor Activities. *ASSAY and Drug Development Technologies*, 13(8), 444-455.

Montag, M., Dyckhoff, G., Lohr, J., Helmke, B., Herrmann, E., Plinkert, P. and Herold-Mende, C., 2009. Angiogenic growth factors in tissue homogenates of HNSCC: expression pattern, prognostic relevance, and interrelationships. *Cancer Science*, 100(7), 1210-1218.

Montagnac, G., Sibarita, J., Loubéry, S., Daviet, L., Romao, M., Raposo, G. and Chavrier, P., 2009. ARF6 Interacts with JIP4 to Control a Motor Switch Mechanism Regulating Endosome Traffic in Cytokinesis. *Current Biology*, 19(3), 184-195.

Montagnac, G., de Forges, H., Smythe, E., Gueudry, C., Romao, M., Salamero, J. and Chavrier, P., 2011. Decoupling of Activation and Effector Binding Underlies ARF6 Priming of Fast Endocytic Recycling. *Current Biology*, 21(7), 574-579.

Moreau, K., Ravikumar, B., Puri, C. and Rubinsztein, D., 2012. Arf6 promotes autophagosome formation via effects on phosphatidylinositol 4,5-bisphosphate and phospholipase D. *Journal of Cell Biology*, 196(4), 483-496.

Morishige, M., Hashimoto, S., Ogawa, E., Toda, Y., Kotani, H., Hirose, M., Wei, S., Hashimoto, A., Yamada, A., Yano, H., Mazaki, Y., Kodama, H., Nio, Y., Manabe, T., Wada, H., Kobayashi, H. and Sabe, H., 2007. GEP100 links epidermal growth factor receptor signalling to Arf6 activation to induce breast cancer invasion. *Nature Cell Biology*, 10(1), 85-92.

Mühlmann, M., Forsten, E., Noack, S. and Büchs, J., 2017. Optimizing recombinant protein expression via automated induction profiling in microtiter plates at different temperatures. *Microbial Cell Factories*, 16(1).

Müller, T., Stein, U., Poletti, A., Garzia, L., Rothley, M., Plaumann, D., Thiele, W., Bauer, M., Galasso, A., Schlag, P., Pankratz, M., Zollo, M. and Sleeman, J., 2010. ASAP1 promotes tumor cell motility and invasiveness, stimulates metastasis formation in vivo, and correlates with poor survival in colorectal cancer patients. *Oncogene*, 29(16), 2393-2403.

Muralidharan-Chari, V., Clancy, J., Plou, C., Romao, M., Chavrier, P., Raposo, G. and D'Souza-Schorey, C., 2009. ARF6-Regulated Shedding of Tumor Cell-Derived Plasma Membrane Microvesicles. *Current Biology*, 19(22), 1875-1885.

Murphy, D. and Courtneidge, S., 2011. The 'ins' and 'outs' of podosomes and invadopodia: characteristics, formation and function. *Nature Reviews Molecular Cell Biology*, 12(7), 413-426.

Myers, K. and Casanova, J., 2008. Regulation of actin cytoskeleton dynamics by Arf-family GTPases. *Trends in Cell Biology*, 18(4), 184-192.

Nakatsu, F. and Ohno, H., 2003. Adaptor Protein Complexes as the Key Regulators of Protein Sorting in the Post-Golgi Network. *Cell Structure and Function*, 28(5), 419-429.

Nie, Z., Stanley, K., Stauffer, S., Jacques, K., Hirsch, D., Takei, J. and Randazzo, P., 2002. AGAP1, an Endosome-associated, Phosphoinositide-dependent ADP-ribosylation Factor GTPase-activating Protein That Affects Actin Cytoskeleton. *Journal of Biological Chemistry*, 277(50), 48965-48975.

Nguyen, D., Bos, P. and Massagué, J., 2009. Metastasis: from dissemination to organ-specific colonization. *Nature Reviews Cancer*, 9(4), 274-284.

Ogasawara, M., Kim, S., Adamik, R., Togawa, A., Ferrans, V., Takeda, K., Kirby, M., Moss, J. and Vaughan, M., 2000. Similarities in Function and Gene Structure of Cytohesin-4 and Cytohesin-1, Guanine Nucleotide-exchange Proteins for ADP-ribosylation Factors. *Journal of Biological Chemistry*, 275(5), 3221-3230.

Okada, R., Yamauchi, Y., Hongu, T., Funakoshi, Y., Ohbayashi, N., Hasegawa, H. and Kanaho, Y., 2015. Activation of the Small G Protein Arf6 by Dynamin2 through Guanine Nucleotide Exchange Factors in Endocytosis. *Scientific Reports*, 5(1), 14919.

Onodera, Y., Hashimoto, S., Hashimoto, A., Morishige, M., Mazaki, Y., Yamada, A., Ogawa, E., Adachi, M., Sakurai, T., Manabe, T., Wada, H., Matsuura, N. and Sabe, H., 2005. Expression of AMAP1, an ArfGAP, provides novel targets to inhibit breast cancer invasive activities. *The EMBO Journal*, 24(5), 963-973.

Osmani, N., Peglion, F., Chavrier, P. and Etienne-Manneville, S., 2010. Cdc42 localization and cell polarity depend on membrane traffic. *Journal of Cell Biology*, 191(7), 1261-1269.

Otani, T., Oshima, K., Onishi, S., Takeda, M., Shinmyozu, K., Yonemura, S. and Hayashi, S., 2011. IKKε Regulates Cell Elongation through Recycling Endosome Shuttling. *Developmental Cell*, 20(2), 219-232.

Otsuka, Y., Sato, H., Oikawa, T., Onodera, Y., Nam, J., Hashimoto, A., Fukunaga, K., Hatanaka, K., Hatanaka, Y., Matsuno, Y., Fukuda, S. and Sabe, H., 2016. High expression of EPB41L5, an integral component of the Arf6-driven mesenchymal program, correlates with poor prognosis of squamous cell carcinoma of the tongue. *Cell Communication and Signaling*, 14(1).

Padovani, D., Folly-Klan, M., Labarde, A., Boulakirba, S., Campanacci, V., Franco, M., Zeghouf, M. and Cherfils, J., 2014. EFA6 controls Arf1 and Arf6 activation through a negative feedback loop. *Proceedings of the National Academy of Sciences*, 111(34), 12378-12383.

Palacios, F., Price, L., Schweitzer, J., Collard, J. and D'Souza-Schorey, C., 2001. An essential role for ARF6-regulated membrane traffic in adherens junction turnover and epithelial cell migration. *The EMBO Journal*, 20(17), 4973-4986.

Palacios, F., Schweitzer, J., Boshans, R. and D'Souza-Schorey, C., 2002. ARF6-GTP recruits Nm23-H1 to facilitate dynamin-mediated endocytosis during adherens junctions disassembly. *Nature Cell Biology*, 4(12), 929-936.

Pan, T., Sun, J., Hu, J., Hu, Y., Zhou, J., Chen, Z., Xu, D., Xu, W., Zheng, S. and Zhang, S., 2014. Cytohesins/ARNO: The Function in Colorectal Cancer Cells. *PLoS ONE*, 9(3), e90997.

Parachoniak, C., Luo, Y., Abella, J., Keen, J. and Park, M., 2011. GGA3 Functions as a Switch to Promote Met Receptor Recycling, Essential for Sustained ERK and Cell Migration. *Developmental Cell*, 20(6), 751-763.

Pasqualato, S., Ménétrey, J., Franco, M. and Cherfils, J., 2001. The structural GDP/GTP cycle of human Arf6. *EMBO reports*, 2(3), 234-238.

Peng, H., Dara, L., Li, T., Zheng, Y., Yang, H., Tomasi, M., Tomasi, I., Giordano, P., Mato, J. and Lu, S., 2013. MAT2B-GIT1 interplay activates MEK1/ERK 1 and 2 to induce growth in human liver and colon cancer. *Hepatology*, 57(6), 2299-2313.

Peters, P., Hsu, V., Ooi, C., Finazzi, D., Teal, S., Oorschot, V., Donaldson, J. and Klausner, R., 1995. Overexpression of wild-type and mutant ARF1 and ARF6: distinct perturbations of nonoverlapping membrane compartments. *Journal of Cell Biology*, 128(6), 1003-1017.

Peyroche, A., Paris, S. and Jackson, C., 1996. Nucleotide exchange on ARF mediated by yeast Geal protein. *Nature*, 384(6608), 479-481.

Pils, D., Horak, P., Gleiss, A., Sax, C., Fabjani, G., Moebus, V., Zielinski, C., Reinthaller, A., Zeillinger, R. and Krainer, M., 2005. Five genes from chromosomal band 8p22 are significantly down-regulated in ovarian carcinoma. *Cancer*, 104(11), 2417-2429.

Powelka, A., Sun, J., Li, J., Gao, M., Shaw, L., Sonnenberg, A. and Hsu, V., 2003. Stimulation-Dependent Recycling of Integrin β1 Regulated by ARF6 and Rab11. *Traffic*, 5(1), 20-36.

Prudêncio, M., Mota, M. and Mendes, A., 2011. A toolbox to study liver stage malaria. *Trends in Parasitology*, 27(12), 565-574.

Qi, Q., Kang, S., Zhang, S., Pham, C., Fu, H., Brat, D. and Ye, K., 2017. Co-amplification of phosphoinositide 3-kinase enhancer A and cyclin-dependent kinase 4 triggers glioblastoma progression. *Oncogene*, 36(32), 4562-4572.

Qin, X., Lin, F., Lii, Y., Gou, C. and Chen, F., 2010. Molecular analysis of ARF1 expression profiles during development of physic nut (Jatropha curcas L.). *Molecular Biology Reports*, 38(3), 1681-1686.

Quilty, D., Chan, C., Yurkiw, K., Bain, A., Babolmorad, G. and Melançon, P., 2018. The Arf-GDP-regulated recruitment of GBF1 to Golgi membranes requires domains HDS1 and HDS2 and a Golgi-localized protein receptor. *Journal of Cell Science*, 132(4).

Radhakrishna, H. and Donaldson, J., 1997. ADP-Ribosylation Factor 6 Regulates a Novel Plasma Membrane Recycling Pathway. *Journal of Cell Biology*, 139(1), 49-61.

Randazzo, P., Inoue, H. and Bharti, S., 2007. Arf GAPs as regulators of the actin cytoskeleton. *Biology of the Cell*, 99(10), 583-600.

Regev-Rudzki, N., Wilson, D., Carvalho, T., Sisquella, X., Coleman, B., Rug, M., Bursac, D., Angrisano, F., Gee, M., Hill, A., Baum, J. and Cowman, A., 2013. Cell-Cell Communication between Malaria-Infected Red Blood Cells via Exosome-like Vesicles. *Cell*, 153(5), 1120-1133.

Ren, X., Farías, G., Canagarajah, B., Bonifacino, J. and Hurley, J., 2013. Structural Basis for Recruitment and Activation of the AP-1 Clathrin Adaptor Complex by Arf1. *Cell*, 152(4), 755-767.

Renault, L., Guibert, B. and Cherfils, J., 2003. Structural snapshots of the mechanism and inhibition of a guanine nucleotide exchange factor. *Nature*, 426(6966), 525-530.

Riggs, B., Rothwell, W., Mische, S., Hickson, G., Matheson, J., Hays, T., Gould, G. and Sullivan, W., 2003. Actin cytoskeleton remodeling during early Drosophila furrow formation requires recycling endosomal components Nuclear-fallout and Rab11. *Journal of Cell Biology*, 163(1), 143-154.

Rosano, G. and Ceccarelli, E., 2009. Rare codon content affects the solubility of recombinant proteins in a codon bias-adjusted Escherichia coli strain. *Microbial Cell Factories*, 8(1), 41.

Rosano, G. and Ceccarelli, E., 2014. Recombinant protein expression in Escherichia coli: advances and challenges. *Frontiers in Microbiology*, 5.

Rueckert, C. and Haucke, V., 2011. The oncogenic TBC domain protein USP6/TRE17 regulates cell migration and cytokinesis. *Biology of the Cell*, 104(1), 22-33.

Sabe, H., Hashimoto, S., Morishige, M., Ogawa, E., Hashimoto, A., Nam, J., Miura, K., Yano, H. and Onodera, Y., 2009. The EGFR-GEP100-Arf6-AMAP1 Signaling Pathway Specific to Breast Cancer Invasion and Metastasis†. *Traffic*, 10(8), 982-993.

Sakagami, H., 2008. The EFA6 Family: Guanine Nucleotide Exchange Factors for ADP Ribosylation Factor 6 at Neuronal Synapses. *The Tohoku Journal of Experimental Medicine*, 214(3), 191-198.

Sangar, F., Schreurs, A., Umaña-Diaz, C., Clapéron, A., Desbois-Mouthon, C., Calmel, C., Mauger, O., Zaanan, A., Miquel, C., Fléjou, J. and Praz, F., 2013. Involvement of small ArfGAP1 (SMAP1), a novel Arf6-specific GTPase-activating protein, in microsatellite instability oncogenesis. *Oncogene*, 33(21), 2758-2767.

Santy, L., Ravichandran, K. and Casanova, J., 2005. The DOCK180/Elmo Complex Couples ARNO-Mediated Arf6 Activation to the Downstream Activation of Rac1. *Current Biology*, 15(19), 1749-1754.

Sargeant, T., Marti, M., Caler, E., Carlton, J., Simpson, K., Speed, T. and Cowman, A., 2006. Lineage-specific expansion of proteins exported to erythrocytes in malaria parasites. *Genome Biology*, 7(2), R12.

Sato, H., Hatanaka, K., Hatanaka, Y., Hatakeyama, H., Hashimoto, A., Matsuno, Y., Fukuda, S. and Sabe, H., 2014. High level expression of AMAP1 protein correlates with poor prognosis and survival after surgery of head and neck squamous cell carcinoma patients. *Cell Communication and Signaling*, 12(1), 12-17.

Scheffzek, K., Ahmadian, M. and Wittinghofer, A., 1998. GTPase-activating proteins: helping hands to complement an active site. *Trends in Biochemical Sciences*, 23(7), 257-262.

Schonteich, E., Pilli, M., Simon, G., Matern, H., Junutula, J., Sentz, D., Holmes, R. and Prekeris, R., 2007. Molecular characterization of Rab11-FIP3 binding to ARF GTPases. *European Journal of Cell Biology*, 86(8), 417-431.

Scopes, R., 1988. Maintenance of active enzymes. In *Protein purification, principles and practice*. 2nd ed. Berlin: Springer-Verlag, pp.317-324.

Schweitzer, J. and D'Souza-Schorey, C., 2002. Localization and Activation of the ARF6 GTPase during Cleavage Furrow Ingression and Cytokinesis. *Journal of Biological Chemistry*, 277(30), 27210-27216.

Schweitzer, J., Sedgwick, A. and D'Souza-Schorey, C., 2011. ARF6-mediated endocytic recycling impacts cell movement, cell division and lipid homeostasis. *Seminars in Cell & Developmental Biology*, 22(1), 39-47.

Senkovich, O. and Chattopadhyay, D., 2004. Plasmodium falciparum ARFGAP: expression and crystallization of the catalytic domain. *Biochimica et Biophysica Acta (BBA) - Proteins and Proteomics*, 1698(1), 127-130.

Self, A. and Hall, A., 1995. Measurement of intrinsic nucleotide exchange and GTP hydrolysis rates. *Small GTPases and Their Regulators Part B: Rho Family*, 67-76.

Serafini, T., Orci, L., Amherdt, M., Brunner, M., Kahn, R. and Rothmant, J., 1991. ADP-Ribosylation factor is a subunit of the coat of Golgi-derived COP-coated vesicles: A novel role for a GTP-binding protein. *Cell*, 67(2), 239-253.

Shan, X., Lv, S., Yu, X., Hu, Z., Zhang, J., Wang, G.,and Wei, Q., 2016. Small RNA interference-mediated ADP-ribosylation factor 6 silencing inhibits proliferation, migration and invasion of human prostate cancer PC-3 cells. *Nan Fang Yi Ke Da Xue Xue Bao*, 36(6), 735-743.

Sherman I. W., 1977. Amino acid metabolism and protein synthesis in malarial parasites. *Bulletin of the World Health Organization*, *55*(2-3), 265–276.

Shiba, T., Kawasaki, M., Takatsu, H., Nogi, T., Matsugaki, N., Igarashi, N., Suzuki, M., Kato, R., Nakayama, K. and Wakatsuki, S., 2003. Molecular mechanism of membrane recruitment of GGA by ARF in lysosomal protein transport. *Nature Structural & Molecular Biology*, 10(5), 386-393.

Shiba, Y., and Randazzo, P., 2012. ArfGAP1 function in COPI mediated membrane traffic: currently debated models and comparison to other coat-binding ArfGAPs. *Histology and Histopathology*, 27(9), 1143-1153.

Shirano, Y. and Shibata, D., 1990. Low temperature cultivation of Escherichia coli carrying a rice lipoxygenase L-2 cDNA produces a soluble and active enzyme at a high level. *FEBS Letters*, 271(1-2), 128-130.

Shome, K., Nie, Y. and Romero, G., 1998. ADP-ribosylation Factor Proteins Mediate Agonist-induced Activation of Phospholipase D. *Journal of Biological Chemistry*, 273(46), 30836-30841.

Shteyn, E., Pigati, L. and Fölsch, H., 2011. Arf6 regulates AP-1B–dependent sorting in polarized epithelial cells. *Journal of Cell Biology*, 194(6), 873-887.

Simon, G. and Prekeris, R., 2008. Mechanisms regulating targeting of recycling endosomes to the cleavage furrow during cytokinesis. *Biochemical Society Transactions*, 36(3), 391-394.

Simpson, R., 2010. Stabilization of Proteins for Storage. *Cold Spring Harbor Protocols*, 2010(5), pdb.top79.

Sinden, R., Talman, A., Marques, S., Wass, M. and Sternberg, M., 2010. The flagellum in malarial parasites. *Current Opinion in Microbiology*, 13(4), 491-500.

Sirirattanakul, S., Wannakrairot, P., Tencomnao, T. and Santiyanont, R., 2015. Gene expression profile in breast cancer comprising predictive markers for metastatic risk. *Genetics and Molecular Research*, 14(3), 10929-10936.

Smythe, W., Joiner, K. and Hoppe, H., 2007. Actin is required for endocytic trafficking in the malaria parasite Plasmodium falciparum. *Cellular Microbiology*, 10(2), 452-464.

Snow, R., Guerra, C., Noor, A., Myint, H. and Hay, S., 2005. The global distribution of clinical episodes of Plasmodium falciparum malaria. *Nature*, 434(7030), 214-217.

Someya, A., Moss, J. and Nagaoka, I., 2010. The Guanine Nucleotide Exchange Protein for ADP-ribosylation Factor 6, ARF-GEP100/BRAG2, Regulates Phagocytosis of Monocytic Phagocytes in an ARF6-dependent Process. *Journal of Biological Chemistry*, 285(40), 30698-30707.

Song, J., Khachikian, Z., Radhakrishna, H. and Donaldson, J., 1998. Localization of endogenous ARF6 to sites of cortical actin rearrangement and involvement of ARF6 in cell spreading. *Journal of Cell Science*, 111(15), 2257-2267.

Spang, A., Shiba, Y. and Randazzo, P., 2010. Arf GAPs: Gatekeepers of vesicle generation. *FEBS Letters*, 584(12), 2646-2651.

Stafford, W., Stockley, R., Ludbrook, S. and Holder, A., 1996. Isolation, Expression and Characterization of the Gene for an ADP-Ribosylation Factor from the Human Malaria Parasite, Plasmodium Falciparum. *European Journal of Biochemistry*, 242(1), 104-113.

Swart, T., Khan, F., Ntlantsana, A., Laming, D., Veale, C., Przyborski, J., Edkins, A. and Hoppe, H., 2020. Detection of the in vitro modulation of Plasmodium falciparum Arf1 by Sec7 and ArfGAP domains using a colorimetric plate-based assay. *Scientific Reports*, 10(1).

Takatsu, H., Yoshino, K., Toda, K. and Nakayama, K., 2002. GGA proteins associate with Golgi membranes through interaction between their GGAH domains and ADP-ribosylation factors. *Biochemical Journal*, 365(2), 369-378.

Talman, A., Domarle, O., McKenzie, F., Ariey, F. and Robert, V., 2004. Gametocytogenesis: the puberty of Plasmodium falciparum. *Malaria Journal*, 3(1), 24.

Tanabe, K., Torii, T., Natsume, W., Braesch-Andersen, S., Watanabe, T. and Satake, M., 2005. A Novel GTPase-activating Protein for ARF6 Directly Interacts with Clathrin and Regulates Clathrin-dependent Endocytosis. *Molecular Biology of the Cell*, 16(4), 1617-1628.

Tawk, L., Chicanne, G., Dubremetz, J., Richard, V., Payrastre, B., Vial, H., Roy, C. and Wengelnik, K., 2010. Phosphatidylinositol 3-Phosphate, an Essential Lipid in Plasmodium, Localizes to the Food Vacuole Membrane and the Apicoplast. *Eukaryotic Cell*, 9(10), 1519-1530.

Toda, K., Nogami, M., Murakami, K., Kanaho, Y. and Nakayama, K., 1999. Colocalization of phospholipase D1 and GTP-binding-defective mutant of ADP-ribosylation factor 6 to endosomes and lysosomes. *FEBS Letters*, 442(2-3), 221-225.

Turner, P., Holst, O. and Karlsson, E., 2005. Optimized expression of soluble cyclomaltodextrinase of thermophilic origin in Escherichia coli by using a soluble fusion-tag and by tuning of inducer concentration. *Protein Expression and Purification*, 39(1), 54-60.

Uchida, H., Kondo, A., Yoshimura, Y., Mazaki, Y. and Sabe, H., 2001. PAG3/Papα/KIAA0400, a Gtpase-Activating Protein for Adp-Ribosylation Factor (Arf), Regulates Arf6 in Fcγ Receptor-Mediated Phagocytosis of Macrophages. *Journal of Experimental Medicine*, 193(8), 955-966.

Ueda, T., Hanai, A., Takei, T., Kubo, K., Ohgi, M., Sakagami, H., Takahashi, S., Shin, H. and Nakayama, K., 2013. EFA6 activates Arf6 and participates in its targeting to the Flemming body during cytokinesis. *FEBS Letters*, 587(11), 1617-1623.

Uhlén, M., Forsberg, G., Moks, T., Hartmanis, M. and Nilsson, B., 1992. Fusion proteins in biotechnology. *Current Opinion in Biotechnology*, 3(4), 363-369.

Vaid, A., Ranjan, R., Smythe, W., Hoppe, H. and Sharma, P., 2010. PfPI3K, a phosphatidylinositol-3 kinase from Plasmodium falciparum, is exported to the host erythrocyte and is involved in hemoglobin trafficking. *Blood*, 115(12), 2500-2507.

van den Boom, J., Wolter, M., Blaschke, B., Knobbe, C. and Reifenberger, G., 2006. Identification of novel genes associated with astrocytoma progression using suppression subtractive hybridization and real-time reverse transcription-polymerase chain reaction. *International Journal of Cancer*, 119(10), 2330-2338.

Weimer, C., Beck, R., Eckert, P., Reckmann, I., Moelleken, J., Br gger, B. and Wieland, F., 2008. Differential roles of ArfGAP1, ArfGAP2, and ArfGAP3 in COPI trafficking. *Journal of Cell Biology*, 183(4), 725-735.

West, M., Bright, N. and Robinson, M., 1997. The Role of ADP-ribosylation Factor and Phospholipase D in Adaptor Recruitment. *Journal of Cell Biology*, 138(6), 1239-1254.

Wickham, M., Culvenor, J. and Cowman, A., 2003. Selective Inhibition of a Two-step Egress of Malaria Parasites from the Host Erythrocyte. *Journal of Biological Chemistry*, 278(39), 37658-37663.

Wilson, G., Fielding, A., Simon, G., Yu, X., Andrews, P., Hames, R., Frey, A., Peden, A., Gould, G. and Prekeris, R., 2005. The FIP3-Rab11 Protein Complex Regulates Recycling Endosome Targeting to the Cleavage Furrow during Late Cytokinesis. *Molecular Biology of the Cell*, 16(2), 849-860.

Wright, J., Kahn, R. and Sztul, E., 2014. Regulating the large Sec7 ARF guanine nucleotide exchange factors: the when, where and how of activation. *Cellular and Molecular Life Sciences*, 71(18), 3419-3438.

Xie, C., Wei, S., Chen, J., Xu, X., Cai, J., Chen, Q. and Jia, L., 2012. Down-Regulation of GEP100 Causes Increase in E-Cadherin Levels and Inhibits Pancreatic Cancer Cell Invasion. *PLoS ONE*, 7(5), e37854.

Xu, K., Gao, J., Yang, X., Yao, Y. and Liu, Q., 2013. Cytohesin-2 as a novel prognostic marker for hepatocellular carcinoma. *Oncology Reports*, 29(6), 2211-2218.

Xu, R., Zhang, Y., Gu, L., Zheng, J., Cui, J., Dong, J. and Du, J., 2015. Arf6 regulates EGF-induced internalization of E-cadherin in breast cancer cells. *Cancer Cell International*, 15(1), 11.

Yagi, R., Tanaka, M., Sasaki, K., Kamata, R., Nakanishi, Y., Kanai, Y. and Sakai, R., 2011. ARAP3 inhibits peritoneal dissemination of scirrhous gastric carcinoma cells by regulating cell adhesion and invasion. *Oncogene*, 30(12), 1413-1421.

Yamaguchi, S., Yamamoto, E., Mannen, T., Nagamune, T. and Nagamune, T., 2012. Protein refolding using chemical refolding additives. *Biotechnology Journal*, 8(1), 17-31.

Yang, C., Heimberg, H., D'Souza-Schorey, C., Mueckler, M. and Stahl, P., 1998. Subcellular Distribution and Differential Expression of Endogenous ADP-ribosylation Factor 6 in Mammalian Cells. *Journal of Biological Chemistry*, 273(7), 4006-4011.

Yang, J., Lee, S., Gao, M., Bourgoin, S., Randazzo, P., Premont, R. and Hsu, V., 2002. ARFGAP1 promotes the formation of COPI vesicles, suggesting function as a component of the coat. *Journal of Cell Biology*, 159(1), 69-78.

Yoo, J., Brady, S., Acosta-Alvarez, L., Rogers, A., Peng, J., Sorensen, L., Wolff, R., Mleynek, T., Shin, D., Rich, C., Kircher, D., Bild, A., Odelberg, S., Li, D., Holmen, S. and Grossmann, A., 2019. The Small GTPase ARF6 Activates PI3K in Melanoma to Induce a Prometastatic State. *Cancer Research*, 79(11), 2892-2908.

Yoo, J., Shi, D., Grossmann, A., Sorensen, L., Tong, Z., Mleynek, T., Rogers, A., Zhu, W., Richards, J., Winter, J., Zhu, J., Dunn, C., Bajji, A., Shenderovich, M., Mueller, A., Woodman, S., Harbour, J.,

Thomas, K., Odelberg, S., Ostanin, K. and Li, D., 2016. ARF6 Is an Actionable Node that Orchestrates Oncogenic GNAQ Signaling in Uveal Melanoma. *Cancer Cell*, 29(6), 889-904.

Yoon, H., Miura, K., Cuthbert, E., Davis, K., Ahvazi, B., Casanova, J. and Randazzo, P., 2006. ARAP2 effects on the actin cytoskeleton are dependent on Arf6-specific GTPase-activating-protein activity and binding to RhoA-GTP. *Journal of Cell Science*, 119(22), 4650-4666.

Yu, X., Breitman, M. and Goldberg, J., 2012. A Structure-Based Mechanism for Arf1-Dependent Recruitment of Coatomer to Membranes. *Cell*, 148(3), 530-542.

Yu, H., Rao, X. and Zhang, K., 2017. Nucleoside diphosphate kinase (Ndk): A pleiotropic effector manipulating bacterial virulence and adaptive responses. *Microbiological Research*, 205, 125-134.

Zangari, J., Partisani, M., Bertucci, F., Milanini, J., Bidaut, G., Berruyer-Pouyet, C., Finetti, P., Long, E., Brau, F., Cabaud, O., Chetaille, B., Birnbaum, D., Lopez, M., Hofman, P., Franco, M. and Luton, F., 2014. EFA6B Antagonizes Breast Cancer. *Cancer Research*, 74(19), 5493-5506.

Zerbs, S., Giuliani, S. and Collart, F., 2014. Small-Scale Expression of Proteins in E. coli. *Methods in Enzymology*, 536, 117-131.

Zhang, Q., Major, M., Takanashi, S., Camp, N., Nishiya, N., Peters, E., Ginsberg, M., Jian, X., Randazzo, P., Schultz, P., Moon, R. and Ding, S., 2007. Small-molecule synergist of the Wnt/β-catenin signaling pathway. *Proceedings of the National Academy of Sciences*, 104(18), 7444-7448.

Zhang, M., Wang, C., Otto, T., Oberstaller, J., Liao, X., Adapa, S., Udenze, K., Bronner, I., Casandra, D., Mayho, M., Brown, J., Li, S., Swanson, J., Rayner, J., Jiang, R. and Adams, J., 2018. Uncovering the essential genes of the human malaria parasitePlasmodium falciparumby saturation mutagenesis. *Science*, 360(6388), eaap7847.

Zhao, H., Ahirwar, D., Oghumu, S., Wilkie, T., Powell, C., Nasser, M., Satoskar, A., Li, D. and Ganju, R., 2015. Endothelial Robo4 suppresses breast cancer growth and metastasis through regulation of tumor angiogenesis. *Molecular Oncology*, 10(2), 272-281.

Zhou, W., Li, X. and Premont, R., 2016. Expanding functions of GIT Arf GTPase-activating proteins, PIX Rho guanine nucleotide exchange factors and GIT–PIX complexes. *Journal of Cell Science*, 129(10), 1963-1974.

Zhu, S., Gong, C., Ren, L., Li, X., Song, D. and Zheng, G., 2012. A simple and effective strategy for solving the problem of inclusion bodies in recombinant protein technology: His-tag deletions enhance soluble expression. *Applied Microbiology and Biotechnology*, 97(2), 837-845.